SAE Aerospace
An SAE International Group

AEROSPACE INFORMATION REPORT

SAE AIR4065 | REV. A

Issued 1993-05
Reaffirmed 2004-11
Stabilized 2012-05

Superseding AIR4065

Propeller/Propfan In-Flight Thrust Determination

RATIONALE

The overall objectives and approach described in this document were intended to provide guidance and benchmarking. Readers may refer to this approach and practice guidance for application, comparison, or extension to their specific related tasks, using the appropriate technical data, requirements and the most current applicable references. The general approach and guidance are considered stable in regards to the above stated intent.

STABILIZED NOTICE

This document has been declared "Stabilized" by the SAE E-33 In-Flight Propulsion Measurement Committee and will no longer be subjected to periodic reviews for currency. Users are responsible for verifying references and continued suitability of technical requirements. Newer technology may exist.

TO PLACE A DOCUMENT ORDER: Tel: 877-606-7323 (inside USA and Canada)
Tel: +1 724-776-4970 (outside USA)
Fax: 724-776-0790
Email: CustomerService@sae.org
SAE WEB ADDRESS: http://www.sae.org

SAE values your input. To provide feedback on this Technical Report, please visit
http://www.sae.org/technical/standards/AIR4065A

FOREWORD

This document presents methods of determining in-flight thrust for the propeller/propfan propulsion system including the mutual interactions between the airframe and propulsion system. The practices and procedures associated with the determination of airframe aerodynamic characteristics are beyond the scope of this document.

The genesis of AIR 4065 begins with the formation of the E33 Committee, "In-Flight Thrust determination" (IFTD) in the late 70's by Dr. Robert Abernethy of Pratt & Whitney and Mr. Gary Adams of the US Air Force. The results of the committee's earlier activities are AIR's 1678 and 1703, addressing uncertainty of IFTD and IFTD respectively. Upon completion of these tasks there were areas of interest not addressed in AIR 1703 such as unsteady IFTD and propeller IFTD. Therefore two subcommittees were formed; subcommittee D for propellers and subcommittee E for unsteady effects. This AIR 4065 presents advisory information from Subcommittee D regarding IFTD for propellers.

This document attempts to present propeller performance accounting and methodology that can be employed to obtain in-flight thrusts. Two methods of quantifying propeller performance are described in this report. The first method relates propeller performance to the traditional parameters of advance ratio, J, power coefficient, C_p, and efficiency, η, and is referred to as the "J" method. The second relates propeller performance to torque or power coefficient , C_q or C_p, reference blade angle, θ, and efficiency, η, and is known as the "Theta" method.

The determination of in-flight thrust can be a complex process. Success depends upon careful planning and meticulous attention to detail throughout the test program. It is important that the participants involved (engine, propulsor and airframe manufacturers, military service, government agency, etc.) agree at the outset on the definitions and the methods to be used for demonstration. Provision for flexibility and redundant methods are important to provide for unforeseen difficulties with a particular method.

There are no industry or government standards for determining in-flight thrust or its associated uncertainty at present. The purpose of this AIR is to present information and guidance on the selection of methodologies to predict and assess propulsion system thrust during flight development programs of conventional aircraft employing propeller propulsion systems,excluding rotors (i.e. helicopters or any vehicle using cyclic pitch propellers/rotors). Methodologies beyond those presented are required in order to evaluate configurations such as vectored thrust or V/STOL aircraft. The document is intended to be used as a technical guide, not as a standard or legal document. In addition to this document, References 1 and 2 describe comprehensive procedures and tasks for implementing the methodologies. Each program should select those tasks that are appropriate to meet its particular objectives.

Uncertainty was not addressed in this AIR, however, the processes involved are amenable to the same uncertainty analysis as enumerated in AIR's 1678 and 1703. Uncertainty as applied to propeller systems may be addressed after completion of the current E-33 committee task.

Particular credit and thanks are owed to the British Aerospace P.L.C., MIDAP group whose document "MIDAP Guide to Drag Estimation of Aircraft & Weapons, Sub-Chapter 5.3 "Propeller Installations" provided a starting basis for the current document. The propulsion accounting system for these counterrotating devices are governed by the same physical laws/characteristics as the existing traditional propellers. This is acknowledged by the document name "Propeller/Propfan In-Flight Thrust Determination"

Mr. Jack Rowse of the Garrett Engine Division of Allied-Signal Aerospace Company, the Sub committee D chairman, led the evolution of the document, and Mr. Todd Havey of the Boeing Commercial Airplane Group, the document sponsor, correlated and edited the many drafts leading to this document. The parent Committee SAE-E33 chaired by John Roberts , United Technologies, Pratt and Whitney Aircraft, deserves special thanks for having endured these drafts and reviews, providing constructive comments.

The following lists the principal authors and E-33 Subcommittee D membership:

Principal Authors:

Jack H. Rowse, E-33D Chairman	Allied Signal Garrett Engine Division
C. Todd Havey, Document Sponsor	Boeing Commercial Airplane Group

Subcommittee D Membership:

Lynn Young, Secretary	Cessna Aircraft Co.
Mahmood Abdelwahab	NASA Lewis Research Center
Dr. Chellappa Balan	General Electric, Evendale
David Barber	deHaviland Div, Boeing Canada
Richard Cybul	Naval Air Propulsion Center
James Diedrich	NASA Lewis Research Center
Donald K. Dunbar	General Electric Evendale
Alexander Hepler, Jr.	Douglas Aircraft Co.
Dan Hofferth	GM Allison Gas Turbines
Roland Lorenz	GM Allison Gas Turbines
Paul N Methven	Dowty Aerospace
Otmar Pozniak	Aircraft Research Assoc. LTD.
Jerry Roan, former E-33D Chairman	Retired (GM Allison Gas Turbines)
Carl Rohrbach	Hamilton Standard - Retired
Phillip A. Simpson	Rolls Royce, Derby
Ronald C. Smith	NASA Ames Research Center
Richard A. Sulkoske	Retired (GM Allison Gas Turbines)
Harry Wainauski	Hamilton Standard
William Wallace, former E-33D Chairman	Allied Signal Garrett Engine Division
Thomas Wynosky	United Technologies, Pratt & Whitney

Other contributors & consultants to AIR 4065:

John Benson	Lockheed Aeronautical Systems Co.
Henry V. Borst	Borst & Associates
Robert J. Jeracki	NASA Lewis Research Center
Margaret M. Kline	Boeing Commercial Airplane Group
Rodney F. Lauer	Calspan Corp./AEDC Operations
Oral Mehmed	NASA Lewis Research Center
Jerry L. Overfield	Allied Signal Garrett Engine Division
Mark T. Pickett	NASA Lewis Research Center
Eugene C. Rooney	Retired but active
Sam Wehofer	Sverdrup Technology, Inc.

This Page Intentionally Blank

TABLE OF CONTENTS

This Page Intentionally Blank

TABLE OF FIGURES

This Page Intentionally Blank

TABLE OF TABLES

This Page Intentionally Blank

1 SCOPE:

AIR 4065, "Propeller/Propfan In-Flight Thrust Determination" addresses steady state propeller thrust as applied to aircraft which are usually powered by gas turbine engines. It includes theory, examples and methods which have been used. Specifically two methods are discussed, the "J" or traditional J,C_p,C_t, η method including the SBAC variation and a new method we call the "Theta" method which is dependent on knowing blade angle, power/torque and flight Mach number. Implementation guidelines are offered as well as overall approaches to flight testing. Appendices include expansions on theory and testing as well as examples.

2 REFERENCES & NOMENCLATURE:

2.1 References:

2.1.1 Society of Automotive Engineers, 400 Commonwealth Drive, Warrendale, PA 15096-0001:

(1) AIR 1678 "Uncertainty of In-Flight Thrust Determination"

(2) AIR 1703 "In-Flight Thrust Determination"

(3) ARP 755 "Gas Turbine Engine Performance Station Identification and Nomenclature"

(4) AS 681 "Gas Turbine Engine Steady State Performance Presentation for Digital Computer Programs"

(5) ARP 1217 "Instrumentation Requirements for Turboshaft Engine Performance Measurements"

(6) ARP 793-66 "Total Temperature Measuring Instruments"

(7) ARP 920-68 "Design and Installation of Pitot-Static Systems for Transport Aircraft"

(8) ARP 921-71 "Flight Test Procedure for Static Pressure System Instrumentation in Subsonic Transport Aircraft"

(9) AS 8005-77 "Minimum Performance Standard Temperature Instrumentation"

(10) AS 8006-88 "Minimum Performance Standard - Pitot and Pitot-Static"

(11) AS 8009-89 "Pressure Altitude Systems"

2.1.2 Other - Referenced

(12) A. H. Fraser-Mitchell et al "MIDAP Guide to Drag Estimation of Aircraft and Weapons - Sub-Chapter 5.'Propeller Installations"'British Aerospace (Kingston), 1980

(13) Stefko, G.L., Rose, G.E., and Podboy, G.G.: Wind Tunnel Performance Results of an Aeroelastically Scaled 2/9 Model of the PTA Flight Test Propfan. NASA TM 89917, July 1987

(14) Stefko, G.L.: New Test Techniques and Analytical Procedures for Understanding the Behavior of Advanced Propellers. NASA TM 83360, April 1983

(15) Stefko, G.L.: Propeller Flow Visualization Techniques. NASA CP-2243 1982

(16) Stefko, G.L.: New Propeller 'Paint Flow" Visualization Technique. NASA TM 83038, 1982

(17) Pope, A.:Wind-Tunnel Testing; Second Edition, John Wiley & Sons Inc., New York, 1954

(18) Glauert, H.: "Wind Tunnel Interference on Wings, Bodies, and Airscrews", R.& M. #1566, British Air Research Committee, 1933

(19) Milne-Thomson, L.M.: Theoretical Aerodynamics, Macmillan and Company Ltd., London

(20) Hamiliton-Standard Publication PDB6101A, Generalized Method of Propeller Performance Estimation

(21) Flight Test Engineering Handbook, Herrington, Shoemacher, Bartlett and Dunlap, USAF, Air Force Systems Command, Air Force Flight Test Center, Edwards Air Force Base, California, Technical Report No. 6273

(22) Performance Flight Testing Theory, USAF Aerospace Research Pilot School, Edwards Air Force Base, Cal., FTC-TIH 64-2005

(23) Young, A.D.: "Note on the Application of the Linear Perturbation Theory to Determine the Effect of Compressibility on the Wind Tunnel Constraint on a Propeller", R.& M. #2113, British Air Research Committee, 1944

(24) Duesterhaus, D. A. and Maywald, P. V.,"Freejet Test Capability for the Aeropropulsion Systems Test Facility", AIAA Paper 89-2537, July 1989.

2.1.3 Other - Non-Referenced

AGARD Conference Proceedings #366, "Aerodynamics and Acoustics of Propellers", containing 33 papers covering: Propeller Analytical Design; Propeller Testing; Propeller Acoustics, October 1984.

Borst, H. V; Sand, E. and Elliot, D. A. Jr.,"Summary of Propeller Design Procedures and Data; Volume I, Aerodynamic Design and Installation", USAAMRDL Technical Report 73-34A, November 1973, AD 774831/2GI

Borst, H. V; Amatt, W. and Bates, W.E.,"Summary of Propeller Design Procedures and Data; Volume II, Structural Analysis and Blade Design", USAAMRDL Technical Report 73-34B, November 1973, AD 774836

Borst, H. V; Sand, E. and Elliot, D. A. Jr.,"Summary of Propeller Design Procedures and Data; Volume III, Hub, Actuator and Control Designs", USAAMRDL Technical Report 73-34C, November 1973, AD 776998

Clifford Bull and George Bennett, "Propulsive Efficiency and Aircraft Drag Determined from Steady State Flight Test Data", SAE Paper 850872, 1985.

Clifford Bull and Philip D. Bridges, "A Method for Flight - Test Determination of Propulsive Efficiency and Drag", AIAA Journal of Aircraft, March 1985, pp 200 -207.

2.2 Nomenclature

A	- Propeller disk area
AEDC	- Arnold Engineering Development Center
AF	- Propeller blade activity factor
ATF	- Altitude test facility
b	- Blade width
b/D	- Propeller blade elemental width ratio (width/tip diameter)
B	- Number of blades
C_D	- Drag coefficient
C_{LD}	- Propeller blade elemental section design lift coefficient
C_{Li}	- Propeller blade integrated design lift coefficient
C_P	- Power coefficient = $P/\rho n^3 D^5$
C_Q	- Torque coefficient = $Q/\rho n^2 D^5$
CR	- Counter rotation
C_T	- Thrust coefficient = $T/\rho n^2 D^4$
C_{Tn}	- Net thrust coefficient
C_{Tp}	- Propulsive thrust coefficient (based on T_p)
C_{Ts}	- Propulsive thrust coefficient (based on T_s)
C_v	- Nozzle velocity (gross thrust) coefficient
D	- Diameter
D_{AFS}	- Throttle independent drag of the airframe system
ΔD_{AFS}	- Change in basic airframe drag due to slipstream effects
ΔD_{exh}	- Exhaust System Drag
D_{iso}	- Drag of centerbody (nacelle) with blades off (tare)
D_{nac}	- Drag of centerbody (nacelle) with blades on = $D_{iso} + \Delta pA_{cb} + \Delta D_{SS}$
$D_{nac,T}$	- Nacelle tare
ΔD_{ss}	- Increase in centerbody (nacelle) with skin friction due to slipstream

D_S	- Spinner Drag Force (Pressure Drag + Skin Friction Drag)
ΔD_S	- Change in propeller spinner force
$D_{s,T}$	- Spinner tare
D_{str}	- Skin Friction Drag due to structure supporting nacelle in the slipstream
f_b	- SBAC Body Correction Factor = 1 - (1.22 S C_D/A) = η_p/η_E
F	- Force
F_{bal}	- Balance reaction force also referred to as metric force
F_{ex}	- Excess thrust, i.e. $F_{ex} = F_{IPF} - D_{AFS}$
ΔF_{exh}	- Throttle dependent force increment due to changing exhaust conditions
F_{G9}	- Core gross thrust
ΔF_{inl}	- Throttle dependent force increment due to changing inlet conditions
F_{IPF}	- Installed propulsive thrust that is obtained from F'_{net} with adjustments for deviations from full scale reference conditions
F_M	- Metric force, also called F_{bal}
FM	- Figure of merit (quasi static efficiency) = .798 $C_T^{3/2}/ C_p$
F_{net}	- Propeller overall net thrust ~ T_s - (D_{iso} + $\Delta p A_{Cb}$+ ΔD_{ss}) - D_{str}
F'_{net}	- Combined overall net thrust of propeller + core ~ F_{net} + Core Thrust
F^*_{Ncore}	- Modified net thrust of the core (AIR1703, Para 2.2)
ΔF_{trim}	- Throttle dependent force increment due to changing aircraft trim conditions
h	- Blade thickness (Not to be confused with retardation factors)
(1-h)	- SBAC Retardation factor = 1 - .254 S/A
h/b	- Propeller blade elemental thickness ratio (thickness/width)
J	- Advance ratio = V/nD
JE	- Effective advance ratio - (1-h)J
J_{Ref}	-Reference advance ratio (related to η_N)
KIAS	- Knots, indicated airspeed
L	- Length

M	- Mass and Meter
MFR	- Mass Flow Ratio
M_{nH}	- Helical Mach number
n	- Revolutions per second
P	- Power
PTR -	Propeller Test Rig
P_0	- Freestream total pressure
P_2	- Core engine face total pressure
ΔpA_{cb}	- Buoyancy force, change in centerbody drag due to propeller pressure field
$\Sigma p\Delta A_{int}$	- Pressure force on rear spinner face
P_{nac}	- Local nacelle static pressure
P_s	- Static pressure
P_{s0}	- Undisturbed static pressure at station 0
Q	- Torque
r	- Propeller blade elemental radius from axial centerline
r/R	- Propeller blade elemental radius ratio
R	- Propeller blade tip radius
R_N	- Reynolds number $=\rho VL/\mu$
RPM	- Revolutions Per Minute
S	- Maximum cross sectional area of nacelle
SBAC	- Society of British Aircraft Contractors
sco	- Spinner cut off ~ xx%R
SR	- Single rotation
T	- Thrust or time
TAF	- Total activity factor = B(AF)
ΔT_{af}	- Thrust increment due to installing T_{net} in the presence of wing and fuselage.
T_{fa}	- Free air thrust aka isolated thrust = $T_s - \Delta pA_{cb} - \Delta T_{pert}$
$T_{net,inst}$	- Installed propeller net thrust in highly integrated wing/nacelle

configuration

T_p - Propeller propulsive thrust = $T_s - (\Delta p A_{cb} + \Delta D_{ss}) = T_{net} - \Delta D_{ss}$

T_{net} - Propeller net thrust = $T_s - \Delta p A_{cb} = T_{fa} + \Delta T_{pert}$

ΔT_{pert} - Change in apparent thrust due to non uniform flow over centerbody

T_s - Apparent thrust, also referred to as shaft thrust

$T_{s,inst}$ - Apparent thrust, T_s, in the presence of aircraft influences

$T_{s,iso}$ - Isolated blade thrust

$\Delta T_{\theta er}$ - Error due to blade pitch measurement between isolated and installed propeller tests.

V - Velocity

V_E - Effective velocity = $(1-h)V_0$

V_0 - Freestream velocity

V_∞ - Core exhaust velocity

w - Increase in slipstream velocities over V_0 due to propeller

W_0 - Mass flow through the core engine ~ lbs/sec

W_9 - Core efflux mass flow = $W_0 + W_f$, lbs/sec

W_{10} - Mass flow through propeller disk

W_f - Fuel mass flow rate ~ lbs/sec

X - Radius ratio = r/R

α - Local section incidence angle

γ - Local section $\tan^{-1}(C_D/C_L)$

η - Propeller efficiency, Power out/Power in = $J\, C_T/C_P$

η_E - Effective efficiency

η_{Net} - Net efficiency

η_P - Propulsive efficiency

η_S - Apparent efficiency

θ - Propeller blade elemental angle

$\theta_{.75}$ - Propeller blade angle at r/R=.75

θ_F - Counterrotating Propeller front row reference angle

θ_R - Counterrotating Propeller rear row reference angle

λ - Propeller blade elemental section sweep angle

μ - Viscosity

π - 3.141592654

ρ - Density of air

σ - Solidity, i.e. ratio of total blade area to swept disk area

ϕ_{plug} - Axial gage force on plug surface downstream of Sta. 9

ϕ_{post} - Axial gage force on post exit streamtube between Sta. 9 and ∞

ϕ_{pre} - Axial gage force on core pre-entry streamtube between Sta. 0 and 1

Ψ - Propeller blade elemental section cone angle.

This Page Intentionally Blank

3 BASIC METHODOLOGY & INSTALLATIONS:

The forces acting on a propulsion system in flight are sometimes difficult to define and are often even more difficult to evaluate. The process of in-flight thrust determination must therefore begin with a definition of the force (thrust) that is to be evaluated. It is particularly important in the case of propeller-driven aircraft that the definition of thrust and drag be well understood by all the parties involved and that there be a proper accounting of all the forces acting on the system. As with the turbofan, the variety of different arrangements adds complication to the thrust/drag accounting process. Three typical locations of the propeller relative to the intake and exhaust stations are discussed in this document. These are: 1. tractor installation, 2. pusher installation with hot exhaust impingement, and 3. pusher installation with no exhaust impingement. Following an analysis of the isolated propeller, all three arrangements are illustrated and analyzed in the following sub-sections. In these sub-sections, reference will be made to a number of terms which are defined in AIR 1703. Additional terms needed to describe forces associated with the propeller will be defined in the text, and in general these are consistent with the definitions used in Reference 12. In AIR 1703 it was assumed that the podded propulsion system used to illustrate the general principles involved was axisymmetric, aligned with the free-stream flow direction, and isolated from the flow field of the remainder of the aircraft. The same assumptions are made here in order to simplify the discussion, BUT IT MUST BE RECOGNIZED THAT THIS SIMPLIFICATION MAY NOT BE CONSISTENT WITH THE PARTICULAR THRUST/DRAG ACCOUNTING SYSTEM BEING CONSIDERED. In addition, the engine support pylon is assumed, initially, to be a symmetrical airfoil at zero angle of attack. The effect of these assumptions is that the only force produced will be exerted in the streamwise (axial) direction. Unless the net swirl in the slipstream is zero, lift and thrust forces will be induced on the other airplane parts by their interaction with the slipstream.

3.1 Thrust:

The general thrust definitions discussed in AIR 1703, Section 2.1 for turbofans are, in principal, also applicable to propeller propulsion systems. However, their application to in-flight thrust determination for the propeller may not be practical

because the secondary or propeller flow has no physical boundary. This lack of a physical boundary appears to make the accurate measurement of flow quantities normally used for in-flight thrust determination very difficult. Alternate approaches have resorted to measuring propeller thrust as an integral force in sub-scale tests. Then, correlations can be made to full-scale via certain parameters determinable in flight, such as flight velocities, shaft torque, blade pitch and rpm.

Several definitions of thrust must be addressed because of the different approaches to thrust/drag accounting in use. The particular approach to thrust/drag accounting chosen for a given application is determined to a large extent by the configuration and by the relative practicality of making certain measurements in flight and in sub-scale tests. These aspects of thrust determination will be addressed later. As in AIR 1703, all of the following developments presume the existence of a frictionless slip surface which separates the propulsive stream from the rest of the flow field.

3.1.1 Traditional Thrust Definitions: This section develops the traditional definitions of thrust used by the propeller industry. These thrust quantities are then related to the overall net thrust given in AIR 1703 whenever practical. Figure 1 summarizes these thrust definitions using the nomenclature used throughout this document.

3.1.1.1 Propeller Overall Net Thrust: Propeller overall net thrust (F_{net}) is defined in accordance with AIR 1703 as the change in momentum flux between far upstream (station '0') and far downstream (station '∞'). It must, therefore include all forces exerted by the internal flow on all surfaces wetted by the internal flow between stations '0' and '∞'.

Overall net thrust,

$$F_{net} = W_{10}\ (V_0 + w) - W_{10}V_0 \qquad (1)$$
$$= W_{10}\ w$$

where: W_{10} = mass flow through the propeller disk

V_0 = freestream velocity

w = increase in slipstream velocity over freestream velocity at station '∞'.

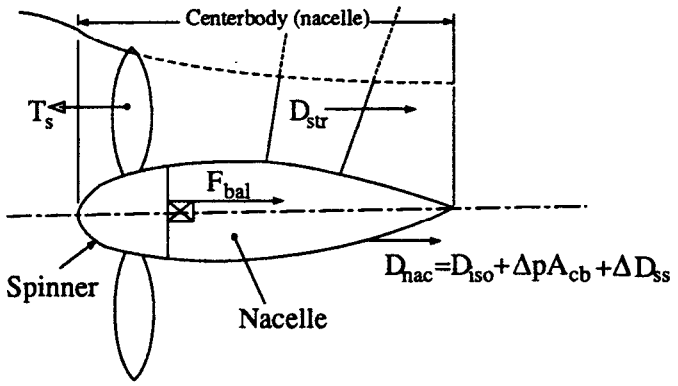

Propeller plus Centerbody

'bouyancy force' = ΔpA_{cb} = increase in centerbody drag due to prop pressure field (determined from the axial component of the integrated pressure readings of the wetted surface)

$= \oint (p_{(blades\ on)} - p_{(blades\ off)})\, dA_{cb}$ over centerbody surface.

$= \int p_{(blades\ on)}\, dA_{cb} - \int p_{(blades\ off)}\, dA_{cb}$

ΔD_{ss} = increase in centerbody skin friction due to slipstream.

D_{iso} = drag of centerbody with blades off

D_{str} = skin friction + pressure drag due to structure

ΔT_{pert} = change in apparent thrust due to non-uniform flow over the centerbody (See Figure 26)

FORCE TERM	SYMBOL	ALTERNATE NAME	DEFINITION
Apparent thrust	T_s	Shaft thrust	Blade Force = F_{bal} corrected for spinner forces
Free-air thrust	T_{fa}	Isolated thrust	T_s with no centerbody and uniform flow, $T_s - \Delta pA_{cb} - \Delta T_{pert}$
Propeller net thrust	T_{net}	Net thrust	$T_s - \Delta pA_{cb}$ or $T_{fa} + \Delta T_{pert}$
Balance reaction force	F_{bal}	Metric force	as measured with hub balance
Propeller propulsive thrust	T_p	Propulsive thrust	$T_s - (\Delta pA_{cb} + \Delta D_{ss})$
Propeller overall net thrust	F_{net}		$T_s - \underbrace{(D_{iso} + \Delta pA_{cb} + \Delta D_{ss})}_{D_{nac}} - D_{str}$ or $T_p - D_{iso} - D_{str}$

Figure 1 - Propeller Thrust Definitions with Strut and Centerbody

3.1.1.2 Free-Air Thrust: Free-air thrust (T_{fa}) is the thrust produced by an ideal propeller or actuator disk operating in a uniform freestream flowfield with no center-body and an infinitely thin drive shaft. (See Appendix A for explanation of actuator disk theory.) This arrangement is shown in Figure 2.

In this case, the only surfaces wetted by the flow in the stream tube between stations '0' and '∞', are the propeller blades themselves. Overall net thrust is therefore equal to free-air thrust for the isolated prop.

$$T_{fa} \text{ in the ideal case} = F_{Net} = W_{10}\, w = A(P_{13}-P_{12}) \qquad (2)$$

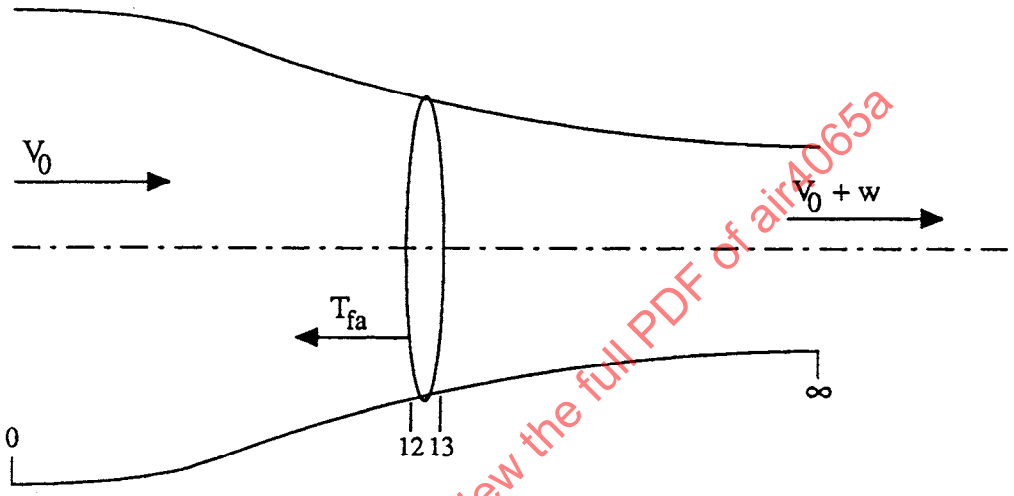

Figure 2 - Free-air Thrust

3.1.1.3 Apparent Thrust : In practice, adjustments must be made to the ideal case for non-uniform inflow caused by the presence of the body around the propeller drive system body and the drag of other structure in the propeller slip stream. Apparent thrust (T_s), sometimes referred to as shaft thrust, is the thrust reacted at the root of the propeller blades as they pass into the hub. It is not the thrust which would be measured on the propeller shaft, as this would include the forces associated with the hub. Note that, for this document, the centerbody is defined as the hub (rotating) plus the nacelle (stationary).

The apparent thrust with no centerbody present is the same as free-air thrust. When a centerbody is introduced behind (or in front of) the propeller, the apparent thrust is altered by two effects as follows:

i) The change of the increased pressure field on the centerbody caused by the propeller results in a 'buoyancy force', term $\Delta p A_{cb}$, which increases both the

apparent thrust of the propeller and the drag of the centerbody. For inviscid flow, the increase in apparent thrust and centerbody drag are equal, and so the effect on overall net thrust will be zero. This force is determined from the axial component of the integrated pressure readings over the wetted surface.

ii) The centerbody will impose a non-uniform velocity distribution on the propeller inflow due to blockage. Any change in the propeller inflow will alter the loading distribution along the blade, which in turn will change the apparent thrust for a given shaft power. The change in apparent thrust ΔT_{pert} (also see Figure 1) is usually small at low Mach numbers, but can be significant for propellers operating at high forward Mach numbers. This is because the reduction of local Mach number in the blade root region, where the blade airfoil sections are working below their critical Mach numbers, can be used to significantly reduce compressibility losses in that region. To achieve such a benefit, the design of the propeller must account for the non-uniform flow due to presence of the centerbody (i.e. the propeller twist has been optimized for the expected non-uniformity at the propeller plane). The apparent thrust of a propeller in the presence of a centerbody may now be related to free-air thrust as follows:

$$T_s = T_{fa} + \Delta p A_{cb} + \Delta T_{pert} \qquad (3)$$

The terms required to relate apparent thrust to propeller overall net thrust are shown in Figure 3.

$$\text{Propeller overall net thrust} = F_{net} = T_s - (D_{iso} + \Delta p A_{cb} + \Delta D_{ss}) \qquad (4)$$

3.1.1.4 Propeller Net Thrust: Propeller net thrust (T_{net}) is defined as the apparent thrust with the 'buoyancy force' term (ΔpA) removed.

$$T_{net} = T_s - \Delta p A_{cb} \qquad (5a)$$

Propeller net thrust differs from free-air thrust only by the effect of inflow velocity distortion caused by the centerbody. Therefore, any reduction in propeller compressibility losses, due to variations in local Mach number produced by the centerbody, will increase the propeller net thrust relative to free-air thrust.

This relationship is expressed as:

$$T_{net} = T_{fa} + \Delta T_{pert} \qquad (5b)$$

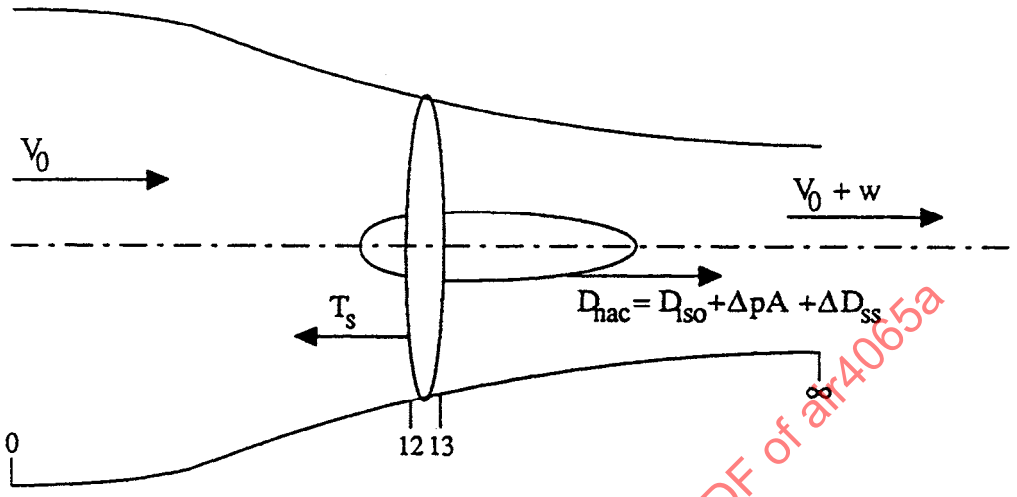

Figure 3 - Apparent Thrust for Propeller plus Centerbody

This equation permits the determination of the flow field distortion effect, ΔT_{pert}, and thus offers an evaluation of how well the propeller has been 'retwisted' for the actual non-uniform flow over the centerbody plus any additional benefit due to reduced compressibility loss. The advanced high-speed propellers known as propfans are designed to operate only in the presence of a centerbody which is specially contoured to take advantage of this effect. Hence, for such props, free-air thrust data would not normally exist.

If compressibility losses are small and the blades are carefully retwisted to account for the distortion of local inflow along the blade, then ΔT_{pert} will be small and propeller net thrust will approximately equal free air thrust. Note that this comparison is to be made at the same rpm, free stream velocity and power, and further assumes that the blade pitch angle has been adjusted to account for the body induced change in mean flow velocity. If the blade angle is fixed, then any change in inflow velocity will result in relatively large changes in both power and thrust.

The relationship between propeller net thrust and propeller overall net thrust is,

$$F_{net} = T_{net} - (D_{iso} + \Delta D_{ss}) \quad (6)$$

3.1.1.5 Propeller Propulsive Thrust: Propeller propulsive thrust (T_p) is traditionally defined as the thrust of the propulsion unit with the propeller blades installed:

$$T_p = T_s - (\Delta p A_{cb} + \Delta D_{ss}) = T_{net} - \Delta D_{ss} \quad (7)$$

3.1.1.6 Thrust Summary for Propeller With Centerbody and Supporting Structure: The foregoing paragraphs have presented a number of different definitions for the thrust of a propeller with centerbody. The relationship of each of these to the Propeller Overall Net Thrust with the addition of supporting-structure drag is summarized as follows:

$$F_{net} = T_s - \left(D_{iso} + \Delta p A_{cb} + \Delta D_{ss}\right) - D_{str} \quad (8)$$

$$= T_{net} - \left(D_{iso} + \Delta D_{ss}\right) - D_{str} \quad (9)$$

$$= T_p - D_{iso} - D_{str} \quad (10)$$

$$= T_{fa} + \Delta T_{pert} - \left(D_{iso} + \Delta D_{ss}\right) - D_{str} \quad (11)$$

Note: - If the AIR1703 definition of Overall Net Thrust were to be strictly adhered to, the TOTAL DRAG of any supporting structure existing within the slipstream boundary would be subtracted as shown above. In the case of highly-integrated propulsion systems, however, a large portion of the airframe may be immersed in the slipstream, making it unreasonable to adhere to the customary definition. In such cases, it is common practice to include only the slipstream-induced or "throttle-dependent" part of the immersed-structure drag in the overall net thrust. Furthermore, other issues arise in separating "thrust" and "drag" when any propulsion system is installed on an airframe. These issues are explored in section 3.1.3.

3.1.2 Practical Application of Thrust Definitions: This section gives an overview of the practical applications of the propeller thrust definitions to a range of configurations. While PROPELLER APPARENT THRUST is used throughout the following illustrations, any of the other thrust quantities summarized in the preceding paragraph may be substituted. In this section, the drag of the

supporting structure is retained as a single throttle-dependent quantity only to maintain consistency with the AIR1703 definition of overall net thrust.

3.1.2.1 Pusher Propeller with Nacelle (No Exhaust Impingement): A pusher arrangement with gas generator efflux aft of the propeller with its station numbering system is shown in Figure 4, below:

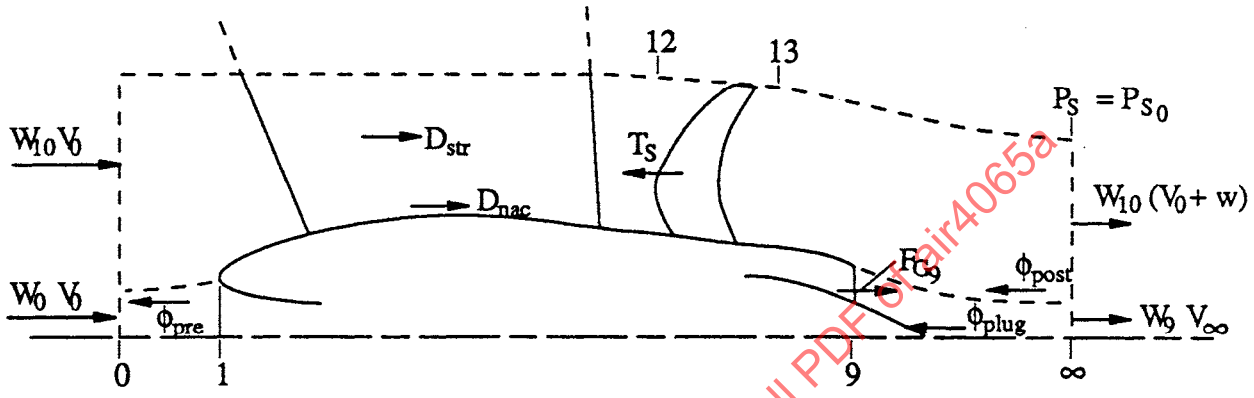

Figure 4 - Pusher Propeller Installation (No Exhaust Impingement)

The combined overall net thrust of the combined propeller and core

$$F'_{net} = W_{10}(V_0 + w) - W_{10} V_0 + W_9 V_\infty - W_0 V_0 \quad (12)$$

$$F'_{net} = W_{10} w + F_{G9} + \phi_{post} + \phi_{plug} - W_0 V_0 \quad (13)$$

or alternatively:

$$F'_{net} = T_S - D_{nac} - D_{str} + F^*N_{core} - \phi_{pre} \quad (14)$$

where the prime (') designates inclusion of core forces as defined in AIR 1703 Section 2.1.

3.1.2.2 Tractor Propeller with Body & Structure: A tractor arrangement with its station numbering system is shown in Figure 5 below.

The overall net thrust of the combined propeller and core is:

$$F'_{net} = W_{10}(V_0 + w) - W_{10} V_0 + W_9 V_\infty - W_0 V_0 \quad (15)$$

$$F'_{net} = W_{10} w + F_{G9} + \phi_{post} + \phi_{plug} - W_0 V_0 \quad (16)$$

or alternatively $$F'_{net} = T_S - D_{nac} - D_{str} + F^*N_{core} - \phi_{pre} \quad (17)$$

For this arrangement the core engine performance is influenced by the presence of

the tractor propeller and vice versa. The engine deck from which $F^*_{N_{core}}$ is

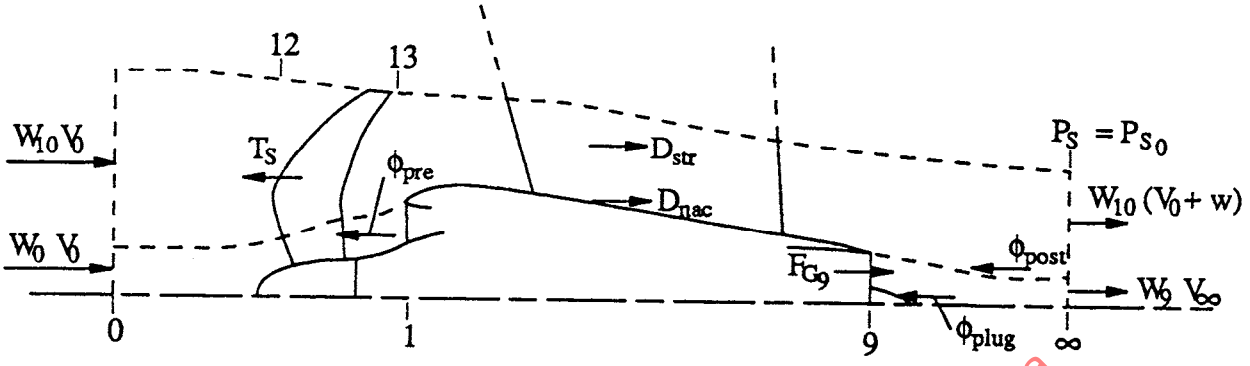

Figure 5 - Tractor Propeller with Body and Structure

derived should be modified to account for an additional stage of compression from the portion of propeller within the inlet streamtube; and the propeller apparent thrust will be altered by the presence of the engine inlet. These effects will be nonuniform and unsteady if the inlet is not axisymmetric and may require time and area averaging.

3.1.2.3 Pusher Propeller with Body (Hot Gas Impingement): A second pusher arrangement with gas generator efflux passing through the propeller plane is shown in Figure 6, below.The combined overall net thrust of the propeller and core is:

$$F'_{net} = W_{10}(V_0 + w) - W_{10}V_0 + W_9 V_\infty - W_0 V_0 \quad (18)$$

$$F'_{net} = W_{10}w + F_{G9} + \phi_{post} + \phi_{plug} - W_0 V_0 \quad (19)$$

or alternatively

$$F'_{net} = T_S - D_{nac} - D_{str} + F^*_{N_{core}} - \phi_{pre} \quad (20)$$

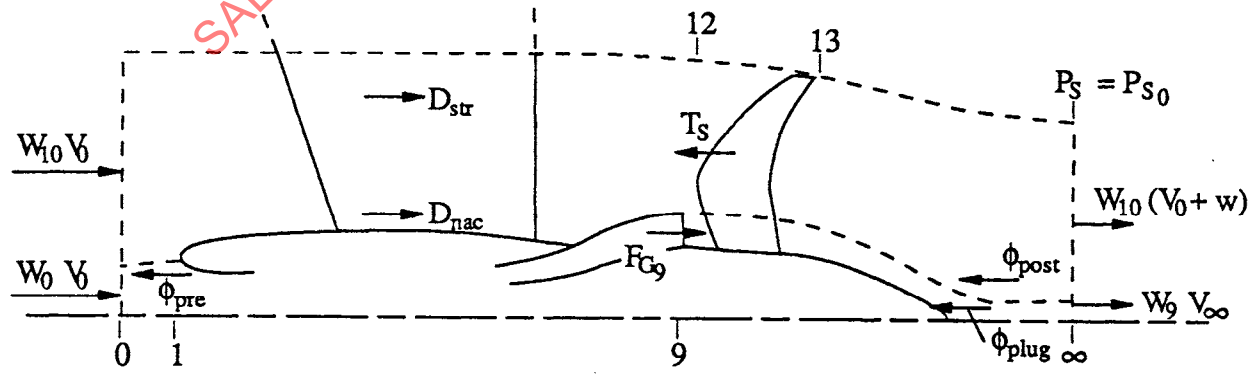

Figure 6 - Pusher Propeller Installation (Hot Gas Impingement)

While the terms in the definition of overall net thrust are identical to the previous case, the interactions between the core and propeller are quite different. Here, the pusher propeller alters the core engine performance through its effect on exhaust nozzle pressure ratio; and the exhaust flow obviously affects the propeller blade forces generated within the exhaust streamtube. Again, these effects will be non-uniform if the exhaust nozzle is not axisymmetric. The above definitions presume T_S includes the effects of flowing inlets and nozzles. If the propeller map does not include the efflux effects on the propeller, it must be accounted for separately. (See Section 4.2.1; Figure 33, ΔT_S due to jet)

3.1.3 Propeller and Nacelle Installed on Aircraft: The definition of "thrust" and "drag" is not straight forward when considering all forces on a total aircraft system. In the previous sections, all the forces associated with the isolated propulsion system were contained within the propeller slipstream, hence the propeller stream tube was a convenient control volume boundary for use in defining Overall Net Thrust. (Note: In this section 'isolated' designates isolated from the aircraft not isolated from the engine as it was previously used). On the aircraft, however, only a portion of the forces of interest are washed by the propeller airflow. While it is tempting to treat forces within the propeller wash as "thrust" and those outside as "drag", this would produce a complicated interface because of the movement of the propeller streamtube boundary with changing flight conditions. For example, Figure 7 shows two propulsion system installations, a wing mount and an aft fuselage mount propeller. As flight speed or propeller flow capacity changes, so does the propeller streamtube. At low speeds, significant portions of the airplane fuselage and/or the wing are contained within the propeller flow field. As speed increases, the propeller capture stream tube decreases in diameter, and the propulsion thrust/airplane drag interface moves. If the streamtube was used as the criterion to differentiate between thrust and drag, it is difficult to imagine a test set-up which would measure "propulsion thrust" and "aircraft drag". Furthermore, the propeller induction and discharge can dramatically impact airplane forces. For example, the recovery of non-axial propeller discharge momentum could produce thrust by increasing pressure on parts of the aircraft surface. The concept of "Negative drag" is not universally accepted, therefore, when trying to define the forces that constitute "thrust" vs. those that should be categorized as "drag", it is obvious that the propeller streamtube is not an appropriate interface.

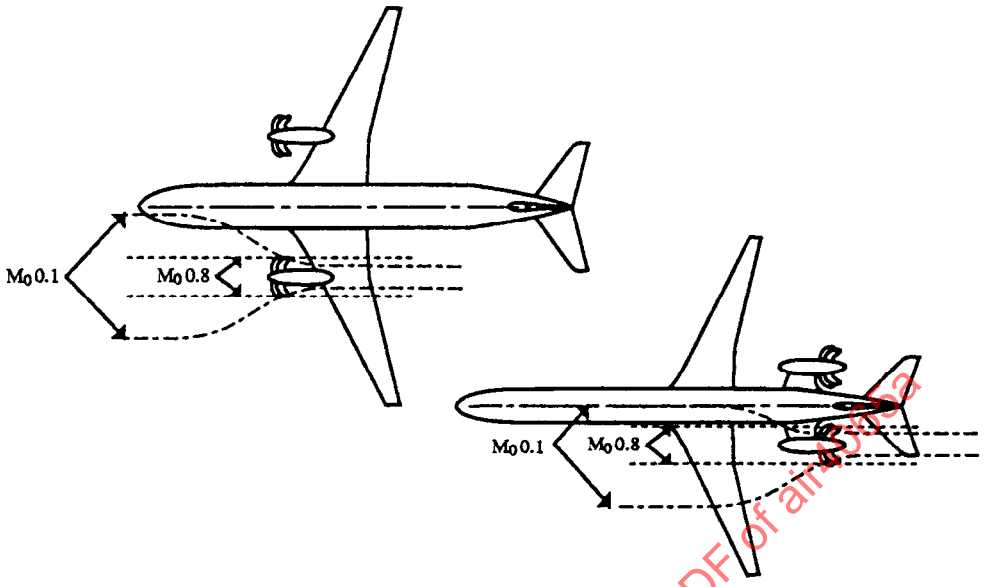

Figure 7 - Propeller Capture Stream Tube Coverage

The installed thrust/drag accounting quantities should be formulated to be compatible with the experimental set-up. For example, wind tunnel models often have multiple force balances to measure the numerous aerodynamic interactions. The total aircraft (including propulsion) system may be on a force balance; while the propeller forces may be measured simultaneously on rotating balances (Figure 8A). The installed apparent thrust, $T_{s,iso}$ can be derived from the difference of the shaft balance measurements with and without blades (with corrections for spinner gap forces). This derivation of apparent thrust includes the force on the blades as well as the changes in the spinner force due to the presence of the blades. These rotating balances also yield isolated apparent propeller thrust, Ts, when the propulsion system is tested separately. Comparing these rotating balance measurements, $T_{s,iso}$ and T_s, allows evaluation of the airplane flow field influence on the propeller performance. In a similar fashion, the difference between the airplane system balance and the installed rotating balance allows evaluation of the propulsion system interaction effects on airframe drag. This is done by comparing the difference between these two force readings to the airplane force data acquired without the propulsion system installed.

Another method of attaining installed interactions with multiple balances is to test with an airplane system balance and with the propulsion system on a pylon balance (Figure 8B). This shifts the airplane/propulsion interface from the root of the propellers to the pylon. This interface also allows segregation of the interactions using methods analogous to those described in the previous paragraph.

The terms and accounting equations are obviously closely tied to the particular experimental methods or agreed upon interfaces being used to initiate the in-flight thrust calculations. Specific examples of candidate test setups and the resulting in-flight thrust projection methodology are addressed in detail in Section 3.2.

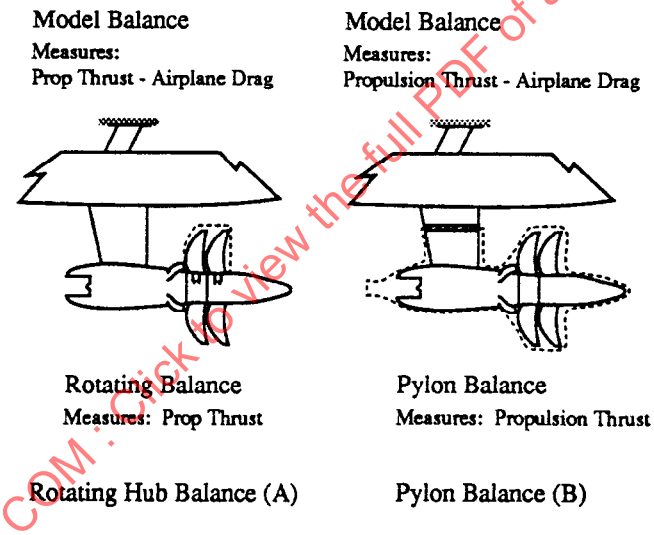

Figure 8 - Examples of Test Set-up Affecting Thrust/drag Definition

3.2 Installed Thrust/Drag Accounting:

This section addresses the accounting methods used for: (l) Podded Configurations and (2) Integrated Configurations where the nacelle cannot be separated aerodynamically from the airplane. For podded configurations the thrust/drag accounting begins with isolated nacelle/propeller wind tunnel tests for propulsion system net thrust, and the airplane bookkeeping uses clean airplane aero force and moment models as a basis for subsequent drag accounting. For integrated configurations the nacelles and wing may be highly contoured to be compatible with the propeller discharge. Therefore isolated propulsion tests are

not meaningful except for comparison; nor are airplane drag tests without propulsion simulation. Consequently, the two types of installations require different accounting methods.

Despite the differences noted, both must account for thrust and drag changes due to throttle excursions. Both start with the selection of a reference condition which establishes a datum for both the overall net thrust and the airframe system drag. Then all changes in either thrust or drag due to throttle changes from that reference condition are normally accounted for as changes in the INSTALLED PROPULSIVE FORCE, F_{IPF}.

The installed propulsive force is defined to be equal to the installed combined overall net thrust at the full scale reference conditions and accounts for all propulsive forces (including throttle dependent forces) acting on the aircraft.

$$F_{IPF} = F'_{net} - \Delta F_{inl} - \Delta D_{exh} - \Delta F_{trim} \quad (21)$$

This method of accounting, then, defines the "drag" side of the equation to be throttle-independent. As before, the amount by which thrust exceeds drag is the EXCESS THRUST, F_{ex}, (available for acceleration and climb),

$$F_{ex} = F_{IPF} - D_{AFS} \quad (22)$$

The inlet and exhaust system throttle dependent force increments for the core engine when operated outside the environment of the propeller are described in AIR 1703 (see 3.2.1 and 3.2.2). When strong interaction exists due to the presence of the propeller, appropriate models will be needed to measure these increments in wind tunnel tests and this topic is covered in Section 4 of this report. These interactions may be numerous and vary from one installation to another. A previously cited example of this (Section 3.1.2.2) is the tractor propeller supercharging effect which should be accounted for in the engine cycle. Furthermore, when the power plant is installed on the airplane, aerodynamic interactions between the propulsion system and airframe often give rise to additional interaction forces. Some of these interactions will be discussed in the following examples of thrust/drag accounting for both integrated and podded

power plants. It is likely, however, that other cases will give rise to interactions not covered here.

3.2.1 Podded Configuration:

3.2.1.1 Typical Accounting System: An isolated nacelle/propeller model establishes the baseline for net thrust determination, while the clean airplane, (no propulsion system simulation) aerodynamic force and moment model, is the baseline for drag as indicated in Figure 9.

The isolated podded performance tests give T_{net}. These must be adjusted for any imperfections in the simulation and for scale effects (described in detail in sections 3.2.3, 4.1 and 4.2). This adjusted model data and associated cycle performance can be combined to project full scale isolated pod net thrust. A specific example of executing this process is presented in Appendix B where the PW-Allison 578DX propfan in-flight thrust determination is given as a numeric example.

The airplane model accounting build up starts with the "force and moment model". This is augmented with airplane model tests using a propulsion simulator. The propulsion simulator can also be tested in an isolated environment (removed from the airplane model). The "force and moment model" drag and the isolated propulsion model thrust can be compared to the force measurement of the installed airplane/propulsion simulator model. The difference between these is interference drag (ΔF_{IPF}). In evaluating an airplane system performance in level flight, the adjusted "force and moment model" drag plus interference drag will equal the isolated pod net thrust.

It is noted that the propulsion tests are usually performed with model propellers large enough for adequate simulation of the full-scale product. The installed airframe/propulsion system model, on the other hand, usually must be built to a smaller scale because of wind tunnel blockage considerations and may not provide adequate simulation of the full-scale propeller. Any thrust difference due to model defects will, in general, not be separable from the airframe interference effects on thrust without some additional tests for scale effects on isolated-propeller thrust. The usual force accounting for such cases will have thrust errors due to scale lumped into airframe interference forces.

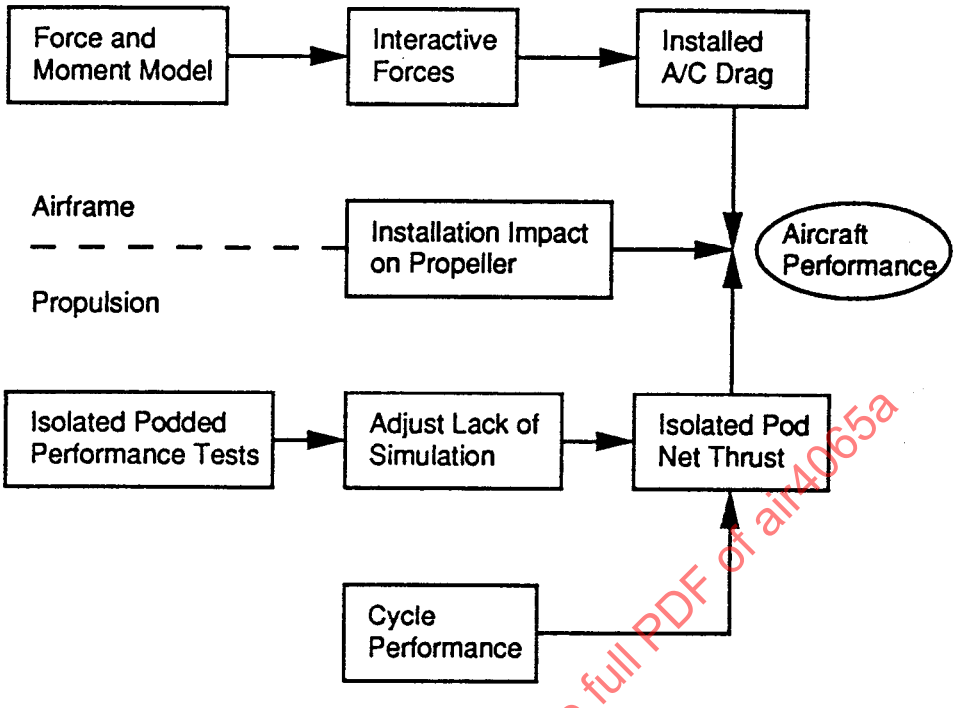

Figure 9 - Podded Installation Accounting System

3.2.1.2 Throttle Dependent Variables: The airframe side of the accounting system in Figure 9 started with adjusted aerodynamic forces and model characteristics which are throttle independent. The interactive force adjustments must include throttle dependent variations to the airplane drag as well as the interference drags that arise from merely putting the reference propulsion system in proximity to the airplane.

These throttle dependent drag increments may include but are not limited to:

- changes in scrubbing drag
- swirl recovery
- slipstream impact on either wing or fuselage pressure drag
- changes in airplane trim drag

The propulsion side of the accounting system, through the combination of cycle analysis and isolated podded performance tests, also accounts for throttle

dependent changes to the reference propulsion system net thrust. These force increments may include but are not limited to:

- changes in inlet spillage drag
- changes in nozzle jet thrust
- changes in core ram drag
- changes in isolated nacelle drag due to spillage, aft-end pressurization and/or flow separation

3.2.2 Integrated Configuration: For integrated systems, the throttle-dependent forces induced by the slipstream are potentially very significant if not treated carefully in the design process. For example, a high-speed, nacelle-wing combination should be designed in the presence of the slipstream in order to avoid excessive interference drag. Such design considerations as wing twist, thickness and camber distributions play a dominant role in the design of the nacelle/wing, especially for the special case of single-rotation props. For this special case, the recovery of the slipstream angular momentum can improve overall system efficiency.

3.2.2.1 Typical Accounting Systems: The general approach to thrust/drag accounting for integrated-nacelle propeller systems is illustrated in Figure 10. Test models needed to set up the accounting are shown in Figure 11. The test models and the indicated analyses provide a reference airframe system drag and the throttle-dependent forces used to determine installed propulsive force for desired operating conditions. For integrated-nacelle installations the nacelle/engine system can not be realistically tested separately from the rest of the airplane. For example the nacelle and wing have been aerodynamically designed to function synergistically, hence, their separation would greatly alter the aerodynamics of each. In such cases, the nacelle and its associated drag are normally included with the throttle-independent airframe drag of the Aero Reference Model, D_{AFS}. The polar representing the reference drag is derived from data from the first three models shown in Figure 11, that is, the basic propeller-off aero model data with adjustments for model scale, inlet and oil cooler drags, sting interference and other differences from flight hardware. The propeller-on version of the basic aero model is used to measure installed-propeller performance and slipstream-induced effects on the airframe. Significant amounts of leading-edge thrust, scrubbing

drag, lift and pitching moment will, in general, be induced on the airframe resulting in new elements of force to be accounted for as throttle dependent forces. The leading edge thrust, scrubbing drag and induced lift will normally be combined into one force component, ΔD_{ss}. This component is evaluated by differencing the untrimmed propeller-off and propeller-on polars. Both ΔD_{ss} and ΔF_{trim} will vary with throttle and airplane lift coefficient. Clearly, the concept of "overall net thrust" is not useful here due to the inseparability of the nacelle and wing. The propeller "thrust" which appears most useful for integrated-nacelle arrangements is the INSTALLED NET THRUST.

$$T_{net,inst} = T_{s,iso} - \Delta p A_{cb} \qquad (23)$$

As noted in the previous section, the installed apparent thrust will be different from the isolated propeller case. And, although one can attempt to predict installed propeller characteristics using the traditional retardation factor, (1-h), (see paragraph 3.4.1.3.1), the achievement of the most accurate in-flight thrust

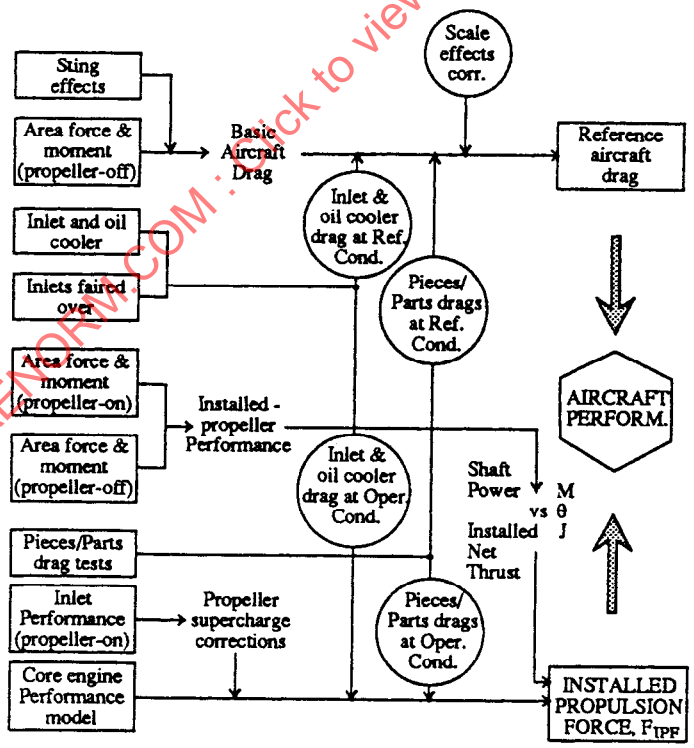

Figure 10 - Thrust/Drag Accounting System Example for Integrated Nacelle Propeller

suggests using the full set of model tests. The installed net thrust is used to adjust the propeller-on polar to its thrust-removed position as indicated in Figure 12. In the absence of installed thrust measurements, an alternate approach uses the isolated propeller characteristics from an isolated test to translate the polar. This approach, illustrated in Figure 13, results in combining the slipstream interference drag with the airframe retardation effect on the propeller thrust characteristics ΔT_{pert}. It also incorporates errors due to blade-pitch-measurement bias between the isolated and installed propeller tests. This potential error is referred to as $\Delta T_{\theta er}$ on the figure. Caution is therefore advised in the use of this method. The installed propulsive force may at full scale reference conditions be summarized as follows:

$$F_{IPF} = T_{net,inst} - \Delta D_{ss} + F^*_{N_{core}} = F_{IPF} \text{ (at full scale reference condition)} \quad (24)$$

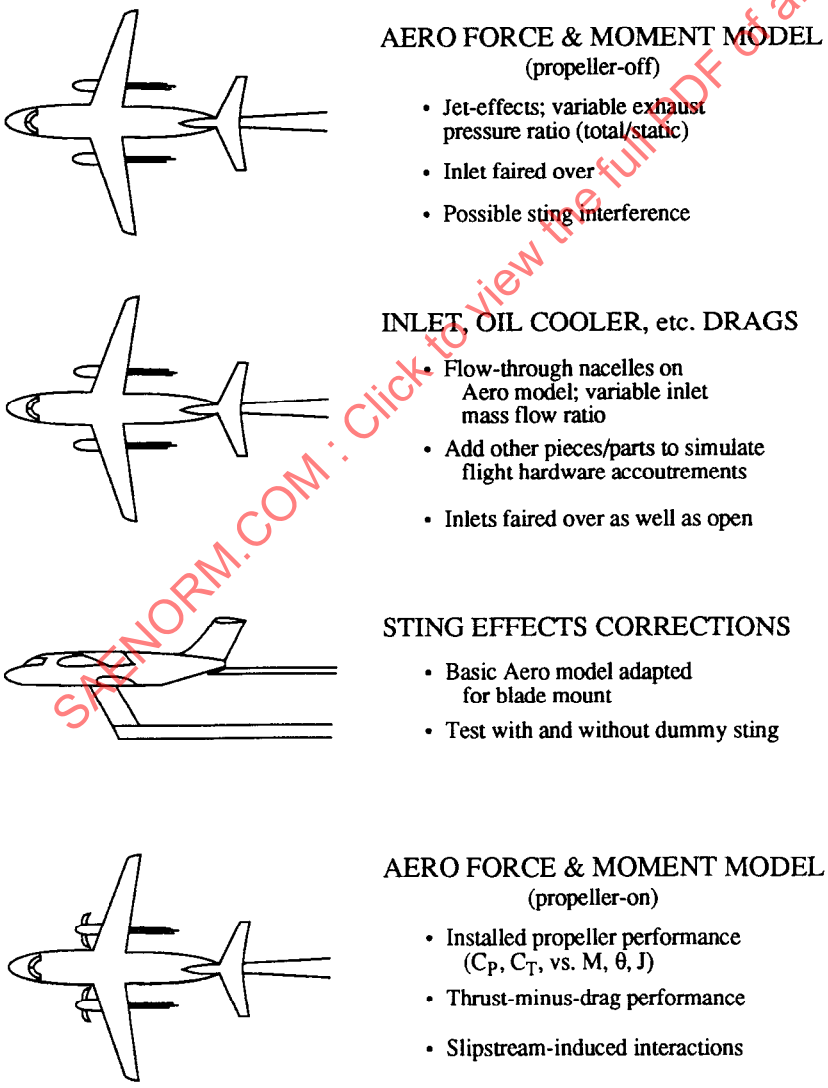

Figure 11 - Test Models for Example Integrated-Nacelle Propfan System

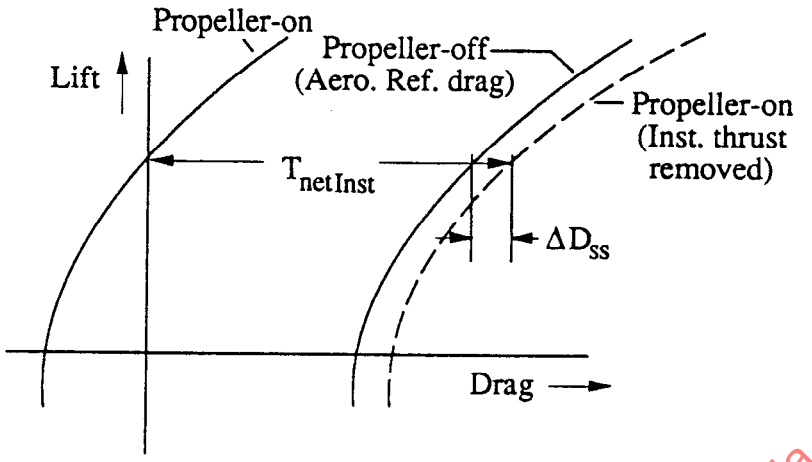

Figure 12 - Drag Polar Differencing for Integrated-Nacelle Propellers; Installed Net Thrust Method

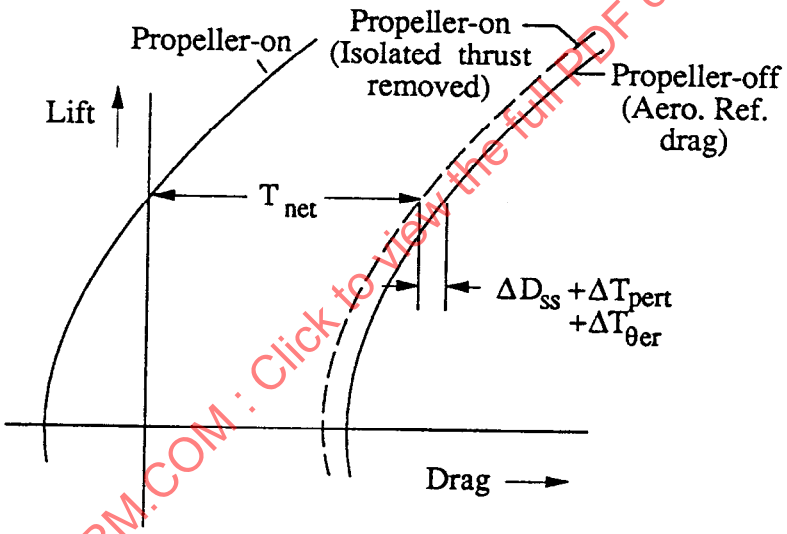

Figure 13 - Drag Polar Differencing for Integrated-Nacelle Propellers; Isolated Net Propeller Thrust (Alternate Method)

or $F'_{net} = T_{net} - \Delta D_{ss} + \Delta T_{pert} \pm \Delta T_{\theta er} + F *_{N_{core}}$ = (Alternate Method) (25)

It is noted that, in the above expression, the throttle-dependent force increments from miscellaneous accoutrements (pieces/parts) are implicit in ΔD_{ss} as are the thrust and induced drag changes due to swirl recovery. For conditions other than the full scale reference condition, throttle increments to F_{IPF} are summarized in section 3.2.3. Among these, the term ΔF_{trim} is the change in trim drag caused by operation of the propulsion system. Propulsion system thrust can alter airplane

aerodynamics in two ways; first by direct thrust action along an axis offset from the c.g. and second, by aerodynamic interaction of the slipstream and exhaust flows with the airframe surface pressures.

3.2.3 Throttle Dependence Considerations: The foregoing discussion of throttle dependent forces is summarized as follows:

	ITEM	SOURCE
ΔD_{ss}	Scrub drag	increase in drag due to slipstream velocity
"	Pieces/parts drag	increase in drag of accoutrements
"	Swirl recovery thrust	streamwise force induced by slipstream
"	Swirl recovery	effective reduction in airplane induced drag due to slipstream-induced lift
ΔF_{trim}	change in trim drag	(see page 2-8, AIR 1703)
ΔF_{inl}	change in inlet force	(see page 2-8, AIR 1703)
ΔF_{exh}	change in exhaust system force	(see page 2-8, AIR 1703)

3.2.4 Thrust/Drag Components: The net thrust of the propulsion system can be shown to be made up of the same basic form for any type of system; however, some terms are system dependent and may be zero or neglected.

These terms can be generally separated into three distinct areas: 1) pre-prop, 2) prop, and 3) post -prop.

Figure 14 presents a chart which provides a summary of major factors which affect the thrust resulting from most propeller installations. It can be used as a check list of parameters to be examined in installation design to avoid overlooking an affect which impacts performance. Many of the factors may be small, but with so many effects to consider, an orderly system helps avoid miss-accounting or double-accounting problems. Pusher installations will have similar factors however the lack of inlet pressure disturbance/increase and the possible impingement effects of exhaust passing through the propeller must be recognized as noted previously.

Propeller installations fall into the pusher or puller (tractor) categories. The choice between pusher or tractor often is made for reasons other than propulsion system effectiveness.

Tractor propeller installations are presently the most numerous type. The tractor installation is affected by the post-propeller surfaces and engine exposed to the propeller wash and the resulting positive and/or negative effects on propeller and engine thrust.

For pusher installations, where the engine exhaust passes through the propeller, the interaction can be significant and should be carefully considered in the system design.

3.2.4.1 Inflow: The manner in which the air enters the propeller disk affects the way the propeller can convert the applied power into thrust because of the local angle of attack of the blade. This local flow into the propeller disk is called "inflow". In practical application this inflow velocity is impacted by the effects of the airframe presence, airframe attitude, wing upwash, or bodies placed behind the propeller itself. Any condition which affects the flow into the propeller must be evaluated to properly account for the inflow effect on the propulsion system thrust. This may be accomplished with the "Retardation Factor" (See Section 3.4.1.3.1).

3.2.4.2 Blockage: Bodies placed directly behind the propeller disk create an adverse pressure gradient against which flow must adjust. In the case of solid bodies, e.g., nacelles, the flow from the propeller at the stations directly in front of the nacelle is forced outward to go around the nacelle.

3.2.4.3 Spinner: The spinner is designed to provide a smooth flow transition into the propeller plane in the case of the tractor or to reduce base drag when returning flow to free stream for the pusher designs. Proper design of the spinner-shank intersection has a large impact on these interference effects, e.g., shank penetration hole covers to prevent leakage into the spinner cavity. This effect is very critical to evaluate the final performance of the propeller and with very little technical information available as a guide to its impact, it will be necessary to measure its impact for each design.

3.2.4.4 Propeller: Propeller performance maps/data packs are generally provided for specific blade geometries and number of blades. Propeller maps may be developed using analytical or testing methods and may be based on free air, apparent, net or propulsive definitions. Care must be exercised to account for differences between the methods of map development and actual nacelle definitions. Hardware inaccuracies and/or aeroelastic effects must also be taken into account. Attempts at improving some of the inherent negative characteristics of propellers are special shaping of the tips to reduce noise levels and counter-rotating propellers to recover the swirl.

3.2.4.5 Inlet-Engine: Depending on the system configuration, the propeller's impact on the inlet may be a factor. For a tractor design, a careful propeller design may favorably impact the engine performance by supercharging the inlet. This can be accomplished by proper placement and design of the propeller radial stations which pass the inlet area. The inlet design must be carefully considered to reduce the impact of the propeller swirl on the inlet flow separation and distortion, thereby affecting the available power output of the engine. Measurements of these effects can generally be accomplished by inlet pressure and temperature rakes. One method of reducing the impact of this low energy flow is to provide a flow diverter channel near the shank area which will have an attendant drag. In order to maximize the thrust capability of the propulsion system, consideration of these effects must be designed into the final system.

Airflow demands made by the engine may not be matched by the inlet. When the demand by the engine is less than that supplied by the inlet, the flow is forced to be diverted around the inlet causing spillage drag. This is a function of the particular inlet-engine design match and is power dependent.

3.2.4.6 Scrub & Interference: The propeller provides thrust by increasing the flow velocity through the propeller. This increase in velocity increases the local dynamic pressure on the surfaces in its wake and increases the drag. It also has the effect of changing the pressure at the intersections of surfaces in its wake, increasing the interference drag. These impacts are technically a function of thrust; therefore, making these effects power dependent.

Tractor Propeller Propulsive Thrust: System Drag and Interacting Effects for Simple or Regenerative Cycles
Summary by Engine/Nacelle Stations

Upstream (0)

1) Velocity Distortion into Prop due to Nacelle and Wing
   a) Retard Factor (1-h)
      • SBAC Method
      • Ham Standard
      • Borst
   b) η_p Increase
      • Borst

Prop/Hub

1) Prop Thrust
   a) η_p Method
   b) C_T Method
   c) θ Method

2) Efficiency Parameters
   • Cp, J, Compressibility
   • Spinner Interference Drag

3) Blockage Factor
   $\int_0^{A\,max} (p_0-p)dA$
   • SBAC Method
   • Ham Standard

4) Spinner Drag

5) Special Blade Effects
   • Proplets
   • Bi-blades
   • Counter Rotating
   • Fixed Pitch
   • Stator Blades
   • Blade Pitch Inaccuracy

6) Trim Drags; Relative Prop Rotation
   • Corotation vs C.R.
   • Prop Normal Forces

Inlet (1)

1) Ram Drag, w/Eng and Cooling Flow

2) Ram Recovery
   • V_0 Recovery
   • Prop Rise

3) Inlet Drags
   • Diverter Channel
   • Spillage

4) Prop Induced Temperature Rise

5) Loss Mechanisms
   • Prop Swirl
   • Spinner Boundary Layer Ingestion
   • Losses between HiLite and Comp Face

6) Heat Transfer from Gearbox and to Inlet walls

Engine (2 to 8)

1) Power to Prop
   a) See Inlet Effects
   b) Back Pressure (P_2/P_0)
   c) Power Extractions
   d) Bleed/Anti-Ice

2) Oil Cooler Drag

3) Exhaust Stub Drag

4) Inlet Distortion Degrading Compressor Performance

Exhaust (9)

1) Boattail Drag
   a) $(P_0-P_8)A$
   b) $(P_0-P)A$

2) Tailpipe Thrust
   • Angle to Flight

3) Effect on Lift by Exhaust Flow on Wing

Nacelle/Wing

1) Prop Swirl Recovery by Straightening

2) Pylon Drag (if used)

3) Nacelle/Wing/Fuselage Interference Drag

4) Increased Drag Due to Slipstream Velocity

5) Thrust Angle Relative to Flight Path

6) Nacelle Cooling Drag

FIGURE 14 - Turboprop In-Flight Thrust Accounting System Considerations

3.2.4.7 Propeller & Exhaust Interaction: For some pusher configurations the engine exhaust passes through the propeller. The exhaust propeller interaction effects must be properly accounted for (see appendix B for an example). For most tractor installations the exhaust nozzle is immersed in the propeller slipstream, causing the local static pressure to be modified. These effects must be accounted for in the determination of nacelle drag and jet thrust.

3.2.4.8 Alpha & Aircraft Trim: The local flow angles behind the propeller are modified by the propeller slipstream. These influences change in the effective angle-of-attack of lifting surfaces in the slipstream. The direction of rotation of the propeller swirl may influence the inboard/outboard differences. These local angle-of-attack differences affect the local sectional drag characteristics which may increase or decrease the drag level depending upon how the affected areas are treated in the wing design. These local differences also may affect the longitudinal stability of the aircraft requiring resetting the trim which affects drag. Direction of rotation significantly effects the lateral stability during the engine-out case resulting in larger changes in drag.

3.2.4.9 Cooling: The components inside of the nacelle have design requirements which limit the temperature to which they can be subjected to maintain their design life and performance characteristics. This requires a cooling air flow which is proportional to the amount of heat rejection of the particular engine into the nacelle compartment. In addition, the engine itself needs to maintain a limiting internal temperature which is generally accomplished with an oil cooler system. With this system, air passes through the oil cooler picking up heat and is then exhausted overboard. There are ram drags associated with both of these cooling requirements which are a function of the air flow designs; however by keeping internal losses under control and with proper design of the oil cooler exhaust, a positive net thrust may be obtained.

3.3 Normalized Parameter Groupings & Definitions:

3.3.1 Propeller Related Items: Propellers operate in a freer environment than turbofans, therefore the nomenclature and geometric characteristics are more numerous and unique. For this reason and to promote broader knowledge of propellers in

general, both performance parameters and geometric characteristics are included in this section.

3.3.1.1 Propeller/Propfan Geometric Characteristics: Before describing performance parameters, it is appropriate to first discuss the blade terminology. Knowing the airfoil families used, a propeller or propfan blade can be completely defined with the data in Figures 15 and 16. Figure 15 describes the blade spanwise distributions of thickness ratio (h/b), width ratio b/D, blade angle, θ, and airfoil section design lift coefficient (C_{LD}). In essence, this Figure defines the characteristics of the individual airfoil sections that comprise the blade geometry orientation. Each section is defined by its thickness ratio, h/b, width, b, and the design lift coefficient, C_{LD}, or camber. With the section geometric characteristics defined, either experimental or analytical two-dimensional airfoil data can then be used to predict the lift and drag characteristics of that section as used in the blade.

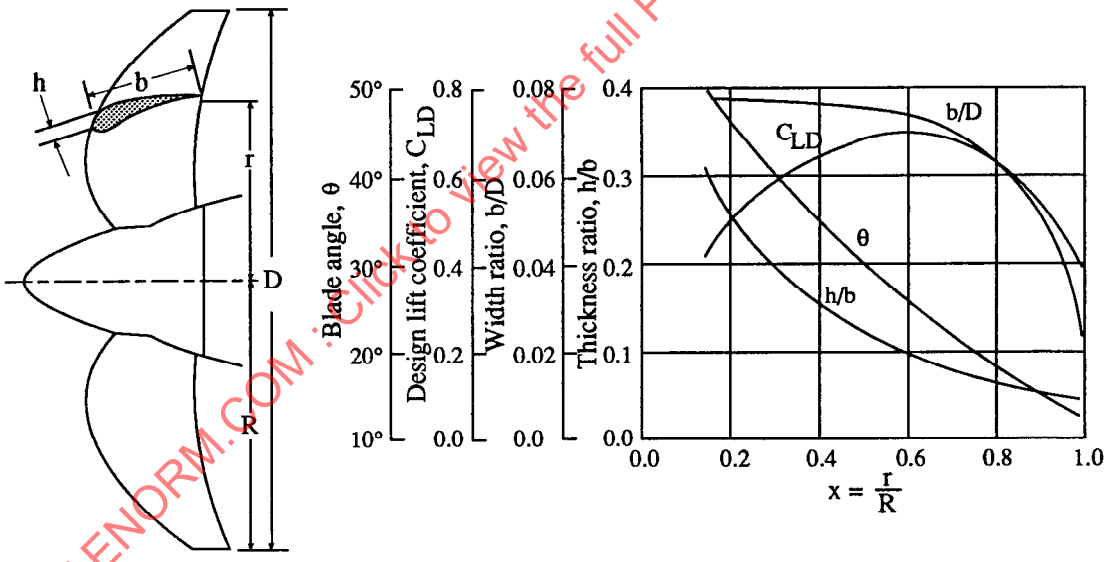

Figure 15 - Typical Blade Characteristic Data Sheet

A feature of some propfan designs is the swept blade planform. Figure 16 shows the graphical means used to describe the geometric blade sweep where:

λ = blade section sweep angle

ψ = blade section cone angle

The blade sweep angle is usually defined as the sweep of the blade mid-chord line. Because of the desire to describe the airfoil section along flow streamlines, the airfoils are laid out on cones of revolution at each radius. These are defined on Figure 16 by the sketch on the left side of the figure.

Two other terms are frequently used in describing the blading of a propeller or propfan which are functions of the blade width and design lift coefficient distributions. These terms are activity factor (AF) and integrated design lift coefficient (C_{Li}).

The activity factor is a non-dimensional function of the blade planform that quantifies the integrated capacity of the blade elements to absorb power.

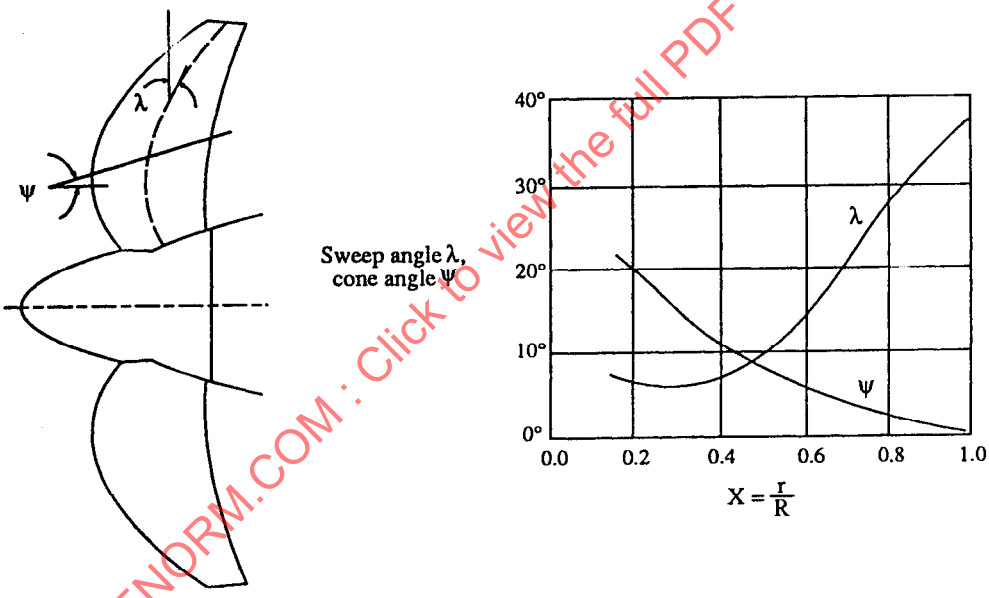

Figure 16 - Definition of Sweep and Cone Angles

It is based on the fact that the ability of a propeller blade to absorb power is a function of the blade area multiplied by the third power of the speed of the air passing over it. The relationships are shown in Figure 17 may be written as:

$$\text{Section Power} \approx (bdr)V^3_{\text{section}}\ \text{Density}(\rho) \tag{26}$$

where blade section area = b dr. Integrating,

$$\text{Blade Power} \approx \rho \int_{sco}^{R} bV^3\, dr \tag{27}$$

However, the section velocity is proportional to the radius:

$$V^3 \approx r^3 \tag{28}$$

Substituting and non-dimensionalizing:

$$P \approx \rho \int_{sco}^{1} b V^3 \, dr. \qquad \text{where } V = \omega r \tag{29}$$

but

$$\approx \rho \int_{sco}^{1} R \; b \; (\omega r)^3 \, d\frac{r}{R} \tag{30}$$

so

$$P \approx \rho \int_{sco}^{1} \left(\frac{D}{2}\right) \left(\frac{b}{D}\right) \left(\frac{D}{2}\right)^3 \left(\frac{r}{R}\right)^3 d\left(\frac{r}{R}\right) \tag{31}$$

and simplifying results in

$$P \approx D^4 \frac{\rho}{16} \int_{sco}^{1} \left(\frac{b}{D}\right) \left(\frac{r}{R}\right)^3 d\left(\frac{r}{R}\right) \tag{32}$$

However, it was found that this factor was very small and cumbersome to use. Therefore, it was decided that an arbitrary multiplier of 100,000 be used and ρ be omitted in defining the activity factor. Thus the activity factor becomes:

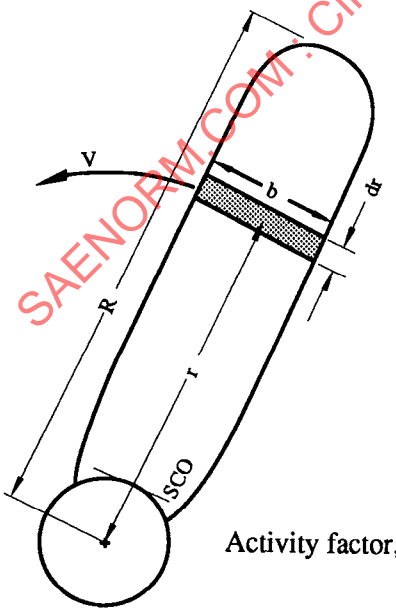

$$\text{Activity factor, } AF = \frac{100{,}000}{16} \int_{SCO}^{1.0} \left(\frac{r}{R}\right)^3 \left(\frac{b}{D}\right) d\left(\frac{r}{R}\right) \tag{33}$$

Figure 17 - Activity Factor

From the above definition, it can be seen that an increase in blade width near the tip is more effective for power absorption than an increase in width near the shank. Total activity factor (TAF) is the product of activity factor (AF) and number of blades (B).

$$TAF = B \times AF \tag{34}$$

Blade activity factor is also a measure of the solidity. The solidity of a propeller is the ratio of blade area to the swept or disk area. In a constant chord blade, the solidity, σ, and activity factor are related by:

$$\sigma \cong 128 \frac{TAF}{100000\ \pi} \left\{\frac{1}{1 + SCO}\right\} \quad \text{(for constant chord blade)} \tag{35}$$

Similarly, the integrated design lift coefficient (C_{Li}) of a blade is mathematically defined as:

$$C_{Li} = 4 \int_{sco}^{1} C_{LD} \left(\frac{r}{R}\right)^3 d\left(\frac{r}{R}\right) \tag{36}$$

The integrated design lift coefficient represents the average section design lift coefficient weighted by the radius cubed and is related to the thrust producing capabilities of a blade, i.e., for a given width blade and ignoring compressibility effects the higher C_{Li} blade will produce a higher static thrust. On the other hand, because of the high cambers used in the blades, high C_{Li} blades tend to be poor performers at high propeller cruise Mach numbers because of low section critical Mach numbers. Thus, propfans which are designed for high flight Mach numbers usually have low C_{Li} with high section critical Mach numbers.

It should be pointed out that AF and C_{Li} are independent of each other. Thus, the C_{Li} level may be associated with a low or high AF blade. The propeller or propfan designer attempts to optimize takeoff, climb, and cruise performance by conducting parametric studies of AF and C_{Li} and selecting the best combination of these two parameters.

To completely describe a propeller or propfan, in addition to the aforementioned blade geometry, it is necessary to define the following four parameters:

1. Number of blades
2. Propeller Diameter
3. Spinner Diameter
4. Stacking Line (blade tilt)

3.3.1.2 Propeller/Propfan Performance Parameters: Before discussing propeller performance data, it is important to first review the terms used in presenting propeller performance. These terms have been in use by propeller designers for many years and their derivations are discussed below.

Generally, the thrust and torque developed by a propeller depend on the flight velocity, rotational speed, diameter, density, temperature or pressure and viscosity. Assuming viscosity and compressibility effects are considered of second-order importance the last three variables may be dropped. Thus,

$$\text{Thrust or Torque} \cong f(\rho, V, n, D) \tag{37}$$

Dimensional analysis can then be used to determine the relationship of the variables. Using the principle that both sides of a real equation must be dimensionally the same the following general dimensional relations result:

$$\text{Thrust or Torque} = K(\rho^a V^b n^c D^d) \tag{38}$$

where K, a, b, c, and d are unknown constants. Using the Mass, Length and Time system, let the variables have the dimensions listed in Table 1.

Table 1 - Mass Length and Time System

Thus, the thrust equation becomes:

$$T = M\,L\,T^{-2} = K\left(\frac{M}{L^3}\right)^a \left(\frac{L}{T}\right)^b \left(\frac{1}{T}\right)^c (L)^d \tag{39}$$

To achieve dimensional equality, the exponents of a given quantity on one side of the equation must equal the sum of the exponents of the given quantity on the other side. Applying this rule for M, L and T respectively, then

$$1 = a$$
$$1 = -3a + b + d$$
$$-2 = -b - c$$

from which

$$d = 4 - b$$
$$c = 2 - b$$

Substituting these values into the thrust equation results in:

$$T = K\rho^{(1)} V^{(b)} n^{(2-b)} D^{(4-b)} = K\rho\, n^2 D^4 \left(\frac{V}{nD}\right)^b \tag{40}$$

However, (V/nD) is dimensionless and may be combined with K to provide the definition of the thrust coefficient.

$$C_T = K\left(\frac{V}{nD}\right)^b \tag{41}$$

This means C_T is a function of (V/nD). Finally then:

$$T = C_T\,\rho\, n^2 D^4 \tag{42}$$

or

$$C_T = \frac{T}{\rho\, n^2 D^4} \tag{43}$$

Similarly, the dimensional equation for propeller torque is:

$$Q = M L^2 T^{-2} = K\left(\frac{M}{L^3}\right)^a \left(\frac{L}{T}\right)^b \left(\frac{1}{T}\right)^c (L)^d \tag{44}$$

from which

$$d = 5 - b$$
$$c = 2 - b$$

so that

$$Q = K \rho n^2 D^5 \left(\frac{V}{nD}\right)^b \tag{45}$$

Defining

$$C_Q = K\left(\frac{V}{nD}\right)^b \tag{46}$$

then

$$C_Q = \frac{Q}{\rho n^2 D^5} \tag{47}$$

Since power, P, is equal to $2\pi nQ$ a power coefficient may be defined as:

$$C_P = \frac{P}{\rho n^3 D^5} \tag{48}$$

Also, the quantity (V/nD) is defined as the advance ratio, J. The advance ratio is a measure of the advance or forward movement of the propeller per revolution. In using these coefficients, it is important to remember that the preceding derivations do not account for Mach or Reynolds number effects. If they had been considered, it could be shown that C_T ,C_Q and C_P would not only be functions of V/nD but also of Mach and Reynolds number.

Reynolds number effects, however, may be neglected if the sectional Reynolds number at the 3/4 radius is above 700,000 (see section 4.1.1). Mach number effects, on the other hand, are important and must be considered at transonic flight Mach numbers. The preceding definitions of thrust, power and torque coefficient and advance ratio are perfectly general and may be applied regardless of the theory used to evaluate them. Thus, they may be utilized in any of the blade element theories.

Lastly, one additional parameter, efficiency, is defined as

$$\eta = \frac{\text{Power Out}}{\text{Power In}} \tag{49}$$

The power out and power in of the propeller are:

$$\text{Power Out} = TV \tag{50}$$

and

$$\text{Power In} = \text{Shaft Horsepower} \tag{51}$$

Thus,

$$\eta = \frac{T\ V}{\text{Power In}} \tag{52}$$

or in terms of the previously defined coefficients

$$\eta = \frac{C_T}{C_P} J \tag{53}$$

Single rotation propellers and propfans tend to have efficiencies in the low to mid 80's and counter rotation propulsors have efficiencies in the mid to high 80's at cruise Mach numbers.

Obviously, this definition of efficiency is not useful at static conditions since at V=0, η=0. In this case, it is customary to use the ratio of C_T/C_P as an indication of static efficiency. For this case, Figure of Merit, FM, is defined as:

$$FM = .798 \frac{C_T^{\frac{3}{2}}}{C_P} \tag{54}$$

The preceding set of standard non-dimensional coefficients retains the same values whatever system of units is used to measure the individual quantities involved, but it is necessary to use a consistent system. Thus, if the thrust is measured in pounds, the diameter in feet and the unit time in seconds, then the velocity must be expressed in feet per second, the power in foot-pounds per second and the density in slugs per cubic foot.

Finally, the above definitions hold whether the propeller operates on the end of an infinitely long shaft or in front of or behind a nacelle. However, care must be taken to specify whether coefficients are free-air, net or shaft (apparent or propulsive as defined in section 3.1.)

3.3.2 Engine/Core Related Items (Ref. AIR 1703)

3.4 Propeller Thrust Method Options

3.4.1 Map (J, Cp, Ct) Method: Two thrust methods are described in this Section;, the "J" method and the "Theta" method. They differ in the way installation and inflow effects are accounted for, i.e. the "J" method relates power coefficient (c_p) and advance ratio (J) to thrust either by way of efficiency (η) or a thrust Coefficient (C_t) and the "theta" method relates power coefficient (c_p) and blade angle (θ) directly to the Thrust coefficient (C_t). The "J" method depends upon modifications to the advance ratio (J) to correct for blockage and inflow effects, etc. The "theta" method bypasses these effects apparently due to a quasi-direct correlation between the blade angle (θ) and thrust at a given power level and RPM, providing an intuitive modification that when these effects are present, the blade angle (θ) changes to absorb the power delivered.

3.4.1.1 Background: Initially, propeller data was obtained from wind tunnel and rig tests on both large and small scale model propellers. These propellers were both fixed and variable pitch types with variations in the prime geometric variables discussed in section 3.3. Moreover, these propellers were tested on a variety of test rigs ranging from bodies representing isolated propellers to simulated nacelles to actual engines. A typical form of the test results is shown in Figure 18. These data are for a fixed pitch propeller and represent the results for one blade angle. With the data non-dimensionalized in the form of C_P, C_T, J and η, these data could then be used to estimate the performance of that particular propeller at any other diameter and RPM by recomputing J.

Many systematic propeller tests were conducted in both private and government facilities. Propeller manufacturers used these data to derive empirical propeller performance manuals. These manuals consisted of the complete performance for a basic propeller geometry and rig configuration with correction factors to adjust the basic plot for the effect of the prime geometry variables. Thus, a user of these empirical methods could predict the performance of any propeller geometry constrained only by the number of propellers making up the data base.

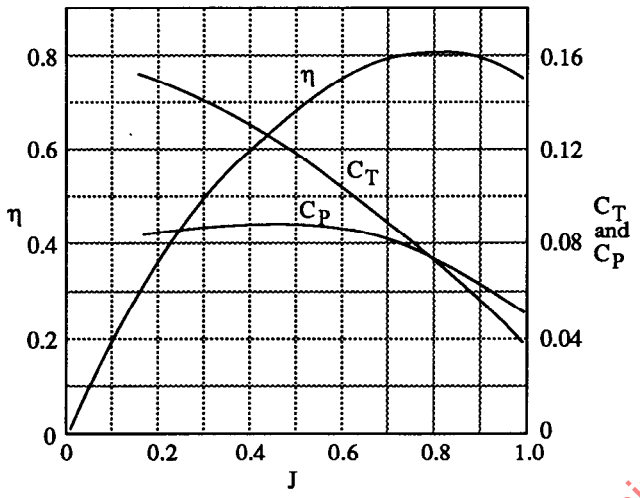

Figure 18 - Typical Performance Curves (Fixed Pitch)

The above method, although largely replaced by analytical predicted performance maps, is still of use today. Non-dimensional experimental data is still used to predict the performance of a given propeller geometry at any given diameter and will be discussed below. A detailed discussion of historical experimental and analytical methods of performance prediction is contained in Sub-section 4.1.

3.4.1.2 Propeller Performance Maps:: The development of propeller performance theories and the advent of the high speed computer allows the propeller manufacturer to predict the performance of a given propeller geometry over a very wide range of operating conditions. Typical analytical maps are shown in Figures 19 and 20 for a given propeller geometry. Figure 19 represents the static or V = 0 performance of a series of propellers while Figure 20 represents the performance at forward velocities. It is obvious that data such as these can be used to estimate the performance for any diameter, velocity, rpm. combination. Propeller manufacturers have developed performance manuals consisting of many charts similar to those above covering a wide range of propeller geometric variables. These manuals allow the aircraft designer to interpolate between configurations and optimize a propeller configuration for his aircraft. However, it is left to the aircraft designer to determine the interference effects between the propeller and the aircraft.

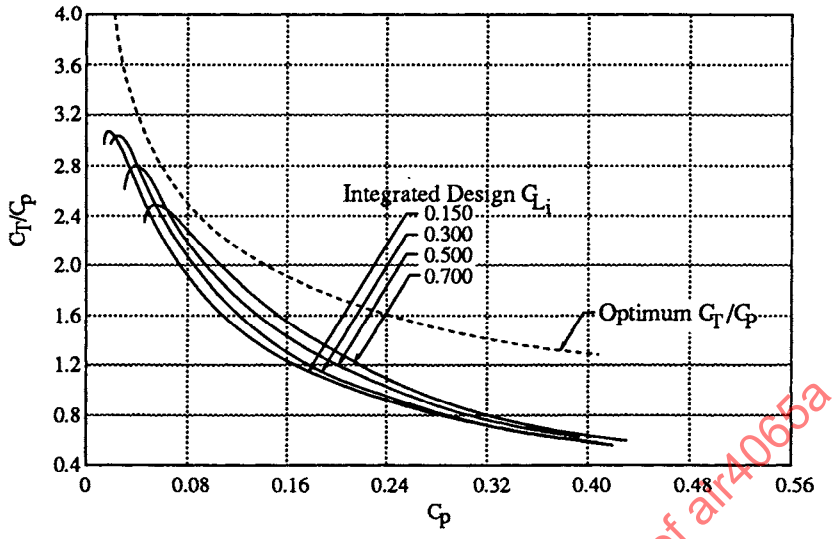

Figure 19 - Typical Static Performance Chart

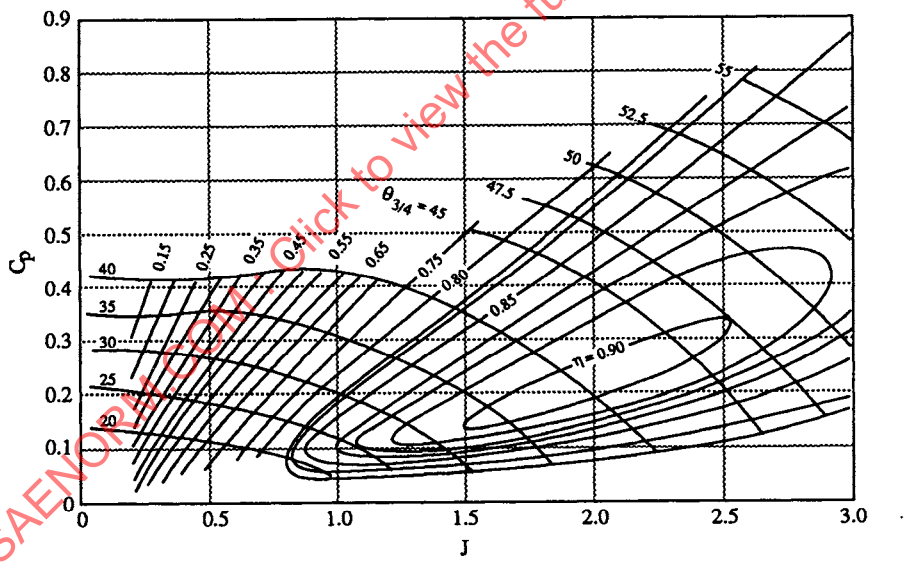

Figure 20 - Typical Propeller Performance Chart

In addition to maps as shown above, performance data is presented in Figure 21 or in the form of computer tapes. In general, the data is presented in non-dimensional form so that it can be used to estimate the performance at any diameter, velocity and rpm.

Mach = 0.7

J	Cp	$C_{T_{Net}}$	η_{Net}	J	Cp	$C_{T_{Net}}$	η_{Net}	J	Cp	$C_{T_{Net}}$	η_{Net}
3.3	1.6	0.4024	0.830	3.5	2.0	0.4646	0.817	3.7	2.3	0.4990	0.803
	1.7	0.4260	0.827		2.1	0.4866	0.811		2.4	0.5173	0.798
	1.8	0.4484	0.822		2.2	0.5058	0.805		2.5	0.5345	0.791
	1.9	0.4703	0.817		2.3	0.5239	0.797		2.6	0.5505	0.783
	2.0	0.4913	0.811		2.4	0.5415	0.790		2.7	0.5657	0.775
	2.1	0.5116	0.804		2.5	0.5580	0.781		2.8	0.5798	0.766
	2.2	0.5313	0.797		2.6	0.5738	0.772		2.9	0.5929	0.757
	2.3	0.5499	0.789		2.7	0.5878	0.762		3.0	0.6051	0.746
	2.4	0.5669	0.780		2.8	0.6005	0.751		3.1	0.6151	0.734
	2.5	0.5833	0.770		2.9	0.6110	0.737		3.2	0.6236	0.721
	2.6	0.5944	0.760		3.0	0.6206	0.724		3.3	0.6297	0.706
	2.7	0.6112	0.747		3.1	0.6294	0.711		3.4	0.6341	0.690
	2.8	0.6228	0.734		3.2	0.6359	0.696		3.5	0.6366	0.673
	2.9	0.6323	0.720		3.3	0.6411	0.680				
	3.0	0.6400	0.704								
3.4	1.8	0.4382	0.824	3.6	2.1	0.4734	0.812				
	1.9	0.4563	0.820		2.2	0.4934	0.807				
	2.0	0.4792	0.815		2.3	0.5119	0.801				
	2.1	0.4994	0.809		2.4	0.5297	0.795				
	2.2	0.5186	0.801		2.5	0.5460	0.786				
	2.3	0.5368	0.794		2.6	0.5419	0.778				
	2.4	0.5547	0.786		2.7	0.5764	0.769				
	2.5	0.5715	0.777		2.8	0.5903	0.759				
	2.6	0.5864	0.767		2.9	0.6030	0.749				
	2.7	0.5993	0.755		3.0	0.6131	0.736				
	2.8	0.6114	0.742		3.1	0.6234	0.724				
	2.9	0.6205	0.728		3.2	0.6313	0.710				
	3.0	0.6289	0.713		3.3	0.6374	0.695				
	3.1	0.6360	0.698		3.4	0.6422	0.680				
	3.2	0.6419	0.682								

Figure 21 - Typical Performance Tabulation

While the foregoing discussion deals with performance data developed analytically, the maps can also be developed from experimental data. Representative samples of such data are shown in Figures 22 through 24 for a conventional propeller, single-rotation propfan and a counter-rotation propfan respectively. The form of the data is identical to that predicted analytically and usually consists of a series of efficiency maps covering a range of Mach numbers. Again, by interpolation the aircraft designer can determine the performance of a given propeller configuration at any diameter and Mach number.

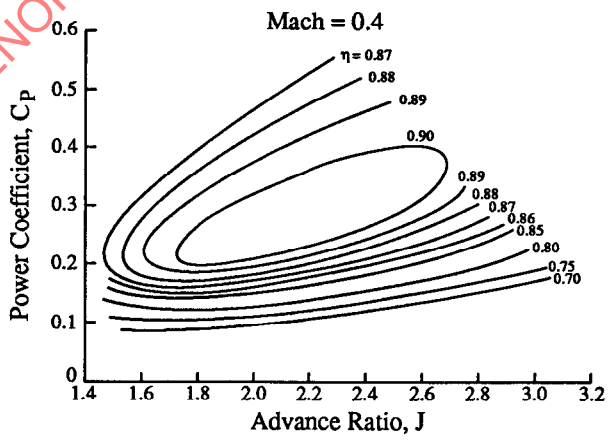

Figure 22 - Efficiency Chart for a Typical Propeller - Mach = 0.4

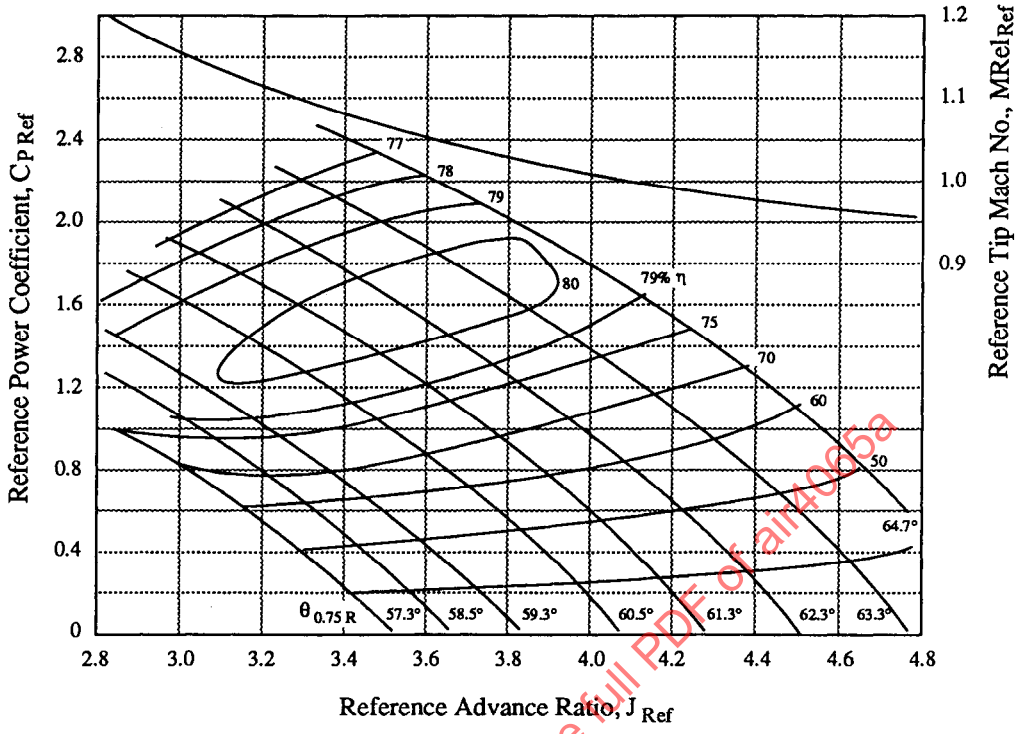

Figure 23 - Propeller Performance at Mach = 0.80

3.4.1.3 Use of Performance Maps: In using these performance maps care must be taken to determine the definition of thrust used to develop the maps. The thrust definitions commonly used to generate maps are:

1. Free-air thrust, T_{fa}
2. Apparent thrust, T_s
3. Propeller net thrust, T_{net}
4. Propeller propulsive thrust, T_p

as defined in section 3.1.1.

To review briefly, the free air thrust is that thrust a propeller would produce if mounted on an infinitely long, thin shaft. The apparent thrust is that thrust produced by the propeller while operating in the presence of a body while the net thrust is the thrust of the propeller operating in the presence of the body minus the incremental pressure drag on the body due to the flow through the propeller. Propulsive thrust is obtained by removing the incremental skin friction on the

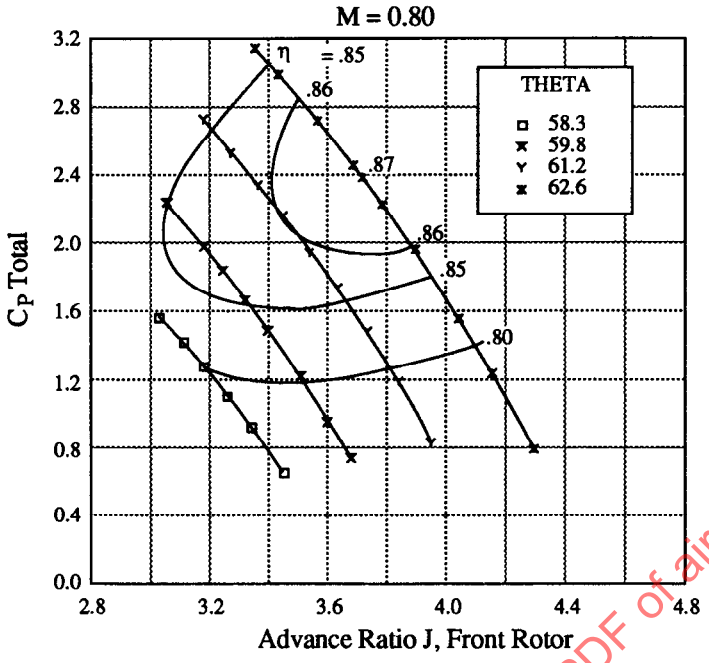

Figure 24 - Partial Efficiency Map (Counterrotation)

body due to the propeller from the net thrust.

Maps should be clearly labeled as to what thrust definition was used in developing the map, and what, if any installation effects have been included in the map. A numeric example to illustrate the use of an apparent thrust, T_S, map is presented in Appendix B.

The preceding discussion applies to either single or counter-rotation propellers. While individual performance maps can be developed either experimentally or analytically for each stage of a counter-rotation propeller, it is more convenient to use maps developed for the combined performance. This eliminates the difficult task of trying to estimate what portion of the body correction factor should be applied to each rotor. Using the combined performance maps with the correction factors discussed below will produce more accurate results.

3.4.1.3.1 Definition of SBAC Body Correction Factors: The Society of British Aerospace Companies (SBAC) body correction factors are used to obtain estimates of installed or propulsive propeller performance from isolated propeller data. They are based on work carried out in the 1920's and 1930's by Glauert and Lock,

among others. Individual isolated data points cannot be readily converted to installed values and use must be made of appropriate isolated performance propeller maps.

The two correction factors used are:

1) A retardation factor is used to allow for the presence of the nacelle or body on the flow through the propeller. This is denoted by (1 - h) and is defined as:

$$(1 - h) = \frac{\text{flow volume in presence of body}}{\text{flow volume with no body}} \quad (55)$$

$$= 1 - \frac{(0.254S)}{A} \quad (56)$$

Where: S = maximum cross sectional area of the nacelle
A = propeller disc area

Where 'propeller' means the disc area which the blades normally rotate within.

In using propeller maps, the value of (1 - h) is used to obtain an effective value of the advance ratio (J).

Since, $$J = \frac{V_0}{nD} \quad (57)$$

Then $$JE = \frac{V_E}{nD} = (1 - h)\, J = (1 - h)\, \frac{V_0}{nD} \quad (58)$$

and $$(1 - h) = \frac{V_E}{V_0} \quad (59)$$

The effective advance ratio (JE) is thus a mean value of the velocity distribution which exists along the propeller blade.

2) A body correction factor to allow for the increase in drag of the parts of the aircraft in the propeller slipstream above the drag in free-stream. The factor thus debits the propeller thrust with the increase in drag due to the increase in slipstream velocity over free stream. This incremented drag factor is defined by:

$$f_b = \frac{\text{propulsive efficiency}}{\text{effective efficiency}} = 1 - (1.22\, S\, C_D/A) \quad (60)$$

$$f_b = \frac{\eta_P}{\eta_E} \tag{61}$$

where: C_D = drag coefficient based on area S

The effective efficiency is often the cause of some confusion as it is defined as:

$$\eta_E = \frac{(T_S\ V_E)}{P} \tag{62}$$

where: T_S = shaft or apparent thrust

V_E = effective velocity or freestream velocity * (1 - h)

This should not be confused with shaft or apparent efficiency, which is defined as:

$$\eta_S = \frac{(T_S\ V_0)}{P} \tag{63}$$

where: V_0 = freestream velocity

Thus,

$$\eta_E = \eta_S\ (1 - h) \tag{64}$$

The empirical values of the two correction factors (1 - h) and f_b can be obtained from the formulae given in the SBAC report (Reference 12). These have been historically obtained from back figuring of wind tunnel test results, but have been found to give reasonable estimates for conventional propellers.

Alternatively, the values of the body correction factors can be determined directly for a given installation. The value of (1 - h) can be measured for a given nacelle as part of a wind tunnel test program, by carrying out velocity measurements in the propeller plane.

The f_b factor can also be determined from wind tunnel tests by carrying out blade-on and blade-off installed tests as shown in Figure 25. Computational Fluid Dynamic code for bodies can also be used to estimate (1 - h).

3.4.1.3.1.1 Use of SBAC Body Correction Factors for Isolated Propeller Maps: The correction factors were originally intended for use with isolated propeller maps by applying the following four steps: 1) Multiply J by (1 - h) to obtain JE; 2) Using this value of JE, obtain values of either CTS or η_E at the required value

of Cp; 3) To obtain propulsive values of either thrust or efficiency, the effective values obtained above are first multiplied by f_b. This will give a propulsive value of efficiency

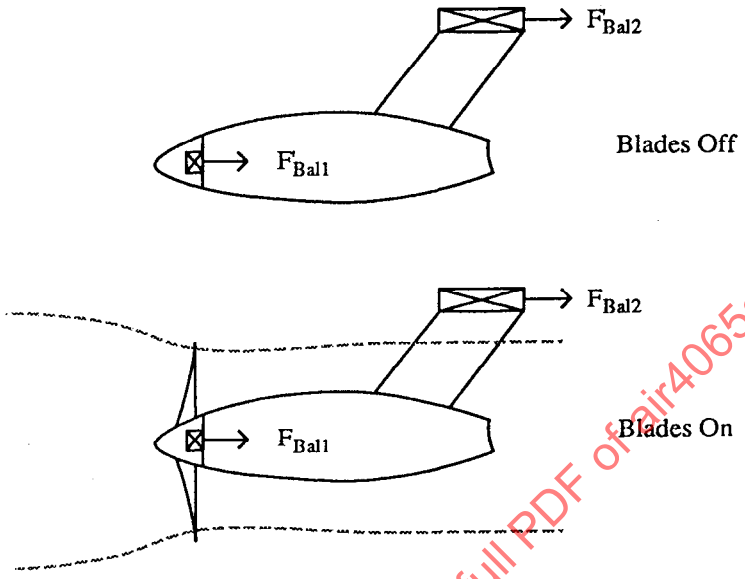

$$T_S = F_{Bal1} - F_{Bal1} \qquad C_{T_S} = \frac{T_S}{\rho n^2 D^2}$$

$$T_P = F_{Bal2} - F_{Bal2} \qquad C_{T_P} = \frac{T_P}{\rho n^2 D^2}$$

$$C_{T_P} = C_{T_S} (1 - h) fb$$

$$\Longrightarrow f_b = \frac{C_{T_P}}{C_{T_S} (1 - h)}$$

Figure 25 - Determination of f_b Factor

directly since f_b is defined as η_P/η_E, but the thrust coefficient or thrust has to be multiplied by (1 - h) as well as f_b. The reason for this is that f_b is related to effective velocity and not free-stream velocity. Thus:

$$f_b = \frac{\eta_P}{\eta_E} = \left(\frac{(C_{Tp}\, V_0)}{C_P}\right)\left(\frac{C_P}{(C_{Ts}\, V_E)}\right) \tag{65}$$

$$f_b = \left(\frac{C_{Tp}}{C_{Ts}}\right)\left(\frac{V_0}{V_E}\right) \tag{66}$$

$$C_{Tp} = C_{Ts}\left(\frac{V_E}{V_0}\right) f_b = C_{Ts} (1 - h)\, f_b \tag{67}$$

4) If values of shaft (apparent) thrust or efficiency are required, they can be determined as follows. Shaft thrust is calculated as part of step 2. above. Shaft efficiency is obtained from effective efficiency by dividing by (1 - h); i.e. $\eta_S = \eta_E / (1 - h)$, since shaft efficiency is related to freestream velocity, whereas effective efficiency is defined relative to effective velocity.

3.4.1.3.1.2 Use of SBAC Body Correction Factors For Shaft Maps: The SBAC body correction factors can also be used to determine installed performance from maps of shaft performance. These maps would correspond to test or analytical data obtained with the propeller in the flowfield of a nacelle or body.

To obtain propulsive values of thrust and efficiency from shaft performance maps, the following procedures should be followed: 1. Obtain values of shaft thrust coefficient and efficiency by using the freestream value of J. 2. Multiply the shaft thrust coefficient and efficiency by both f_b and (1 - h). The reason for multiplying by both correction factors is the same as that explained in step 3. for isolated maps above. Figures 26 and 27 relate the definitions and usage of SBAC correction factors to propulsion test rig data.

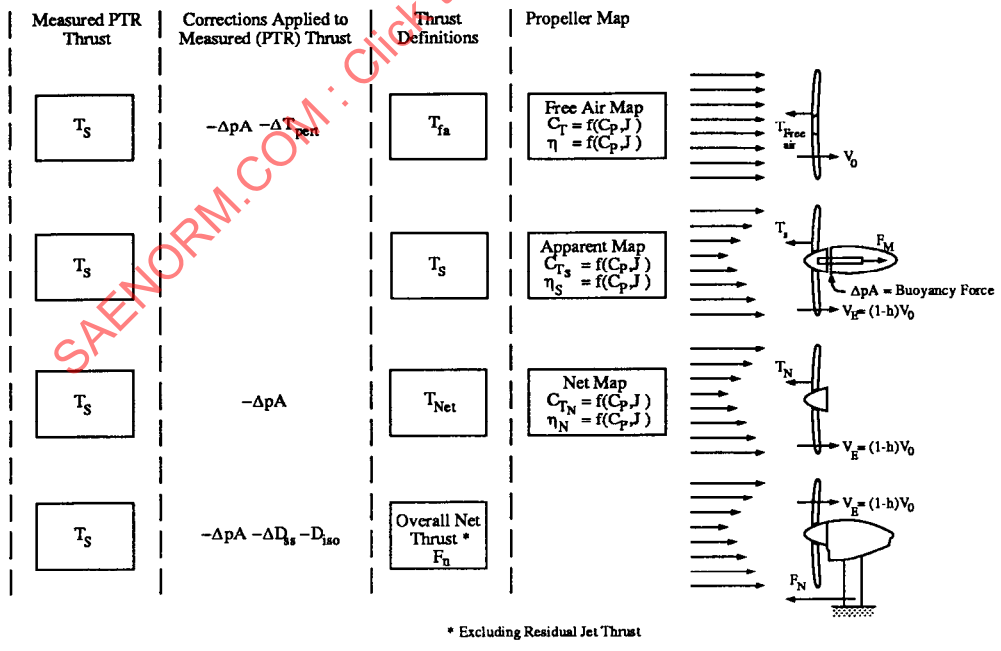

Figure 26 - Free Air, Apparent and Net Map Definitions

3.4.1.3.2 Alternative Body Correction Methods: With the advent of advanced high speed propellers and advanced computational methods, it has become common to present propeller maps in terms of net performance (C_{T_n}). These maps represent the performance of a propeller in the flowfield of a representative nacelle and already have the incremental pressure drag due to the propeller (buoyancy force) removed from the propeller shaft thrust. Moreover these maps base the advance ratio on the flight velocity. Thus it is not necessary to apply the SBAC correction factors to these propeller maps. Since the incremental pressure force has been removed from the net thrust, then, to obtain propulsive thrust it is only necessary to subtract any incremental skin friction force, i.e.:

$$C_{Tp} = C_{Tn} - \Delta D_{SS} \tag{68}$$

The incremental pressure force is normally found by taking the difference in analytically or experimentally determined pressures integrated over the nacelle for the blades-off and blades-on cases. This can then be subtracted from the measured shaft thrust to obtain net thrust.

3.4.2 "Theta" Method

3.4.2.1 Discussion: One of the uncertainties in obtaining propeller thrust using the traditional map methods is knowing the actual value of J entering the propeller disc. For example, a propeller operating statically will have a J=0 as defined in the classical sense, however, the propeller will actually induce an in-flow velocity profile at the propeller face. Also, with forward flight, installed propeller J is for the most part an estimate by various calculations and/or assumptions to account for the impact of the nacelle and airframe on the propeller in-flow conditions. These realities were discussed in the previous subsection.

In an effort to circumvent this uncertainty, it has been proposed that J be eliminated by relating thrust to power as a function of blade angle (θ) and flight Mach number. The function of J, which represents a helix angle, is then replaced by the blade angle which may be more precisely determined by geometric measurement. Table 2 presents a comparison of method elements for the two systems.

	Correction for buoyancy force $(1-h)=1-.254\ s/A$	Correction for ΔD_{ss} $f_b = 1 - \frac{.1308 \times \text{Drag}}{D^2}$ (Drag of parts @ 100 fps)
Free Air Map $C_T = f(C_P, J)$ $\eta = f(C_P, J)$	$J_E = (1-h)J$ Using free air map obtain: $C_{T_E} = f(C_P, J_E) = C_{T_S}$ $\eta_E = f(C_P, J_E)$	Calculate Propulsive Coefficients: $C_{T_P} = C_{T_S}(1-h)\, f_b$ $\eta_P = \eta_E f_b$ $= \eta_S\ (1-h)\, f_b$
Shaft Map $C_{T_S} = f(C_P, J)$ $\eta_S = f(C_P, J)$	Derive an equivalent value of (1-h) for the velocity distribution used in the production of the shaft map. This value of (1-h) is obtained by an area weighted integration of the velocity distribution where the velocity distribution is in terms of: $\frac{V}{V_0}$ *	Obtain C_{T_S} and η_S from shaft map by inputting the free stream value of J and C_P $C_{T_P} = C_{T_S}(1-h)\, f_b$ $\eta = \eta_S\ (1-h)\, f_b$
Net Map $C_{T_N} = f(C_P, J)$ $\eta_N = f(C_P, J)$	If the nacelle used in the production of the net map is different than the aircraft's nacelle, correction for ΔT_{pert} must be made.	

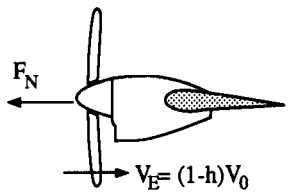

Propulsive Thrust

$T_P = C_{T_P} \rho\, n^2 D^4$

$= \frac{\eta\ 550\ Shp}{V_0}$

$-D_{iso} = F_{net}$

(Excluding Residual Jet Thrust)

* The inlet velocity ratio $\frac{V}{V_0}$ is usually presented for values of fractional radius $\frac{r}{R}$, for example:

$\frac{r}{R}$ =	.2	.25	.3	.45	.6	.7	.8	.9	.95	.975
$\frac{V}{V_0}$ =	.905	.923	.939	.970	.987	.994	.998	1.0	1.0	1.0

$\frac{V}{V_0}$ = (1-h) = Area weighted integration of the above $\frac{V}{V_0}$ distribution

Thrust correction factors due to compressibility effect are given as a function of J, C_P and $M_{.7}$ where the helical Mach No. at .7 radius is $M_{.7} = M_{Flight} \sqrt{1 + (\pi \times .7 J)^2}$

ΔT_{pert} for low speed propellers is negligible.

Figure 27 - Typical Low Speed Map Usage

Data generated using this system results in propeller characteristics that tend to be independent of installation effects or wind tunnel wall effects. This is because a change in effective advance ratio tends to move the operating point up or down a constant Theta line. Appendix C presents results of applying the Theta Method.

3.4.2.2 Method Description: By plotting thrust coefficient against torque coefficient (or power coefficient) at constant values of blade angle, the result of changes in effective advance ratio can be minimized. This means that if inflow conditions into the propeller are changed, by altering nacelle blockage or by introducing wall effects for example, there will be virtually no change in the propeller performance characteristics. This will hold true providing compressibility losses are not significantly altered, and providing the inflow changes do not cause blade airfoil sections to stall. Figure 28 shows a generalized example of this effect, where Figure 28a comes from Reference 12.

3.4.2.2.1 "Theta" Method Linear Characteristics: Another interesting feature of plotting the propeller data in this format, is that over certain parts of the propeller operating envelope, the constant blade angle characteristics are nearly linear. This allows the relationship between thrust and torque coefficients to be expressed in the form of a simple linear equation:

$$C_T = m\,C_Q + c \tag{69}$$

where: m = slope (dC_T / dC_Q)

$c = \frac{-b}{m}$

b = intercept of C_Q axis (i.e. $C_T = 0$)If we consider blade element theory (see Appendix E), it can be shown that:

$$\frac{dC_T}{dC_Q} = \frac{2\,R\,/\,r}{\tan\left(\theta - \alpha + \gamma - \tan^{-1}\left(\frac{0.5\sin\left(2[(\gamma_0-\gamma)-(\alpha_0-\alpha)]\right)}{C_Q/C_{Q_0} - \cos^2\left((\gamma_0-\gamma)-(\alpha_0-\alpha)\right)}\right)\right)} \tag{70}$$

Table 2 - Elements Origin of Method Comparison

	J METHOD			THETA METHOD		
	Meas.	Calc.	Est.	Meas.	Calc.	Est.
M	✓			✓		
J			✓		✓*	
C_p	✓			✓		
C_t		✓			✓	
Theta				✓		

* J can be calculated accurately from test results

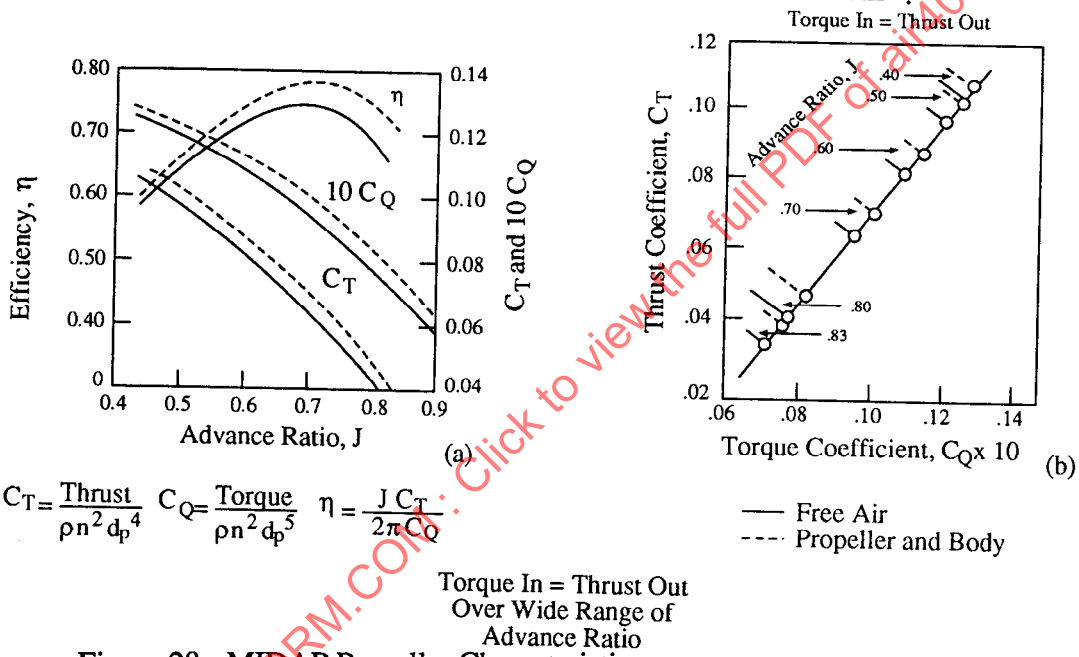

$$C_T = \frac{\text{Thrust}}{\rho n^2 d_p^4} \quad C_Q = \frac{\text{Torque}}{\rho n^2 d_p^5} \quad \eta = \frac{J\,C_T}{2\pi C_Q}$$

Torque In = Thrust Out
Over Wide Range of
Advance Ratio

Figure 28 - MIDAP Propeller Characteristics

where R = propeller radius
r = local section radius
θ =local blade angle
α = local section incidence angle
γ = local section $\tan^{-1}(C_D/C_L)$
suffix 0 = values at $C_T = 0$

Assuming conditions on the blade at a r/R of 0.7 are representative and that $C_Q >> C_{Q_0}$ then this expression simplifies to:

$$\frac{dC_T}{dC_Q} = \frac{2.857}{\tan\left(\theta_{.7} - \alpha_{.7} + \gamma_{.7}\right)} \tag{71}$$

Since $\alpha_{.7}$ and $\gamma_{.7}$ are generally small and in the equation tend to cancel, then the slope (dC_T/dC_Q) is primarily a function of $\theta_{.7}$. This assumption breaks down when α or γ become large, i.e.. at low speed or high Mach numbers.

Also from blade element theory, the intercept with the C_Q axis can be shown to be:

$$C_{Q_0} = \frac{\pi^2 c_{.7}}{8 R}\left(\frac{C_{D_{0.7}}}{\cos^3\left(\theta_{.7} - \gamma_{.7}\right)}\right) \tag{72}$$

where $c_{.7}$ = chord at r/R = 0.7
$C_{D_{0.7}}$ = drag coeff.at r/R = 0.7 and $C_T = 0$

Since $\gamma_{.7}$ is generally small, the C_{Q_0} is a function of $C_{D_{0.7}}$ and $\theta_{.7}$. $C_{D_{0.7}}$ is primarily a function of helical Mach number at r/R = 0.7 ($M_{nH_{.7}}$)) and so:

$$C_T = m\,C_Q + c$$

where $m = f(1/\tan\theta_{.7})$

$$c = \frac{-b}{m}$$

$b = f(M_{nH_{.7}})\ ),\ 1/\cos^3\theta_{.7})$ (73)

This implies that the propeller characteristics can be represented by a slope and intercept which are functions of blade angle and helical Mach number only. Figure 29 gives an example of the performance of a single rotation advanced propeller using this technique.

The following points should be remembered when using this technique (i.e. linear assumption): i) Inaccuracies become greater as the propeller operates further from its design point because the small value assumptions begin to break down. ii) As mentioned, the technique is unique in that it is not related directly to flight conditions (i.e.. V, rpm) but is related only to a blade angle,θ, and torque Q.

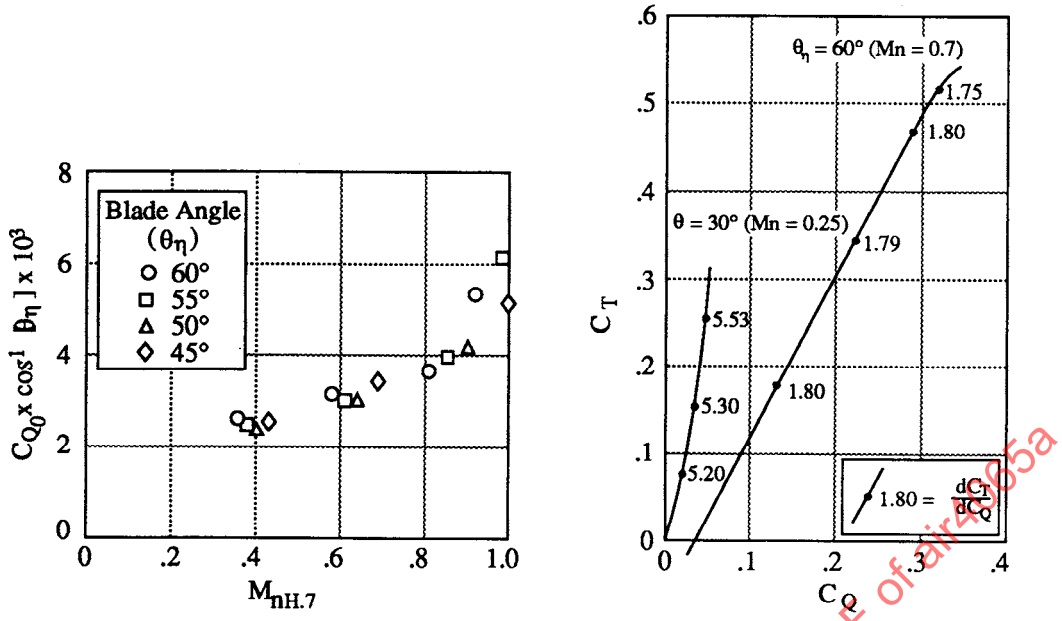

Figure 29 - Linearity of Constant Blade Angle Plot

3.4.2.2.2 "Theta" Method Non-Linear Characteristics: As noted above, treating the Theta Method as a totally linear approach introduces some errors as the measured data falls further from the design point. Therefore the Theta Method can be treated as another type of "map" method with the characteristics represented by a series of curves and /or tables, which in turn provide reasonable accuracy throughout the entire flight envelope.

3.4.2.3 Method of Implementation: There are several choices to make in implementing the theta (θ) method. These choices include a measurement procedure of blade angle, a method of power determination, and a method of data reduction. Blade angle measurement is the largest source of uncertainty in the theta method.

3.4.2.3.1 Blade Angle (θ) Measurement: There probably are several approaches to the measurement of θ. First is the use of potentiometers or other displacement measuring device in the propeller hub which, when calibrated, relate the position of the blade at its point of retention at any flight condition. This method must take into account the torsional stiffness of the blade to calculate the actual θ at .75R. The case study in Appendix C was able to yield an accuracy to 0.1 degree using this method. A second method conceivably could incorporate a laser system

which would be calibrated to measure angle changes of a reflective surface on the blade at the .75R station. Another system might relate a measure of apparent chord width with θ from a given perspective, etc.

3.4.2.3.2 Power Determination: The most obvious method of power determination is the use of a built in torque measuring system and sensing output shaft RPM. The placement should be between the propeller and the gearbox (if one is used), however a torque meter between the engine and gearbox is only slightly less accurate due to high gearbox efficiencies. If it is not possible to use a torque meter then a gas generator power/power turbine analysis will have to be used along the same procedures as presented in AIR 1703.

3.4.2.3.3 Limitations of Data Consolidation Methods: Multiple relationships can be generated in the forms illustrated in Section 3.4.2.2.1. Use of these relationships will require a large number of tables and high order interpolation procedures which minimizes errors, i.e. degrees of curve fit. Another simpler procedure might be to reduce the tabulated data to curve fits and simply apply as an algorithm. The choice made should be based on accuracy required after an uncertainty analysis.

Note that because advance ratio is eliminated from this approach, correlation with flight measurements can only be made using the measured flight blade angle, flight Mach number and rpm.

This Page Intentionally Blank

4 THRUST PROJECTIONS TO FULL SCALE:

4.1 Projection of Model Performance Data to Full Scale

The amount of adjustment needed to correct a model to full scale performance is of course, a function of the rigor taken in the modeling technique. Geometric similitude is extremely important. Conventional propellers have historically been aeroelastically stiff with only minor deflections. Hence, these can be scaled directly to model coordinates which are usually also stiff. However, modern lighter weight flexible blades will deflect, and analysis shows that these deflections can have significant effects on performance. The first order effect causing geometry distortion is the dynamic forces on twisted or swept blades. Aerodynamic loading can also contribute to the deflections. Preferred design practice would have the model blade construction achieve geometric similitude with full scale under dynamic and Aero loaded conditions. The state of the art for these calculations has progressed to the point where adequate simulation is achievable with high confidence. Other geometric similitude concerns are surface finish and contour irregularities. Nacelle and pylon geometries which may affect inflow or outflow aerodynamic properties should also be modeled. If similitude is not achieved, analytical performance predictions should be made for both the model and full scale blade geometries. The incremental differences between these performance predictions should then be used to adjust the model test to predict full scale performance.

The preferred modeling technique is for the model scale to be large enough to minimize or eliminate the need for Reynolds number corrections. Published data from numerous sources shows that the drag coefficient corrections for transonic airfoils will be small for models having Reynold's numbers in excess of 700,000 based on the chord length at 0.75R. For atmospheric wind tunnels, this would require propeller model diameter of nominally two feet or more. Because of drive motor horsepower limitations and/or wind tunnel blockage considerations, a smaller model producing Reynold's number (R_N) less than 700,000 might have to be used. For these cases performance adjustments will be necessary. Data correlations such as that shown in Figure 30 may be usefull. Another approach would be to use analytical prediction methods that have been validated over a range of Reynold's numbers. Figure 31 shows good agreement of "J" Method

calculations (described in Section 3.4.1) with data over a wide range of propeller sizes.

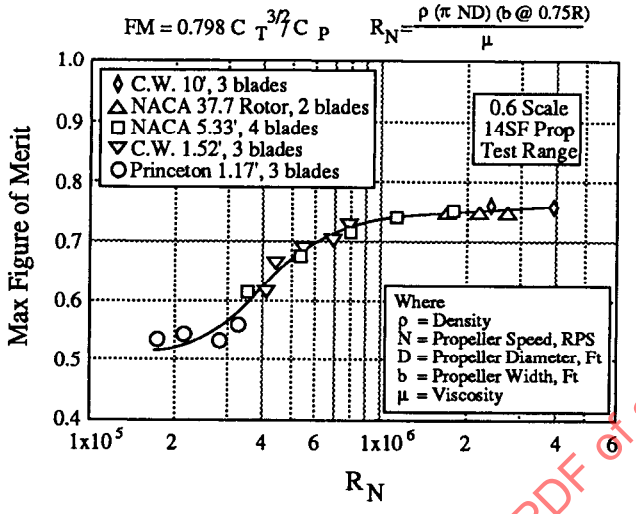

Figure 30 - Sample of Performance Correction

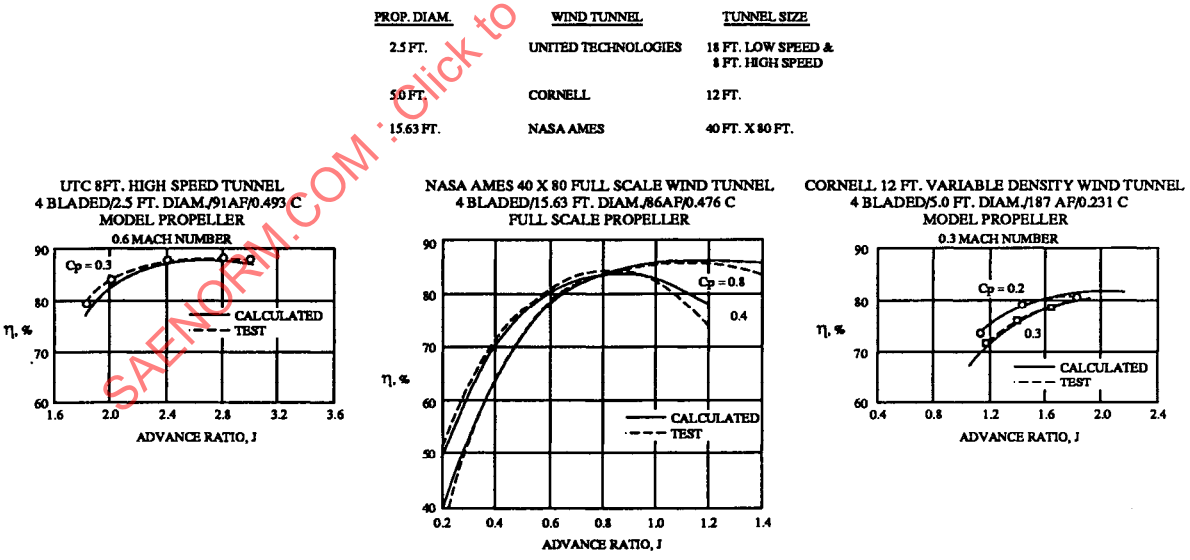

Figure 31 - Validation of Predictions by Test

Simulating flowing inlets and/or nozzles greatly complicates the propfan model. Flowing inlets for pusher propfan test rigs should not be necessary because the nacelle/propeller interactions are far enough removed that the resulting

interference forces should be small. Good design practice would be to contour the capped inlet in such a way that the surface velocity on the nacelle ahead of the propeller is the same velocity that the full scale engine would have at the inlet mass flow ratio of interest. A separate test would be needed to determine inlet total pressure recovery.

Chin or annular inlets in close proximity to tractor propfans are more likely to produce forces because of interaction with the propeller and should be modeled. The capture streamtube of a chin inlet located in close proximity behind the blades causes flow diffusion that will act like a back pressure blockage effect. The model should simulate this with either a flow-through inlet or with a faired inlet that produces the same back pressure effect. The flow-through model is preferred because it facilitates measuring the chin inlet pressure recovery and swirl simultaneously. The faired inlet simulation requires traversing to get information of the supercharging effect of the propeller on inlet recovery. In either case, these data can then be adjusted from model scale to full scale using standard boundary layer analysis.

Nozzle efflux impact on the model blades may also be a consideration when projecting the wind tunnel results to full scale. Pusher propellers may have the warm exhaust of an air/oil cooler heat exchange system and/or the core engine nozzle efflux flowing into the propeller. This will change the local blade entrance velocity diagram producing a performance effect. Appropriate analytical or experimental method adjustments should be used to adjust the data for such effects. Nozzles exhausting behind the pusher propfans will produce less of an effect. If the model is aft sting mounted, it should be contoured to simulate the full scale backpressure behind the prop. A separate nozzle test will be needed to obtain thrust coefficients which can then be projected to full scale flight conditions using turbofan methods. Nozzles for tractor propfans are normally far enough removed that any interactions with the propeller are insignificant. However, there may be significant effects of the slipstream on nozzle performance.

As in all these cases, nozzle thrust coefficients, profile effects, scaling methods, inlet pressure recovery adjustments, bleed ducts, steps, gaps,excrescences, etc., can be projected to full scale using the methods for turbofans as outlined in AIR 1703. Having performed all the above mentioned adjustments to the model data

introduces uncertainty in the accuracy of the full scale flight projection. An experiment to validate the entire process is the most straight forward way to put a determine the accuracy of the final answer. Figure 32 presents propeller test history, presenting observations by experienced experimentalists of measurement accuracy for validation of model to full scale conditions.

The success in projecting model thrust to full scale for turbofan engines leads one to consider analogous methods for turboprop systems. The procedure used for turbofans is as follows:

(1) Model and test the sea level static and flight conditions in sub-scale.

(2) Adjust the model data to full scale using appropriate compressibility and Reynold's number corrections and other increments to adjust for any other differences between the model and flight hardware.

(3) Conduct full-scale static engine tests at sea level and simulated altitude conditions.

(4) Apply appropriate adjustment to close model with full scale static engine performance.

With turbofans, this projection method can be validated with a full scale flight test or in an altitude facility. With propellers, however, this validation method is less precise or even inappropriate due to the lack of corrected airflow measurements which are used to establish turbofan thrust whether it is for sub or full-scale at static or flight conditions.Thus the present methods for projecting propeller thrust to full scale rely almost entirely on extrapolation of wind tunnel test results, using the best available advanced computations to augment test data as needed. Since large scale ground test facilities do not exist to provide even low speed validation of the projection of propeller data to full scale, present procedures are forced to go directly to flight test.

Propeller Performance Validation

Technique	Instrumentation	Basic Measurement	Technical Feasibility	Accuracy
Flight - Full Scale - Test Aircraft or Intended Aircraft	° Backfigured Propeller Performance from Basic Aircraft Flight Data	° Installed Thrust, T'_{net}	° Historic Technique, Difficult to Separate out Propeller Performance	
	° Thrust and Torque Meters	° Apparent Thrust, T_S	° Attempts to Build Accurate, Reliable Thrust Meter Generally Unsuccessful, Expensive, Long Dev. Time - Could Be Troublesome	
	° Wake Measurements	° T, $T_{S\,INST}$	° Wake Measurements in Flight are Difficult Due to Variation of Flow. Feasibility Not Established. Tried by Others Including NASA for Blade Loading Distribution	
Wind Tunnel - Full Scale - Complete Propulsion System - With Engine	° Floor Balance - Load Cell	° $T_{net} - \Delta D_{SS} = F_S$	° Basic, Proven Approach, Limited Number Large W.T. - Limited to (T-D)	±2-3%
	° Thrust and Torque Meters Nacelle Skin Balance	° $T_S, T_{net}, T_{S\,INST} T_{JET}$	° Nacelle Skin Balance Feasible and Demonstrated Thrust and Torque Load Cells Proven. Special Hardware Required. Arrangement of Load Cell with Engine a Big Task. Problems Similar to Flight Thrust Meters.	±?%
Wind Tunnel - Full Scale - Prop/Nacelle - Electric	° Thrust and Torque Meters Nacelle Skin Balance	° $T_S, T_{net}, T_{S\,INST}$	° Proven Instrumentation, Limited Number Large W.T. Drive System Available - Skin Balance Needed, - Could Be Troublesome to Model, Full Nacelle with Existing Drives	±1-2%
	° Thrust and Torque Meters Nacelle Skin Balance	° $T_S, T_{net}, T_{S\,INST}$	° Several Wind Tunnels, Drive Systems Limited, Nacelle Skin Balance Needed, - Could be Troublesome to Model Full Nacelle with Existing Drives	±1-2%
	° Thrust and Torque Meters Nacelle Skin Balance	° $T_S, T_{net}, T_{S\,INST}$	° Many Wind Tunnels, with Prop Dynamometers, Low RN Possible Problem, Skin Balance Needed, - Could be Troublesome to Model Full Nacelle with Existing Drives	±1-2%

Figure 32 - Propeller Performance Validation

To bridge this gap and thereby eliminate associated risk, consideration is being given to conversion of large altitude facilities, like AEDC, into free jet test facilities for open rotor engine tests (see 4.5.3). At the present time, it appears that these facilities may provide a feasible test set up for validation of open rotor propulsion systems sized for general aviation aircraft, but are too small for propulsion systems sized for large commercial or military transports. Other possibilities that have been proposed to permit testing of larger units are: self induced forward velocity indoor stands; combinations of either free-jet or indoor stands with shrouds around the props which have been carefully contoured closely to the shape of the propeller streamtube, or a full scale entry into a large wind tunnel such as the ONERA 8 meter S-1 Tunnel in Modane, France.

4.2 Propeller Installation

4.2.1 Isolated Powerplant with Uniform Onset Flow: The Net Thrust (F'_{net}) of an isolated propulsion system is the summation of many contributing sources. Figure 33 illustrates these for isolated tractor and pusher installations.

The control volumes shown in this figure encompass the airflow passing through the engine which are provided by the engine manufacturer. The engine companies also provide the necessary exhaust conditions for computation of the nozzle gross thrust. The other terms are determined by experiment and/or analysis by either airplane, engine, propeller or nacelle manufacturers.

For total propulsion system performance demonstrations, measurements of engine fuel flow and net thrust are the principal concern, and all the thrust and drag contributors do not need to be segregated. However, large commercial transport engines are too big for high speed isolated tests. The largest high speed wind tunnel in the free world is the ONERA 8 meter tunnel mentioned in the preceding section. Testing here still would require model corrections to adjust to an isolated condition. Also, these tests are very expensive for propulsion system development during which engineers attempt to isolate the performance of each thrust drag contributor. Reliance is therefore placed on subscale wind tunnel propulsion models.

Subscale wind tunnel models can not simulate all these propulsion force elements at the same time. As mentioned earlier in this document, geometric simulation of the propulsion systems must be compromised and subsequently accounted for. Typically, inlets may be capped rather than flowing, nozzle efflux may not be properly simulated, air/oil cooler systems may not be simulated, and the back end

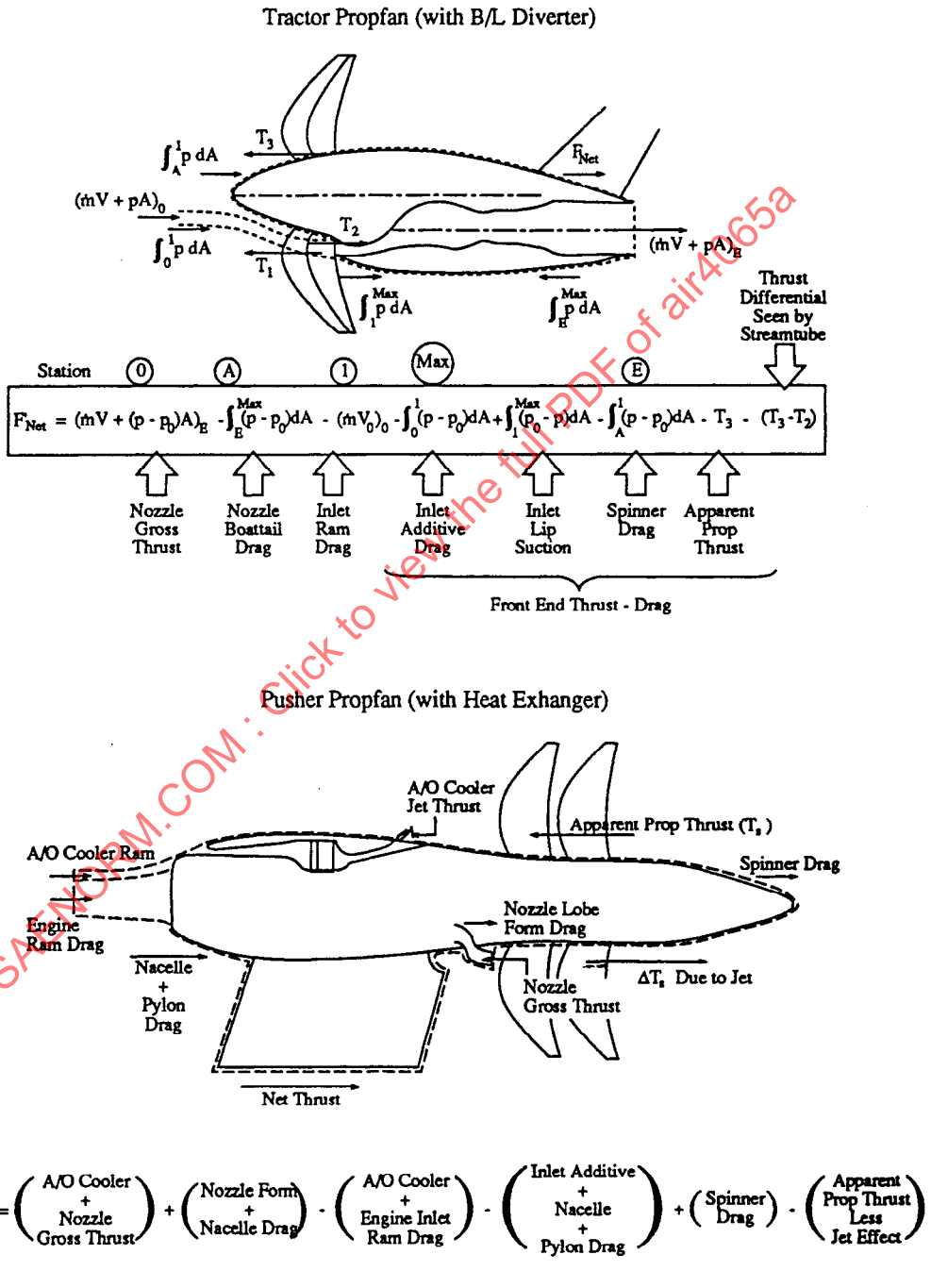

Figure 33 - Thrust and Drag Contributions to Net Thrust of an Isolated Propulsion System

contours might have to be compromised when aft-end drive systems are used. The next section describes some of the test models and drive systems that were used extensively in the past two decades for isolated propeller/propfan model performance testing. Lack of simulation will be pointed out and the methods for correction will be described.

4.2.2 Methods of Quantifying

4.2.2.1 Model Tests: There are numerous types of drive systems for powering propeller models and various sizes of propeller models. Two popular sizes of powered propeller models employ nominally 1 foot diameter props, or 2 foot diameter props. The 1 foot simulators are principally used for installed airplane model testing. Because of wind tunnel blockage considerations, airplane models are relatively small, normally l/10th to 1/15th scale. The 1 foot simulator is well suited for this scale. However, this is too small for propeller blade aerodynamic development testing (refer to Section 4.1). Its principle use is to pump flow, creating a propeller/airplane flow field discriminating streamline that converges in a similar fashion to the full scale item. Hence, it is mainly used for studying the impact of the propeller flow field on the airplane performance where as the influence of the airframe on propeller performance may not be reliably represented.

Isolated propeller aerodynamic testing is usually accomplished with simulators, nominally two feet or greater in diameter. Figure 34 shows a tractor propeller test drive system employing a large electric motor, which was used for the initial propfan testing in the early 1970's. Thrust and torque were measured at the rear of the assembly, and initially, the nacelle behind the propeller was grounded to the static housing. Static pressure taps on the nacelle were integrated to allow computation of propeller apparent thrust (refer to Figure 3). Later enhancement was made by separating the nacelle from the static housing and mounting it on a drag balance in order to study inlet/propeller interactions. Flow-through inlets mounted in the nacelle as shown in Figure 35 allowed quantification of the net thrust of the propulsion system forward of the maximum nacelle diameter. Adding the shaft thrust of the propeller/hub assembly to the drag of the nacelle/flow-through inlet assembly (once the tare drags were removed) yielded the front end performance of the propulsion system. It should be noted that the

tare drags included the loss of momentum of the flow passing through the inlet,which was determined analytically. Total pressure probes in the inlet quantify the supercharging effect of the propeller on the flow being induced into the engine. The inlet's internal diffuser total pressure recovery losses are subtracted from the inlet entrance total pressure to quantify the conditions entering the gas generator. A cycle analysis or test, combined with nozzle thrust prediction or a test, and aft-end drag predictions or test are needed to supplement this front-end data to determine net thrust of the total propulsion system.

The testing in the early 1970's provided the proof that propfans were capable of maintaining high levels of efficiency at flight speeds typical of commercial jet and turbofan powered aircraft. The fuel shortages and subsequent major increases in fuel prices in the min/late '70's launched the aircraft industry into serious study of propfans for these applications. New improved test rigs were built, Bulky electric drive motors were replaced with more compact air turbine drive systems.

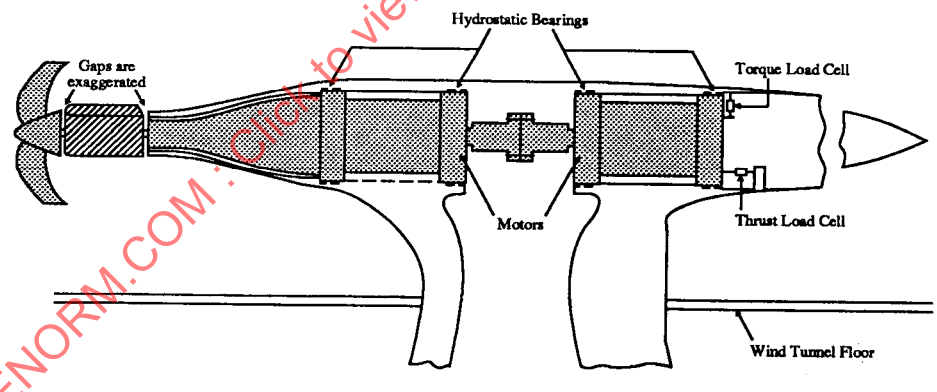

Note: Shaded components are metric on thrust and torque load cells.
Cross hatched components are on a piggy back drag balance.

Figure 34 - Propeller Test Rig in a Wind Tunnel

It was known that the residual swirl, inherent with single rotation (SR) propellers, if recovered, could result in further performance enhancements,hence the counter-rotating (CR) propeller concept came into being. Extensive testing was performed on both CR and SR configurations as evidenced by a sample of the test configurations shown in Figure 36.

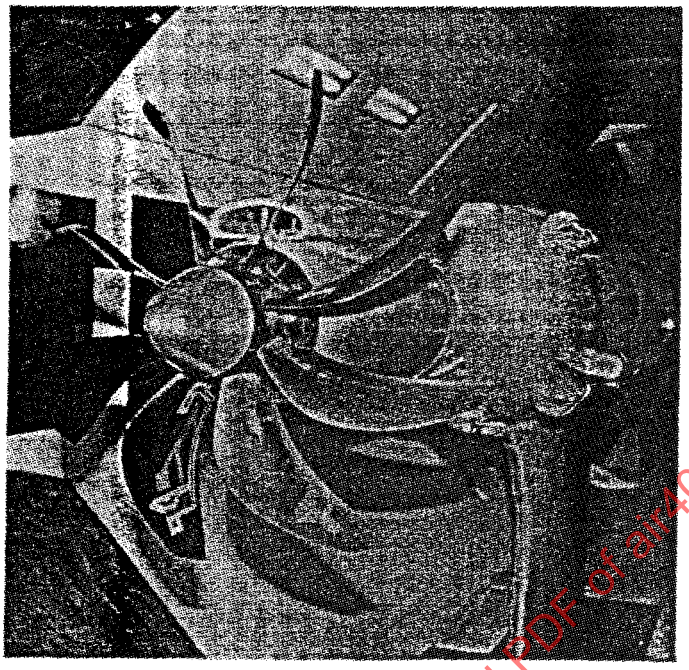

Figure 35 - Single-scoop Inlet with Diverter

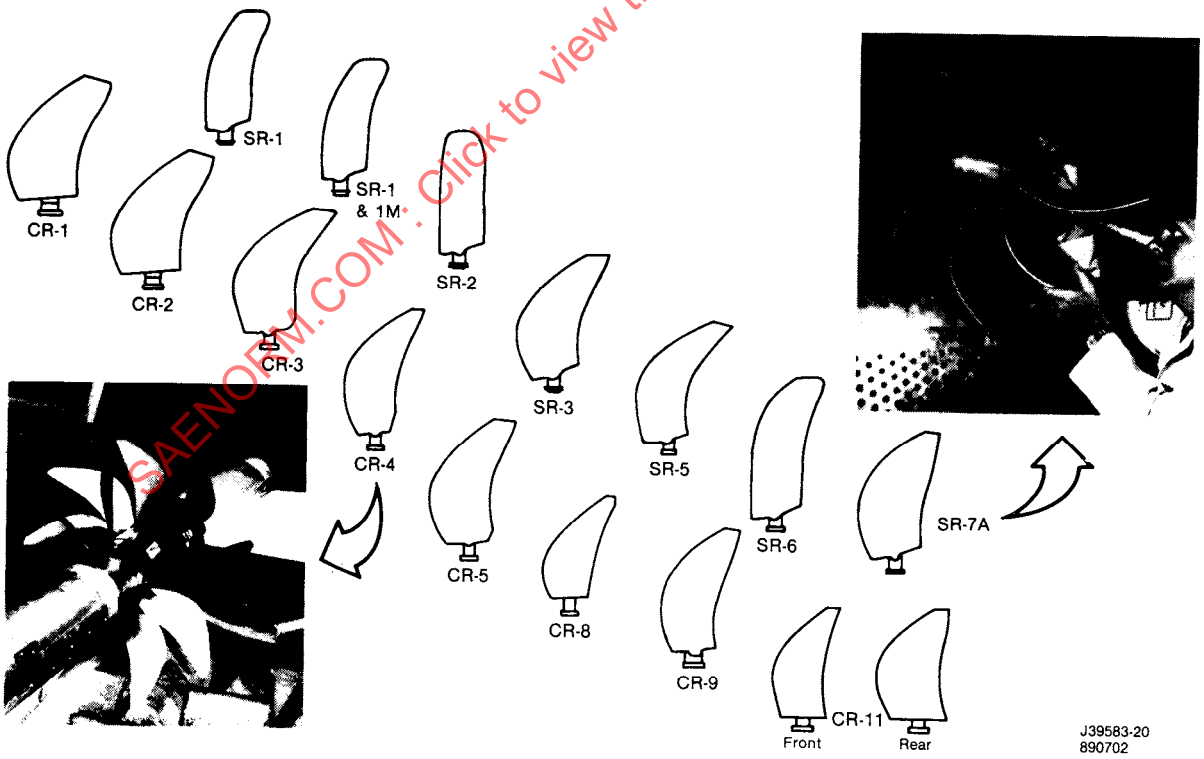

Figure 36 - Extensive Model Testing

As installation studies progressed, it became evident that pusher propfans were better suited than tractors for fuselage mounted applications. Closure of the fuselage allowed tucking the propulsion systems closer. Also, having the propeller aft of the aircraft rear pressure bulkhead was preferable from a cabin noise and safety standpoint. Consequently, tractor model drive systems were modified to simulate the pusher systems, and new pusher model test rigs were built. The tractor to pusher conversion was accomplished by removing the nose cone and placing a non-metric simulation of the nacelle, pylon and nozzles (if appropriate) ahead of the propeller. New pusher rigs employed an aft-drive, and cantilevered a non-metric simulation of the nacelle forward of the propellers. This precluded simulating nozzle flow into the prop, but does make angle of attack testing easier. Both rigs are shown in Figure 37.

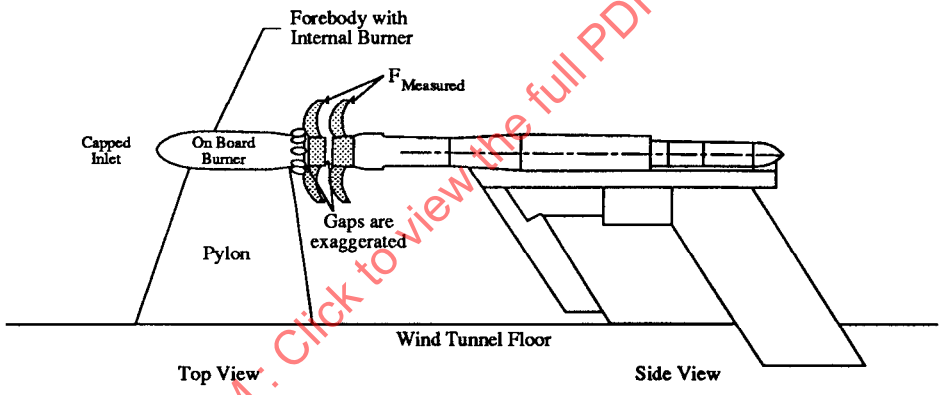

Tractor modified to simulate a Pusher Propulsion Systems

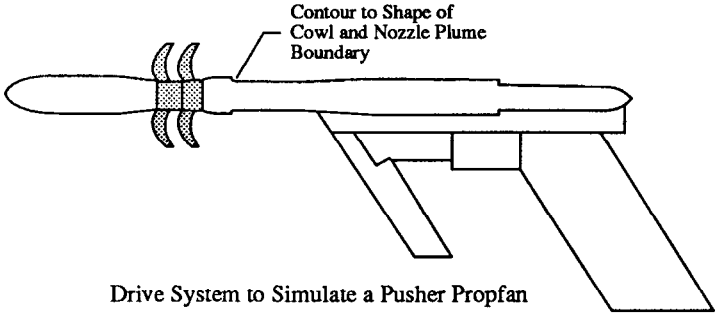

Drive System to Simulate a Pusher Propfan

Figure 37 - Propfan Test Rigs for Pusher and Tractor Configurations

Both rigs have the blades and hubs mounted on rotating thrust and torque balances located in close proximity to the propellers. Running with blades on and then with blades off, and subtracting the two measurements, eliminates many tare force concerns and gives propeller net thrust.

The pusher engine inlet, unlike the tractor installation is far enough removed from the propeller that there should be no significant inlet/propeller aerodynamic interaction. Consequently, simulation of a flowing inlet is not necessary. Typically the inlet is merely capped. Normal design practice is for the contour of the cap to be made to produce a static pressure distribution closely approximating that which would exist over the external portion of a flowing inlet. The inlet drag and nacelle drag contributions are determined by other experiments using standard test methods. Note that isolated unpowered inlet/nacelle drag tests do not simulate propeller induction effects. Integration of nacelle pressure data in front of the propeller test rig, with and without blades on, can give this incremental force. A preferred approach would be to make the nacelle metric. However, in either event, a flowing v.s. capped inlet adjustment is needed, and in all likelihood, will lead to isolated nacelle tests.

The aft nacelle simulation of pushers requires a greater amount of attention because of closer proximity to the propellers. Contours and pressure distributions coming into and leaving the propeller can significantly impact propeller performance. Also the engine exhaust nozzle efflux could significantly impact the propeller aerodynamics if it's located ahead of the propellers. The GE UDF and the Pratt-Allison 578DX demonstrator engines are examples of installations having nozzles behind and in front of their propellers respectively. (Figure 38).

With the engine exhaust nozzle behind the prop, there should be little impact of the nozzle flow on the propeller performance. Standard rig design practice is to contour the body behind the props to the same shape as the nozzle cowling, continuing along with a contour shaped to conform with the outer boundary of the nozzle plume. This simulation should go as far aft as possible until this contour fairs into the aft drive system support sting. However, the propeller efflux combined with the cowling shape will have a profound effect on the flow field enveloping the nozzle, thereby affecting nozzle mass flow and thrust. These

contributions to the isolated propulsion system thrust may require a separate experiment.

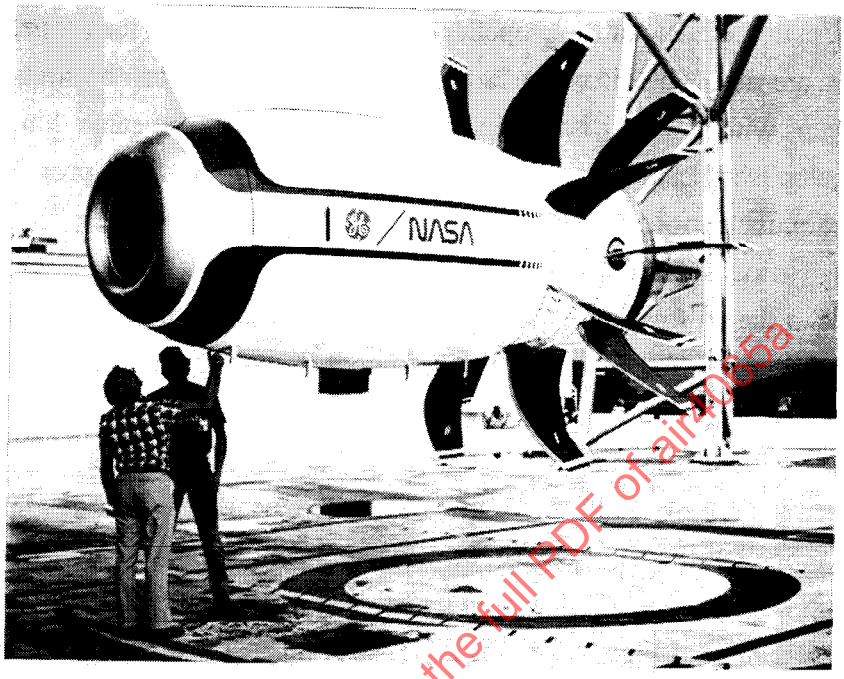

GE UDF Demonstrator with exhaust nozzle behind propellers.

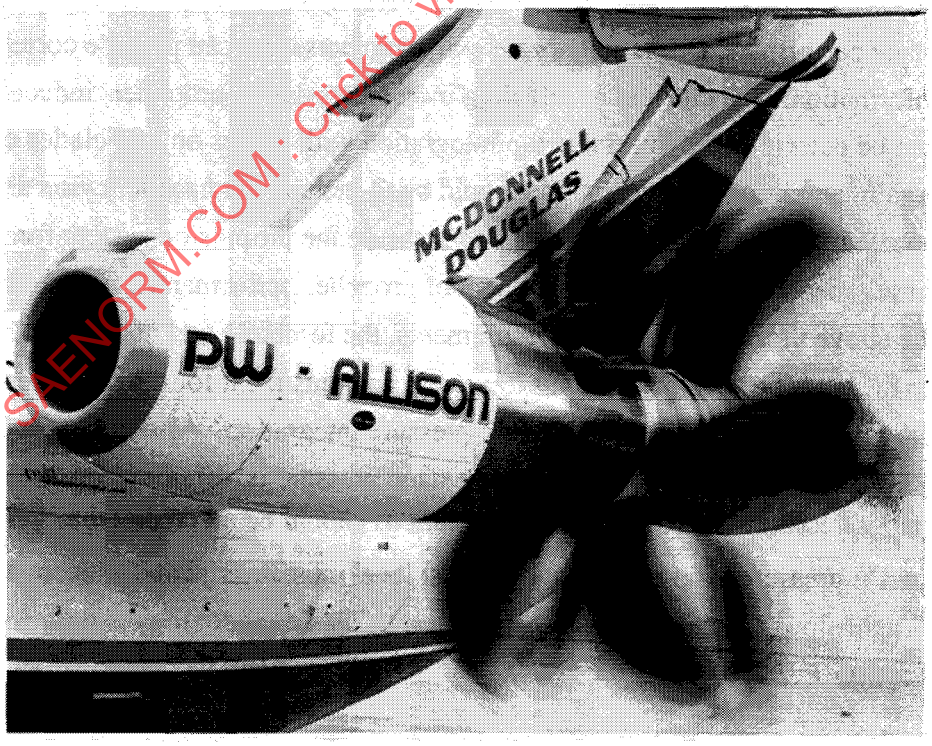

PW-Allison 578DX Demonstrator with exhaust nozzles ahead of propellers.

Figure 38 - Examples of Nozzle Installations

Blown nozzle thrust minus drag tests can be conducted in a wind tunnel but not in the standard way. Propeller efflux simulation is required. There are several candidate methods of accomplishing this: Ejectors within a tube surrounding the model in the plane of the propeller can be used to simulate the propeller total pressure rise. The discharge radial velocity distribution can be simulated by screens with a radial distribution of varying solidity. The same thing can be accomplished using a large tube contoured to the shape of the propeller streamtube surrounding the nozzle which then can produce a simulation of the longitudinal static pressure field. Each method is fraught with difficulty. The state of the art for these types of nozzle experiments is relatively immature. This also holds true for the aft spinner drag contribution for propulsion systems with nozzles ahead of the propeller.

When the nozzle is in front of the propeller, depending on it's axial proximity to the propeller, the jet thrust can be affected by the propeller-induced flow field. A much larger effect though, is the jet exhaust impact on the propeller. The test set-up on the top of Figure 37 can be used to simulate the temperatures and pressures of the nozzle efflux. Temperature simulation is necessary because the absolute level of jet velocity changes the propeller velocity vectors thereby impacting the blade performance. Internal nozzle exit static pressures can provide correlating information. Nacelle and nozzle drag increments due to propeller- induced effects can be determined by pressure tap integration with blades on and blades off. Again, a preferred test technique would be to include the nacelle, pylon and nozzle mounted on a thrust balance to measure the propulsion system forces simultaneously with the measurement of propeller performance. In the absence of the above thrust minus drag measurements, the forebody and nozzle can be tested propeller-off to get thrust minus drag with an adjustment for the propeller-induced drag increments from external static pressure integration. Also, a nozzle jet thrust adjustment is required if the local exit static pressure is different from the ambient static pressure. Static nozzle C_v correlations should be entered at the true local nozzle pressure ratio and the static thrust level must be adjusted to account for the "local minus ambient" pressure x area term. This methodology is described in Section B.7.2.2.

Heat exchangers, particularly with geared propfans, whether exposed to the freestream air or ducted, will figure into the thrust/drag equation. The total

momentum change through the heat exchanger is usually determined in a separate full scale experiment and its contribution included. The isolated propeller test rig should simulate any major bulges or contour changes associated with installing the heat exchanger, particularly if located in close proximity to the propeller. Flow-through tests of the engine inlet and heat exchanger inlet provide inlet drag increments that are added to the nacelle drag. Heat exchanger exhaust thrust can be computed as described above, or measured in a nozzle performance test.

4.3 Test Considerations:

4.3.1 Introduction: In-flight thrust projections would ideally use accurate wind tunnel data taken with models that properly simulate geometry, Reynolds number, blade tip Mach number and J. Practical considerations generally lead to compromises. At a given free stream Mach number, atmospheric wind tunnels have higher velocities than would occur at high altitudes because ambient temperature is not simulated. Overspeeding the propeller provides for compensation to simulate J, but mechanical limitations or available drive power may impose limits. Reynolds Number simulation is also difficult because model size will be limited by model drive power and blockage considerations in the wind tunnel. The considerations that went into these design decisions are discussed in the following paragraphs.

4.3.2 Test Approach: The selection of a particular procedure is made on the basis of the ability of that approach to fulfill the program requirements together with obtaining the most effective compromise of the following factors:

4.3.2.1 Complexity: The complexity of an approach is determined generally by the technology level and the test facilities available and can range from measurements on a single test vehicle (such as an aircraft model with flowing air intakes and powered propellers) to measurements on several test vehicles (such as model nozzle tests linked to isolated intake and isolated propeller tests). The degree of complexity allowable should be the minimum necessary to satisfy the program requirements within the constraints of the following considerations.

4.3.2.2 Cost: Cost will always be a major consideration in the selection process. The simplest test exercise should involve at least a model propeller test at a reasonable scale in a large wind tunnel (with all other effects perhaps deduced empirically or

analytically). At the other extreme lie aircraft flight tests, full powered aircraft model tests or full scale self powered aircraft model tests or full scale self-powered sea level, flight simulation rigs.

4.3.2.3 Risk: There are three principal categories of risk which have to be considered here:

(1) The technology risks lie in activities such as the design and manufacture of complex wind tunnel models or of an apparently simple but previously untried full scale ground test rig. Such activities, involving innovative devices and/or test concepts incur the risk of a potentially long and expensive development exercise.

(2) There is a risk when considering complexity vs cost trade offs, of over-simplifying the test model. Such simplifications can lead to large errors when projecting model test results to full scale.

(3) The test scheduling risks lie with the scheduling and availability of the relatively scarce specialist (large) wind tunnels, ATFs or flying test beds which may be needed.

4.3.2.4 Accuracy/Credibility: Accuracy involves both the precision of the various measurement systems and any associated bias from their position errors (ie. inadequate pressure profile sampling) and calibration traceability together with the bias from the methodology used, whether experimental or analytical. Precision can usually be predicted adequately beforehand and confirmed after completion of the test. Bias is more difficult to quantify in advance because it includes the inherent bias from the various components of a particular procedure, such as the effect of Reynolds Number on the interference drag obtained from a small scale wind tunnel model or accumulated bias due to linking together the component parts of the propulsion matrix. The projection of model data to full scale must include aeroelastic effects and the linking of the individual contributing factors from the thrust accounting system. The whole question of the total accuracy of a proposed thrust determination route must be examined using the most realistic component accuracy assumptions in order to establish credibility. AIR 1678 may be used as a guide incorporating the turbofan analogy.

4.3.3 Candidate Test Methods

4.3.3.1 Wind Tunnel Model Tests: Wind tunnel experiments are usually performed to determine both propulsion system and airplane performance. The propulsion tests are normally isolated tests of the various thrust contributing elements. The airplane performance tests normally begin with an unpowered clean wing configuration to define a basic drag polar. Installed power tests then allow quantification of mutual interference effects between the propulsion system and the basic airframe. Accounting systems to accomplish this were described in 3.2.2.1. The critical part of relying solely on model data is the potential errors associated with extrapolation to full scale flight conditions.

4.3.3.2 Full Scale Tests (Isolated): Full scale propeller testing at higher flight speeds is normally not conducted because of facility limitations. These categories of test (i.e. Altitude Test Facility (ATF), Wind Tunnel and Ground Test) are in general going to be treated only as a 'scale' correlation link used to extend a complete range of scale model data to the full scale level; unlike turbofan methodology where a 'connected airflow' ATF forms a major part of some of the in-flight thrust determination procedures. This restriction on the usefulness of large Wind Tunnels and ATFs lies mainly in their inability to provide the large 'free stream' airflow required for a full scale propeller test (a connected test is obviously impossible for a propeller).

4.3.3.2.1 Altitude Test Facility (ATF) Tests: In order to minimize or avoid 'wind tunnel' constraint effects on the propeller tip flow (for example) it is necessary to have free stream line flow equivalent to a minimum of $1\frac{1}{2}$ to 2 times the propeller diameter in order to carry out useful ATF tests on a complete (isolated) propulsion system installation (Reference 18). Except in the case of very small propeller diameters, 2 to 3 feet, such testing is beyond the capabilities of even the largest ATFs. It is possible however to accept a small freestream ATF test and use a small scale wind tunnel model to establish the tunnel constraint effects. In addition to the cost of the total exercise, this type of approach exhibits the questionable aspects of complexity, risk, accuracy and credibility factors mentioned previously in 4.3.2.

4.3.3.2.2 Wind Tunnel Test Facilities: There are very few wind tunnels in the world capable of carrying out simulated flight tests on even a moderate size propeller because of speed and size constraints. The largest ones have limitations on available Mach Number. One, ONERA, has the required speed capability, but even its 8 meter test section diameter requires data correction for wall interference.

In addition, these wind tunnels (not being ATF's) have operating temperatures and pressures unrepresentative of altitude flight conditions. A summary of the large wind tunnel facilities in the western world is enumerated in Table 3.

Table 3 - Large Wind Tunnels

Location	Size	Max Mn
NASA Ames	40 ft x 80 ft	0.45
NASA Langley	30 ft x 60 ft	0.11
ONERA (France)	8 M Diameter	1.00
NAE (Canada)	30 ft x 30ft	0.20
DNW (Holland)	9.5 M x 9.5 M	0.18

4.4 Model Test Requirements

4.4.1 Aerodynamic Performance Testing: Model testing for aerodynamic performance may be carried out with a single powered, highly-instrumented model to determine directly the net propulsive force. Alternatively, various increments contributing to the net propulsive force might be tested separately using different models of various scales in different facilities. The case for using a larger propeller for "isolated" propulsion integration model, for example has been discussed in 4.1. In the next sections, the model and measurement techniques which have been used successfully to determine the force components are discussed in detail. In all cases, great care is taken to establish model similitude and correct flow field simulation.

4.4.1.1 Rotor Thrust and Torque: Basic measurements are obtained from a rotating force balance which measures thrust and torque of the propeller and spinner. These rotating force balances are custom-designed for each installation. The design of such balance systems is a field of specialization and requires considerable time to produce a finished design. The rotating balance system requires extensive calibration to establish the operating procedures and techniques and establish the confidence of the operating personnel. The desired accuracy of the rotating balance system is usually 0.10% of full scale. (Experience indicates that 0.5% is more realistic.)

4.4.1.2 Determination of Propeller Net Force: This term is defined as the propulsive force of the propeller blades operating in the presence of the spinner and the nacelle flow field without the increase in thrust from the mutual interaction between the propeller blades and the spinner nacelle combination. It is necessary to conduct separate tare tests without the propeller blades to evaluate the external spinner aerodynamic drag and the nacelle pressure drag.

In the tare test, the spinner and propeller blades are replaced by a separate "dummy" hub which is faired to a smooth, continuous contour in the vicinity of the blades. A special series of experimental runs are made to define the spinner aerodynamic and nacelle pressure drag for the same range of test Mach numbers as would be tested with the model blades. The spinner drag ($D_{s,T}$) is measured directly from the force balance and corrected for the pressure-area forces on the internal cavity of the spinner,with the hub rotating. The nacelle pressure drag ($D_{nac,T}$) is determined by integration of the longitudinal, area-weighted static pressure orifices on the nacelle surface. Figure 39 shows the appropriate tare and blades-on forces.

In Figure 39a, summing the forces yield the following set of equations:

$$\sum F = 0 \quad (\rightarrow +) \tag{74}$$

$$D_{s,T} = -\sum pA_{int,T} + F_{bal,T} = 0 \tag{75}$$

$$D_{s,T} = -\left(F_{bal,T} - \sum pA_{int,T} \right) \tag{76}$$

$$D_{nac,T} = \int (p_{nac} - p_0)\, dA_{nac} \tag{77}$$

Where: p_{nac} is the local nacelle static pressure measurement.
p_0 is the reference static pressure.

With the propeller blades installed and thrusting, the force balance measures the algebraic sum of the propeller thrust, the spinner drag, and the internal pressure area forces. The model forces are as shown in Figure 39a.

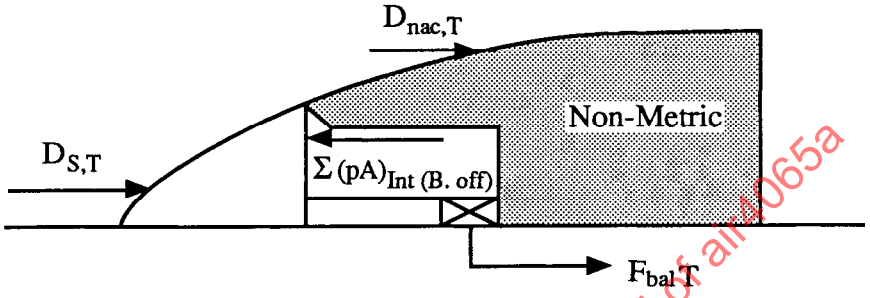

a). Blades-off Configuration

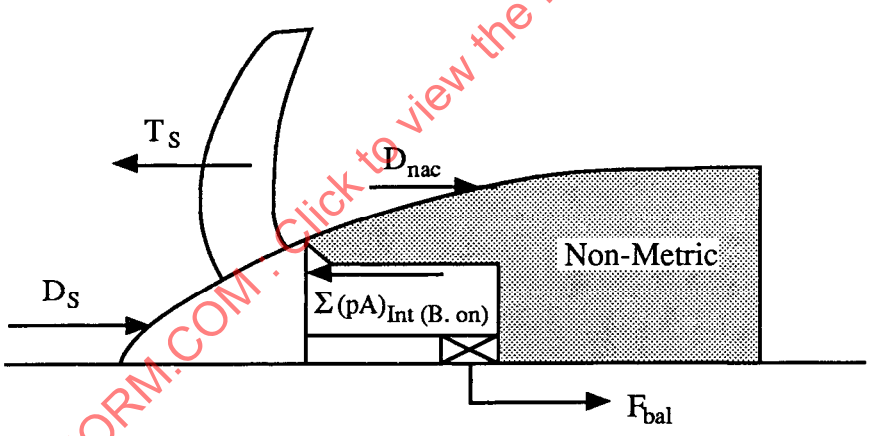

b). Blades-on Configuration

D_{nac} = Nacelle Drag Force
D_s = Spinner Drag Force (Pressure Drag + Skin Friction Drag)
F_{bal} = Balance Reading
$\sum pA_{int}$ = Pressure Force on Rear Spinner Face
T_s = Apparent Propeller Thrust

Figure 39 - Model Propeller Test with Hub Force Balance

$$\sum F = 0 \quad (\rightarrow +) \tag{78}$$

$$- T_s + D_s - \sum pA_{int} + F_{bal} = 0 \tag{79}$$

$$T_s - D_s = F_{bal} - \sum pA_{int} \tag{80}$$

Add equations (76) and (80):

$$T_s - D_s + D_{s,T} = \left(F_{bal} - \sum pA_{int}\right) - \left(F_{bal,T} - \sum pA_{int,T}\right) \tag{81}$$

Let $\Delta D_s = D_s - D_{s,T}$ and substitute:

$$T_s - \Delta D_s = \left(F_{bal} - \sum pA_{int}\right) - \left(F_{bal,T} - \sum pA_{int,T}\right) \tag{82}$$

The objective of the propeller test rig (PTR) is to determine as accurately as possible the isolated blade thrust, $T_{S,ISO}$, excluding any hub forces. In practice, a slipstream induced force increment may be implicit in the $T_{S,ISO}$ force measured in PTR experiments. For our purposes we will include the induced slipstream force component in the $T_{s,iso}$ term.

Finally define $T_{s,iso}$ = isolated blade thrust and

$$T_{s,iso} = \left(F_{bal} - \sum pA_{int}\right) - \left(F_{bal,T} - \sum pA_{int,T}\right) \tag{83}$$

Next, the nacelle pressure drag is obtained from the integration of nacelle surface pressure measurements:

$$D_{nac} = \int \left(p_{nac} - p_0 \right) dA_{nac} \tag{84}$$

The change in nacelle pressure drag, ΔD_{nac}, is obtained from the difference between the test run and tare run data:

$$\Delta D_{nac} = D_{nac} - D_{nac,T} \tag{85}$$

Finally, the net thrust, F_{net}, is determined from the isolated propeller thrust, $T_{s,iso}$.

$$F_{net} = T_{s,iso} - \Delta D_{nac} \tag{86}$$

Or in terms of apparent propeller thrust, T_s:

$$F_{net} = T_s - \Delta D_s - \Delta D_{nac} \tag{87a}$$

It is important to note that $T_{s,iso}$ is a "blades-only" thrust and is ideal for screening individual blade designs during the development phase of a turboprop propulsion system. F'_{net} is also a "blades only " but includes the effects of the nacelle on the isolated rotor thrust. F'_{net} can be combined more directly with a nacelle drag estimate to obtain a propulsion system thrust minus drag value.

4.4.1.3 Alternate Propeller Net Force Determination: The net thrust of the propeller may be measured with a wind tunnel test rig in which the propeller and nacelle forebody are mounted together on a balance. The buoyancy forces arising from interaction between these components are then eliminated by mutual cancellation. Nacelle forebody base pressures are measured to correct the balance data. A nacelle base drag is established for the spinner and nacelle prior to mounting the propeller blades. The model forces are shown in Figure 40.

Therefore using the Figure 40 balance arrangement, F_{Net} is calculated as follows:

$$F_{net} = F_{bal} + (D_{nac,T} + D_{s,T}) - \Sigma p A_{int} \tag{87b}$$

$$= F_{bal} - F_{bal,T} - \Delta\Sigma p A_{int}$$

(87c)

4.4.1.4 Net Rotor Efficiency: The net rotor efficiency can now be calculated from the expression:

$$\eta_{net} = \frac{F'_{net}\, V_0}{\text{Shaft Power}} = \frac{C_{Tn}\, J}{C_P} \tag{88}$$

It can be seen in equation (88),that the rotor net efficiency is a function of freestream velocity. Consequently, it is important to accurately measure the freestream velocity in the test section at the plane of the model propeller rotor to obtain the accuracy desired. In recent experiments conducted at the NASA Lewis Research Center, it has been estimated that the net efficiency was repeatable within 0.5% or less. This value is indicative of the repeatability of the combined effects of the rotating balance system and the variation of the local freestream

velocity in the test section of the wind tunnel (Reference 13). Usually several model propeller blades are instrumented with strain gages and their impact on performance must be accounted for. This correction term is of the order of 0.40% to 0.51% for the experiments conducted at NASA-Lewis (Reference 14).

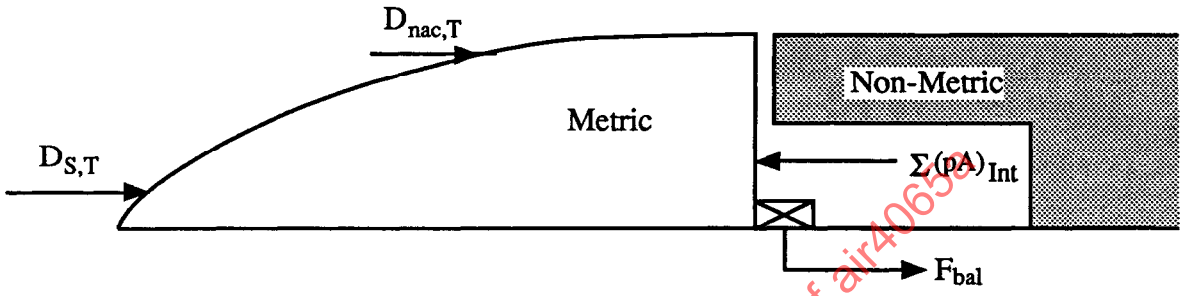

a). Blades-off Configuration

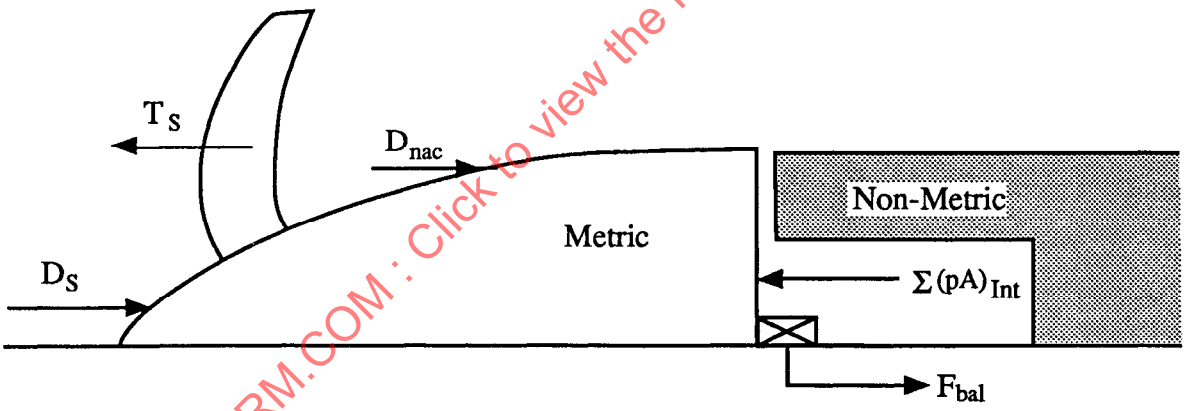

b). Blades-on Configuration

D_{nac}	= Nacelle Drag Force
D_s	= Spinner Drag Force (Pressure Drag + Skin Friction Drag)
F_{bal}	= Balance Reading
$\sum pA_{int}$	= Pressure Force on Rear Spinner Face
T_s	= Uncorrected Propeller Thrust

Figure 40 - Alternate Model Propeller Test with Hub Force Balance

4.4.2 Flow Field Investigation:

4.4.2.1 Flow Field Measurements: The spanwise distributions of the thrust and power coefficients as computed from the probe data can be used to determine if the propfan blades are being loaded as designed and to suggest possible explanations for any discrepancies which may occur between the predicted and measured performance. In order to obtain detailed information of the flowfield downstream of the model propeller, a translating wake survey probe is used to measure the radial distributions of static and total pressure and total temperature in the wake of the propeller for a series of different tunnel and model operating conditions. When combined with the tunnel freestream conditions, these measurements are used to compute the spanwise distributions of elemental thrust and power coefficients, $dC_T / d(r/R)$ and $dC_p / d(r/R)$. The radial distributions of axial, radial and tangential velocity and the wake flow angularity are also obtainable from these measurements. The probe measurements, therefore, provide a more detailed understanding of the propfan performance than can be obtained with the rotating balance, which provides only the integrated thrust and power coefficients, C_T and C_p. The probe should measure total temperature, total pressure, static pressure, and flow angle. A typical probe is shown in Reference 17.

4.4.2.2 Flow Field Visualization Techniques: It frequently becomes desirable to examine the flow across the propeller blades to determine if vortex flow or local flow separation is present. This is most readily done by employing various methods of flow visualization. One method involves coating the blades with fluorescent oil and operating the propeller at the desired condition. After the propeller returns to rest, the blades are illuminated with an ultraviolet light source. The surface flow patterns are clearly visible and the separated regions and vortex patterns are readily discernible. The method is described in more detail in Reference 16.

Fluorescent "mini-tufts" are used to examine the blade surface flow patterns on a rotating propeller. Small "mini-tufts" of nylon having the approximate dimensions of .001 inch dia. x .5 inch long are attached to the propeller blade surface. These tufts are coated with a fluorescent compound. The propeller is illuminated with an ultraviolet flash while the blades and tunnel are at operating conditions and photos are taken. The resulting photographs indicate the blade surface flow condition at operating conditions. Additional details are contained in References 15 and 16. A chemical sublimation technique is also described in

Reference 14 and is useful in locating boundary layer transition locations and possibly separated flow regions.

Frequently it becomes necessary to examine local shock wave structure in the vicinity of the propeller tips. One method is to employ a conventional Schlieren system in either the continuous or flash mode. The resulting shock wave patterns are then used as a diagnostic tool to study the blade loss mechanisms and interference of the shock wave system with the model support. Another method is to use a Paint Flow Technique described in References 17 and 19.

4.4.3 Facility Considerations -Wind Tunnel Blockage: The conditions under which wind tunnel models are tested, as compared to those in free air, differ primarily because of the constraints imposed by the physical boundaries of the tunnel walls. There are three types of wind tunnel test sections that shall be discussed, each presenting its own problems. These different configurations are closed, ventilated (slotted or porous), and open or free jet. The wall corrections that need to be made are the greatest in the closed section and decrease in amount as we move toward the free jet. The two most important corrections that need to be looked at for a thrusting model are as follows; 1. Solid Blockage - The reduction in wind tunnel cross sectional area due to the model in the test section, leads to an increase in the velocity of the air flowing around the body. In a solid wall wind tunnel, this blockage has the effect of an increase in dynamic pressure. To contrast the wind tunnel extremes in an open test section, where the airflow is free to expand around the blockage, this effect is minimal (Reference 17, also see par. 4.5.3 & Figure 42) and has even an opposite effect on the model nacelle forces. In solid wall wind tunnels the effect of this blockage limits the size of the model that can be tested at high subsonic speeds. 2. Wake Blockage - Any model in an airflow will produce a wake behind it. Because of energy losses associated with this wake, the velocity will be below that of the freestream. In view of the law of continuity, the airflow outside the wake will have an increased velocity and has the effect of increasing the drag on the model. For an open test section this effect is usually negligible since the airflow is free to expand around the model (Reference 17, also see par. 4.5.3 & Figure 42)

The interference experienced by a propeller in a wind tunnel is somewhat different than that of other models in that a thrusting propeller produces a stream of

increased velocity behind the propeller model. Because of the continuity of the flow in the wind tunnel, a region of decreased velocity and increased static pressure surrounds the wake. This condition behind the propeller reacts back to change the relationship between thrust and the rate of advance of the propeller for a given rate of rotation. The use of an equivalent free airspeed to represent the tunnel interference has been developed by Glauert (Reference 18) and Pope (Reference 17). This equivalent free airspeed is valid only when the propeller is operating at a positive rate of advance (forward thrust) or when it is acting as a windmill with a slipstream of conventional type but reduced velocity.

In particular, the static condition (zero rate of advance) cannot be reproduced, since the propeller itself will induce a flow through the tunnel. Problems also exist for determining the behavior for a propeller operating with negative thrust. Instead of finding an "equivalent free airspeed", Milne-Thomson (Reference 19) computed the correction to the thrust due to the improper expansion of the slipstream.

Several deficiencies in the classical theories are apparent. First, only solid wall tunnels are considered. Most modern wind tunnels use slotted or porous test sections to minimize wall interference effects. Also, the consequences of allowing mass flow through the tunnel walls is not considered. Effects caused by compressibility are also not considered in these theories, although work on this has been done by Young (Reference 23). The presence of a nacelle and supporting structure are not taken into effect. Yet any blockage effects are important. Finally, the tunnel interference effects change with tunnel speed and are substantially higher at transonic speeds than in the low speed range. See Appendix D for further details on this and wind tunnel safety issues.

4.5 Validation/Adjustment Techniques

The calibration techniques for turbofans using a connected (i.e.. without freestream flow round the engine) altitude test facility (ATF) test series linked to an outdoor static test is a fundamentally good one. It does not involve scale or Reynolds number factors in the 'flight' envelope tests; ram ratio and thus nozzle pressure ratio are the only things which change in the transfer from ground

(static) to flight conditions. The following full scale turboprop calibration test techniques are available for comparison with appropriate scale model tests.

4.5.1 Outdoor Test: The propeller outdoor test is analogous in principle to the outdoor ground test on a turbofan and should be similarly free of thrust bias. However, there are a number of features which have to be considered before undertaking this type of test; 1) The large inlet airflow stream tube makes the involvement of ground boundary layer (and consequent vorticity) effects probable. The use of a ground vortex mat would avoid a local vortex filament but the general ground effect would still be there and would have to be represented in the model testing. 2) The lack of a ducted inlet to the propeller leaves measurement levels and stability vulnerable to even the smallest variations in strength and direction of the natural winds. 3) Under static conditions, the performance of a propeller, which is dependent on forward speed, is different from that in normal flight operation. Even if the blade tip flow is not stalled, there is a migration of propeller blade boundary layer along the blade due to the greater centrifugal forces. This boundary layer effect will be influenced by Reynolds number, making direct comparisons (or calibrations) with scale model propellers difficult if other differences exist. A major problem is the confusion of the effects of incorrectly identified blade flexibility with actual Reynolds number effects. Most models of course can be regarded as being rigid but very large models which undergo deformation may add to the uncertainty level.

4.5.2 Large Wind Tunnel Test: A turboprop test in a large wind tunnel was noted in Section 4.3 to be less than ideal as an element of determining inflight thrust . One, however the ONERA wind tunnel at Modane, France has sufficient size to accommodate large propulsion systems and operate at cruise mach number approaching 1.0. It could therefore be used as a proof of methodology test to validate sub-scale projections to full scale. Even though it has a large test cross section (8 meter diameter), model corrections would still be needed, namely testing scale models in a wind tunnel and in an isolated environment to get appropriate corrections for wind tunnel constraint effects. Full scale tests in this wind tunnel will have compressibility effects, but Reynold's Number adjustments will still be required. It should be noted that these tests are quite expensive which would probably limit the number of tunnel runs/entries.

4.5.3 Altitude Test Facility (ATF) Freejet Tests: As explained by H. Glauert (Reference 18),"it is to be expected that the tunnel constraint on an airscrew in a free jet will be negligibly small since the stream surrounding the slipstream can contract and thus maintain the same velocity and pressure as the undisturbed stream in front of the airscrew." Glauert further states that "...the interference of an airscrew in a freejet does not become appreciable until the diameter of the airscrew exceeds 60 percent, or perhaps even 70 percent, of the diameter of the jet.'

The freejet test concept is used in today's propulsion altitude test facilities to provide the means to simulate flight external flow conditions and patterns which occur within the aircraft operating envelope. Freejet flow simulation is accomplished using an air supply plant to condition the intake air to the pressure and temperature representative of the flight airspeed and altitude, a nozzle to shape and guide the flow to the desired flight airspeed and aircraft altitude and an exhaust plant to maintain the test cell at the proper altitude static pressure.(Figure 41). To date, ATF freejet facilities have primarily been employed for ramjet and turbojet missile system tests with limited propeller engine and propeller unit tests.

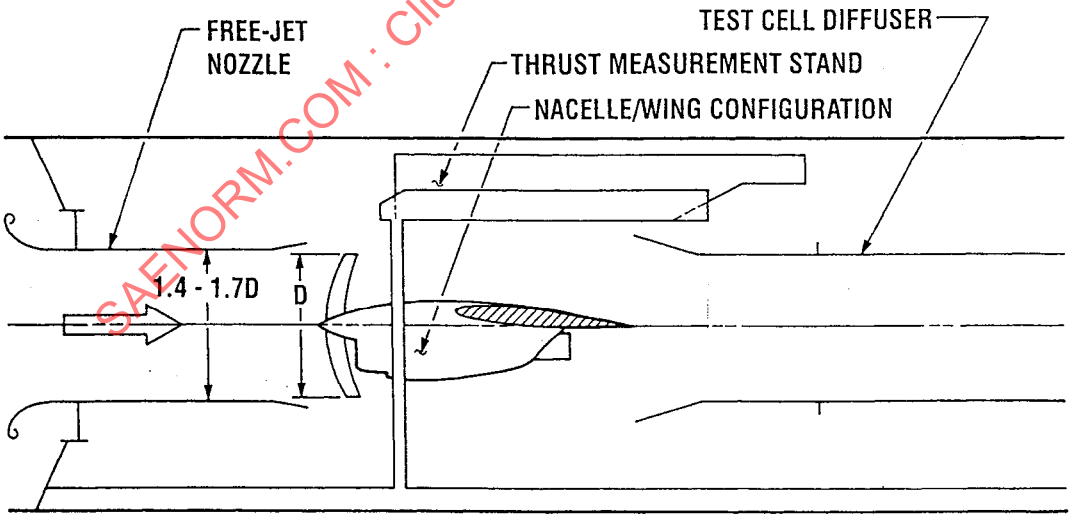

Figure 41 - Turbo-Prop/Engine Freejet Test Installation Schematic

A freejet test installation used for an aircraft with a 7.5 ft diameter, three bladed constant speed propeller is presented in Figure 42. The aircraft fuselage was installed in the test cell with the centerline of the propeller aligned with the air supply duct and the propeller plane one foot downstream of an 8.5 ft exit diameter air supply nozzle. The divergence of the air supply nozzle from 8 to 8.5 ft diameter was intended to relieve the upstream air blockage effect from the spinner. The aircraft wingmounts were used to support the fuselage on shock mount fixtures located in the test cell. The test cell mounting fixtures had a six degree pitch capability from the horizontal plane. A propeller wake survey total pressure rake with seven probes was used to measure the total pressure profile behind the propeller. Although the propeller to freejet diameter ratio of the test exceeded Glauert's guidelines (i.e., 0.88 vs. 0.6 -0.7), the total pressure survey immediately down stream of the propeller produced profiles which compared favorably with flight test results (Figure 42). These results are not absolute proof of the facility viability, but does show promise that a free jet may provide acceptable results in a low speed regime.

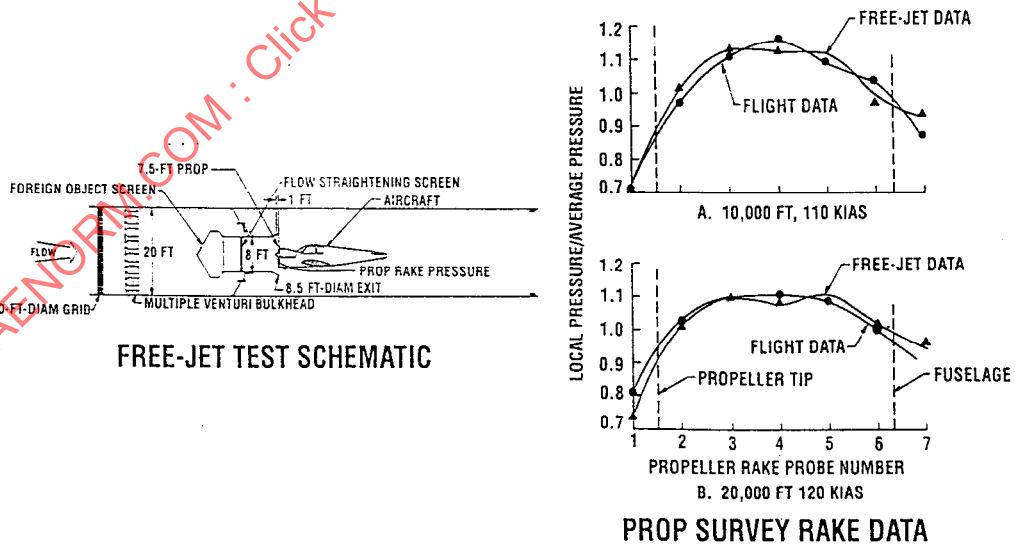

Figure 42 - Comparison of Propeller Wake Survey Data

A freejet test installation used in an altitude performance evaluation of a propeller driven ram air turbine (RAT) unit is presented in Figure 43. The RAT was a four-bladed, axial-flow variable pitch turbine with a propeller blade diameter of twenty-one inches. The RAT was mounted on a support cart which could be remotely positioned along fixed guide rails. During the tests, an airstream survey rake was used to correlate air speed in the flow nozzle with the airspeed profile at the propeller inlet. The propeller to freejet diameter ratio used for this test was 0.5. No direct flight flowfield data were available for comparison with the freejet flow simulation; however, the turbine power output performance for the ground and flight tests were the same throughout the entire operational envelope.

A proposed freejet installation for a full-scale, propfan-powered cruise missile which uses an integrated thrust balance measurement system is shown in Figure 44. The force balance system employed is similar in concept to the force balance systems used in wind-tunnel model tests.

An advanced freejet test facility concept that can be used to support propeller testing is under development at the Arnold Engineering Development Center (Figure 45) and is scheduled to be operational in early 1992 (Reference 24). This facility has a combined capacity to test full-scale engines and vary freestream flow Mach number and flow angularities at rates representative of today's subsonic cruise missles. The facility's freejet flow field is provided with a subsonic nozzle which has an exit area of 77 ft^2 with and aspect ratio of 0.72. The nozzle attitude positioning mechanism provides continuous nozzle pitch capability from 45 degrees positive to 10 degrees negative with a combined yaw capability of plus or minus 10 degrees. Using Glauert's criteria, the facility with the 77 ft^2 nozzle can test an engine with a 4 - 5 ft propeller diameter. The facility freejet operational envelope with the 77 ft^2 subsonic nozzle is shown in Figure 46. This same facility also has an auxiliary test leg that, based on Glauert's criteria, can test a nominal 8 ft diameter propeller at 0 degree pitch and yaw attitude. It should be pointed out that this technique has not been validated for high speed propeller performance. Validation of the methodology with a subscale freejet and wind tunnel testing may be required.

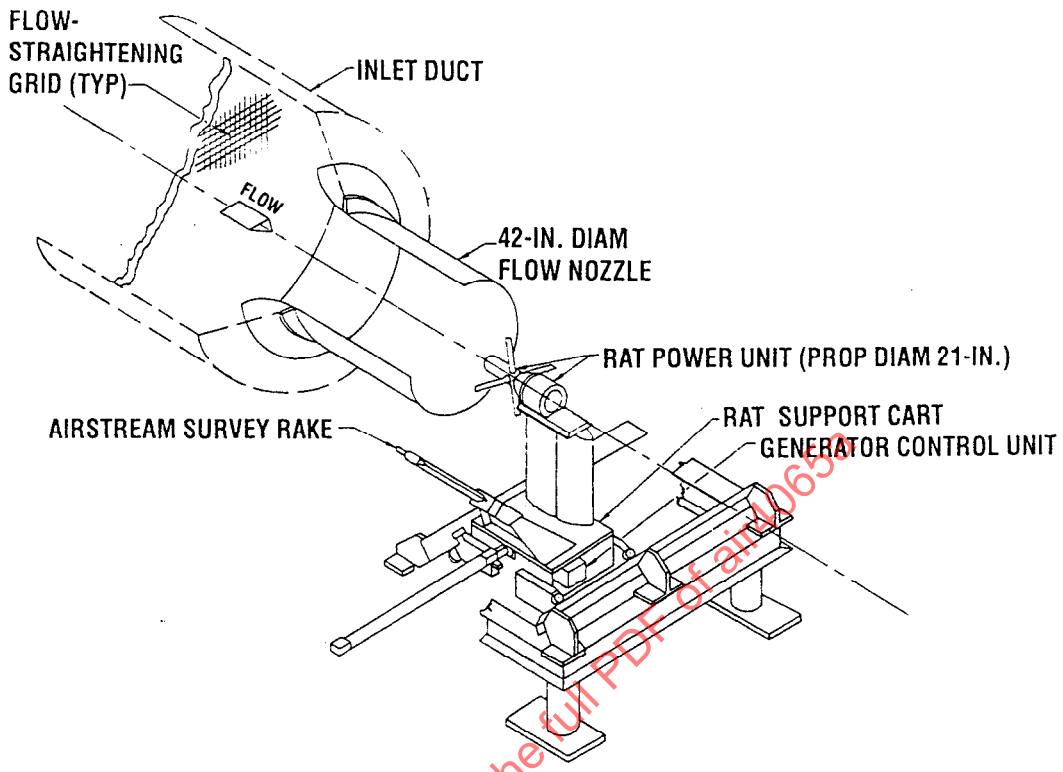

Figure 43 - Freejet Ram Air Turbine Test Installation Schematic

4.5.4 Full Scale Self-Powered Rig: The concept of such device is shown in Figure 47; it can function as a calibration vehicle in the same manner as the large wind tunnel of Figure 48 but with the advantages of on-site availability and relative cost. Figure 48 shows how it or a large wind tunnel function in the process of calibrating small scale wind tunnel model data and extending it over the flight envelope at full scale. The rig imposes constraints on the propeller operation, compared to 'free air' or a good wind tunnel and these effects have to be identified by a separate exercise (see Figure 49)

Three other points should be mentioned: 1) A design data bank does not exist specifically for a self powered rig, therefore a certain amount of caution should be exercised in the initial design. Additionally a propeller is a poor compressor, i.e. the static pressure rise through the disk is small. Since the rig is an open

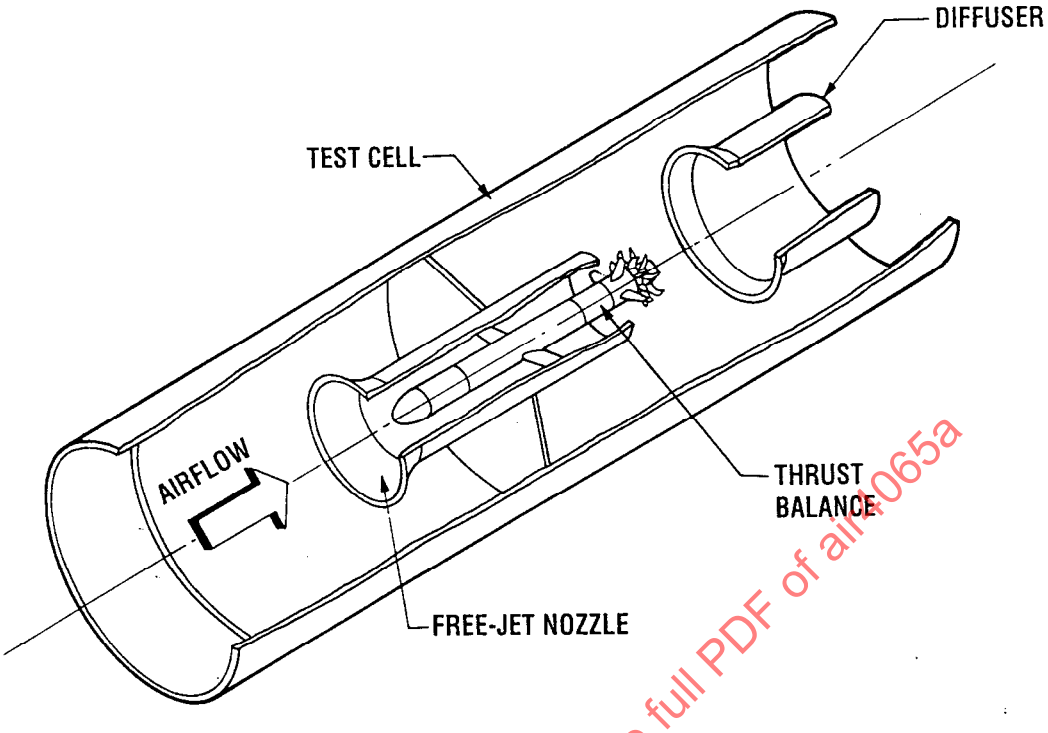

Figure 44 - Proposed Propfan Cruise Missle Freejet Test Installation Schematic

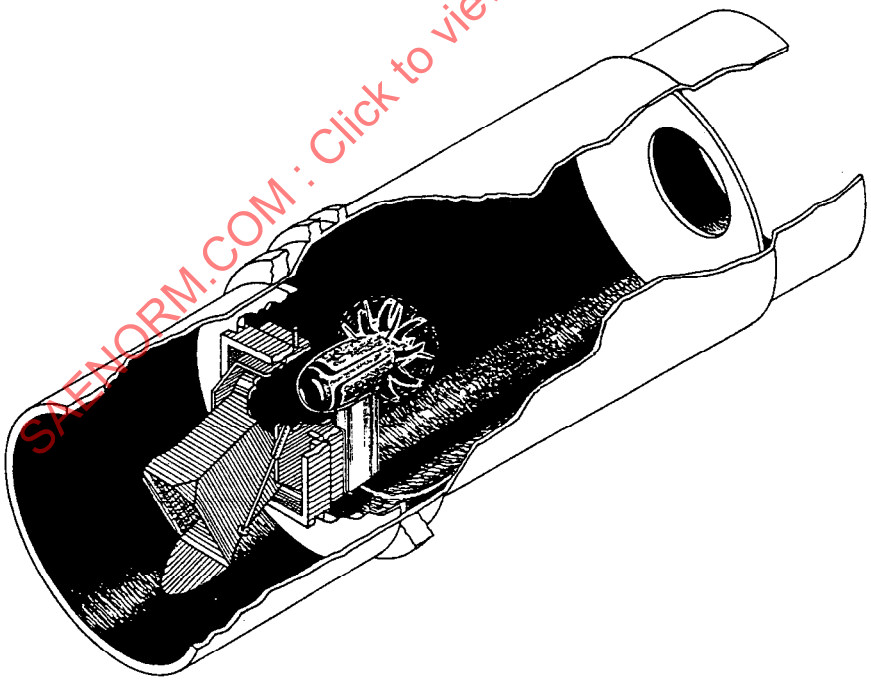

Figure 45 - AEDC Subsonic Freejet Installation with Pitch/Yaw Capability

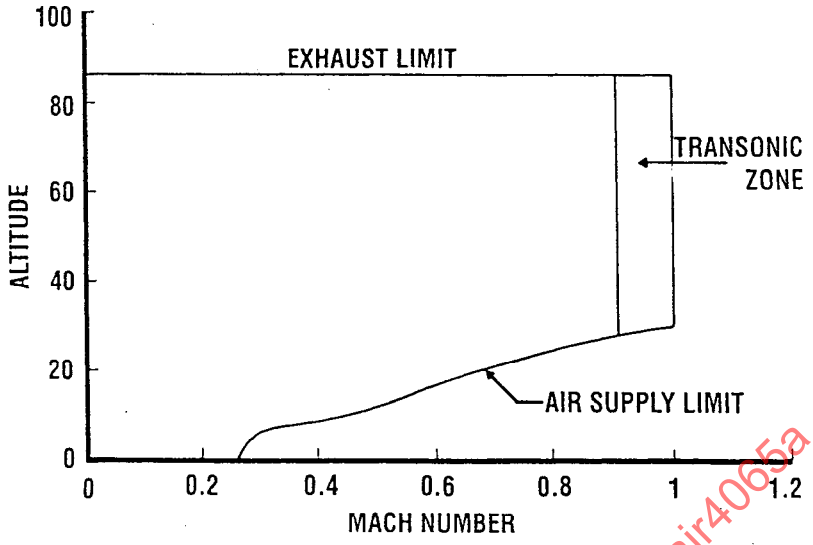

Figure 46 - AEDC Freejet Capability with 77 ft^2 Subsonic Nozzle

circuit device, with the air starting and finishing at ambient static pressure, total pressure losses in the circuit should be minimized, requiring that flow straightening devices, silencing devices and turbulence control devices be very carefully designed. The flow process may be usefully enhanced by incorporating an efficient diffuser in the exhaust system. It can be seen that

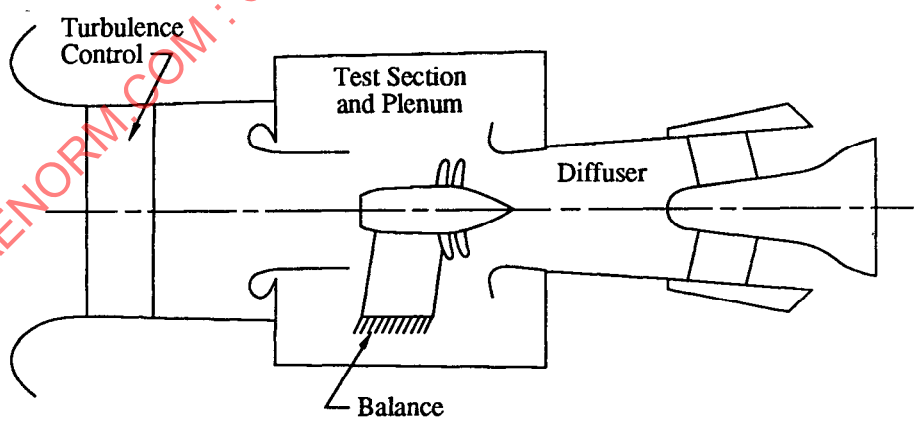

Figure 47 - Full Scale Self Powered Rig

the effective 'forward speed' produced depends on the success of the detail design and the precise degree of simulation may not be known until first test. 2)

Mechanical resonance, induced by 'organ piping' may be a community noise problem, as well as a mechanical problem, requiring a separate development

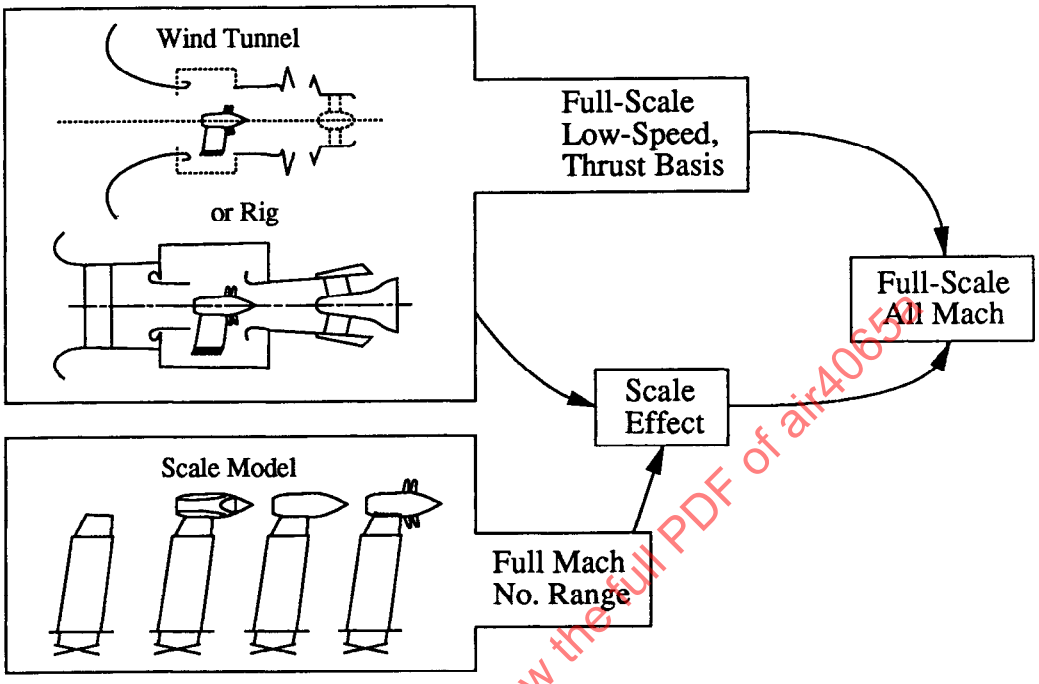

Figure 48 - Thrust Substantiation

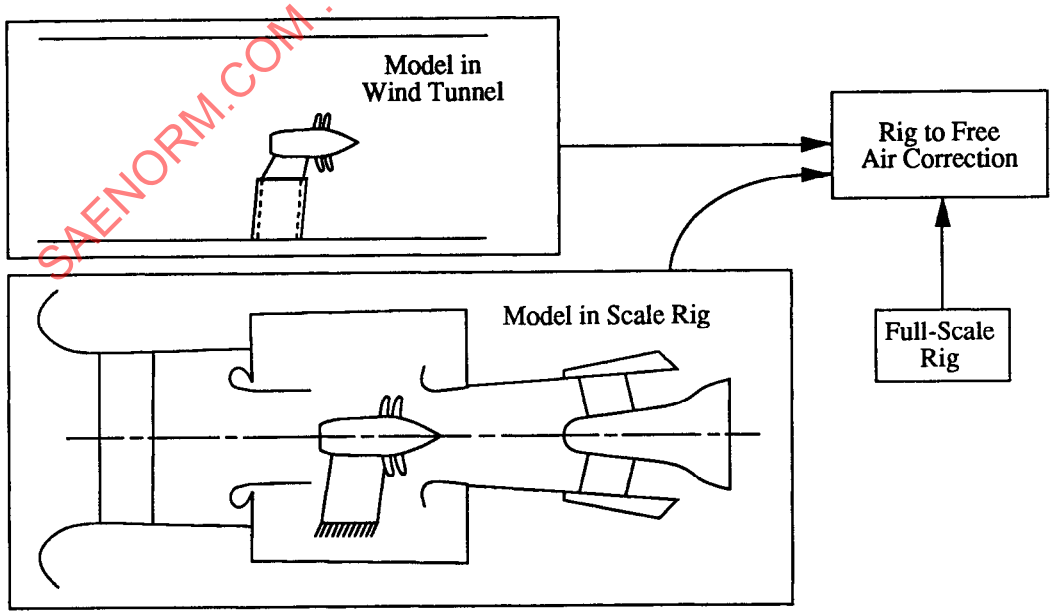

Figure 49 - Rig to Free Air

program on the rig itself. 3) The calibration procedure is complicated, involving a prior calibration of rig constraint effects. As with the large wind tunnel calibration procedure, there is the danger that the genuine scale effects (Reynolds number and manufacturing details) may be obscured or corrupted by poor flexibility simulation of the scale models.

4.5.5 Aircraft Flight Tests: The large propeller stream tube requires a thorough examination of the interference effects between propeller/nacelle and powerplant/aircraft using wind tunnel model and/or analytical techniques. When accomplished, it is possible to relate propeller speed, pitch and power to powerplant net thrust.

Direct measurements of pylon (strain-gauged) thrust or propeller wake (traverse) momentum are not only difficult but of limited use because of mechanical/flow interferences. It can be seen from the foregoing that an aircraft measurement procedure can exhibit all the uncertainties of Section 4.3.2. It can however provide a potentially satisfactory result if a means of resolving the differences between aircraft drag and powerplant thrust which occurs because of mutual interference is logical and available. General guidelines for flight testing are discussed in Section 5.0.

This Page Intentionally Left Blank

5 FLIGHT TEST APPLICATION SUGGESTIONS:

Flight testing of an instrumented aircraft and propulsion system is the final step in the thrust determination process. It is through careful flight testing that the integrated values of thrust and drag used to develop the aircraft performance model do, in fact, accurately describe the aircraft performance. If flight test data and analytical model predictions disagree, further tests or analytical rationalization should be pursued until a reasonable degree of agreement is reached. This section addresses the basic requirements and some considerations which should be observed to extract the maximum benefit from the flight test validation portion of the thrust prediction process.

Historically, there have been several propeller powered aircraft programs that attempted to compare the in-flight thrust projection based on propulsion system data to the in-flight thrust implied from airplane drag characteristics. In general these attempts resulted in a thrust estimate discrepancy of several percent. The open literature is void of information where these discrepancies were resolved or attempted to determine if the inaccurate projection was attributable to the propulsion thrust prediction or to the airplane drag prediction. In all cases the difference was attributed to an undefined airplane/propeller interaction and the total aircraft system performance was adjusted accordingly.

This document attempts to present methods of determining in-flight thrust for the propeller/propfan propulsion system including the mutual interactions between the airframe and propulsion system. The practices and procedures associated with the determination of aerodynamic characteristics are beyond the scope of this document. AIR 1703, Appendix C (Aerodynamic Characteristics and In-Flight Drag Determination) presents methods for determining turbofan powered drag characteristics. The performance of the propulsion system is determined by ATF tests and based upon this the airframe drag is determined. In the case of the propeller/propfan propulsion system, the interactions of the propulsion system on the airframe and the airframe on the propulsion system may preclude the validation of the propeller/propfan system by ATF testing and requires a build up of the propulsion system increments.

Propulsion system and airframe scale model tests may be required to form the basis of an accounting system for the validation of flight test results. These models must be as large as practical to minimize Reynolds number effects.

5.1 Fundamental Program Requirements:

There are two basic requirements for a successful flight test performance validation program; 1) An appropriate analytical model must exist. 2) The flight test program should be meticulously conducted using appropriate procedures and equipment. Comments regarding these two requirements are presented below.

5.1.1 Basic Analytical Model Requirements: The following factors regarding the analytical model should be considered prior to initiating a flight test program.

5.1.1.1 Analytical Model: The analytical models are normally developed from a combination of airframe and propulsion system performance, analytical estimates and wind tunnel test results. When complete, they should provide the two following basic functions; 1) The propulsion model should predict the thrust available from the propulsion system for all operating conditions. This propulsion simulation combines the engine and propeller characteristics and predicts the available thrust for any aircraft operating condition. Essentially, this simulation calculates the available shaft horsepower from the engine parameters that will be monitored during the flight tests. The engine simulation may be presented in the form described in Reference 4. The simulation then converts power to propeller thrust using either the J or Theta method. Secondary propulsion system thrust/drag effects, such as core thrust, are also included in the analytical model.

2) The airframe analytical model should describe the aero force and moment characteristics of the aircraft for all operating conditions, including the effects of the numerous interactions of the propulsion system. This portion of the analytical model is usually presented in the form of drag polars, or lift/drag characteristic plots. Discrete polars are generated for each significant aircraft configuration or condition (e.g. gear, flap and spoiler positions, Mach number, etc.). Aircraft performance may then be predicted by combining these two portions of the model.

5.1.1.2 Documentation: The data, procedures and (wind tunnel) test results used to develop the model should be clearly recorded. This foundation provides an easily traceable path in the event that later investigation are required to resolve disagreement between the model and the flight test data.

5.1.1.3 Model Availability: It is advisable to have the analytical model well defined prior to the initiation of the flight test. This allows the performance engineers to review factors which may potentially affect performance and thus guide decisions on the types of instrumentation and tests to conduct.

5.1.1.4 Bookkeeping: The airframe and propulsion system performance engineers should agree on the form of the model and on the book-keeping system to be used. This agreement should help focus efforts on the resolution of later problems and help to avoid unproductive disagreement on how to handle potential model/flight test differences. Reference 4 provides nomenclature which can be used to standardize the model description.

5.1.2 Basic Flight Test Program Requirements: Two general categories of testing are usually involved in the performance validation process. The first category includes all flights and ground calibration which are required to establish the detailed effects on thrust and drag of significant aircraft components. These tests should include, but not limited to the following:

Aircraft static pressure instrumentation calibration

Engine air inlet ram recovery and temperature rise tests.

Engine exhaust flow characteristics measurement tests.

Aircraft outside air temperature probe calibration tests.

Flow field surveys, particularly in the propeller flow field.

Engine heat exchanger cooling flow effects.

(See Appendix B for additional items)

Many other detailed tests may be necessary depending on the potential effects of each component. In more elaborate programs, tests may be conducted to investigate the effects of most of the factors identified in Paragraph 3.2.3. In many practical cases, these tests are limited, however, by schedule or cost restraints.

The second category of flight test includes the flights dedicated to total aircraft performance measurement. This type of test provides the data required to determine the basic lift and drag characteristics of the aircraft for particular conditions. The following paragraphs provide further discussion of the flight test data, instrumentation and methods required.

5.2 Flight Test Data Required:

There are several types of flight test that can be performed to determine in-flight thrust. (Reference AIR 1703) Level cruise operation with appropriate airplane wind tunnel drag data gives a direct indication of the propulsion system net thrust. Climb gradients and rates of acceleration also provide an indication of the propulsion system thrust. There are two approaches that can be pursued to determine the net thrust 1) Aircraft characteristics can be measured and adjusted with appropriate wind tunnel data to quantify the airplane drag, hence inferring a propulsion system thrust. 2) Measure the pertinent engine parameters and after adjustments with appropriate propulsion wind tunnel model data project what the propulsion system thrust is. If executed correctly these two approaches should yield the same answer within uncertainty constraints.

5.2.1 Aircraft Aerodynamic Data: In virtually all flights, the basic aircraft operating condition should be defined. This includes the aircraft configuration and the basic aerodynamic condition of the aircraft. The aircraft configuration data includes a record of the aircraft weight and center of gravity and the configuration of flaps, gear and spoilers. Figure 50 illustrates the relation of the sensed parameters to the calculated parameters for the basic aerodynamic data including airspeed, altitude and temperature. This relation is valid not only for the general aircraft flowfield, but for instrumentation in other specific flow field, such as the engine air inlet.

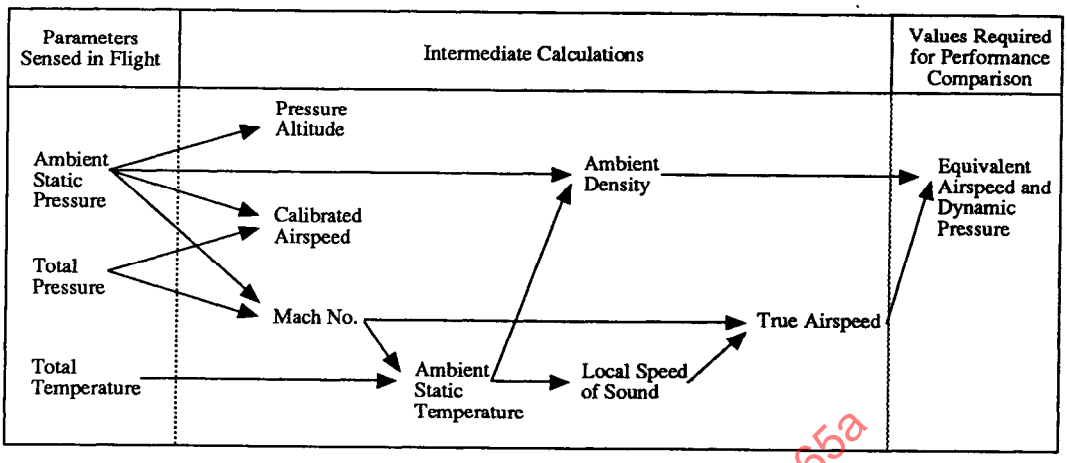

Figure 50 - Relation of Sensed Parameters to Required Performance Aerodynamic Data

5.2.2 Propulsion System Data: All flight tests pertaining to performance should acquire data which defines the propulsion system condition. This includes the following typical parameters which may be derivations and /or measurements:

Basic condition of each engine (operating, windmilling, feathered)

Basic power output level

Shaft power

Shaft rotation speed

Shaft torque

Accessory power extraction

Bleed air extraction

Secondary power output level

Exhaust thrust

Significant Drag Parameters

Cooling system

Vents

Excrescences etc.

Other power setting or measuring data is also normally recorded. This data provides information required to set power (in flight test and later in normal operations) and it provides data relating to engine health. Examples include:

Engine fuel flow
Engine turbine temperature
Engine rotor speeds
Propeller blade angle

Figure 51 illustrates the relation between the basic propulsion system operational measurements and the parameters normally used for thrust determination in the analytical model.

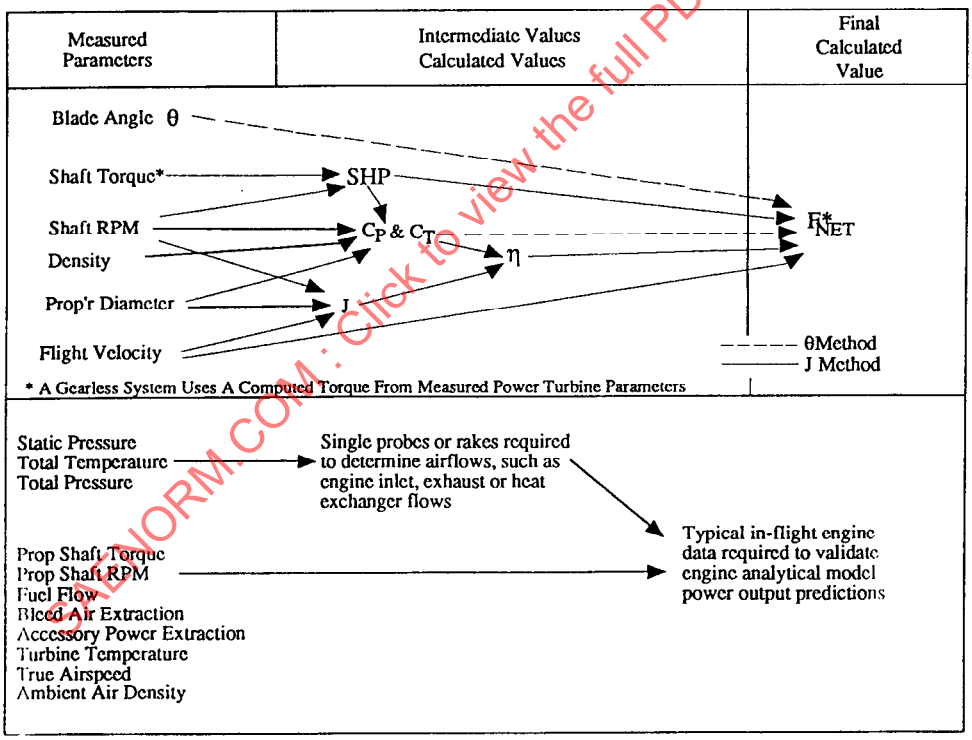

Figure 51 - Relation of Measurements to Parameters Required for Thrust Determination

5.3 Instrumentation Considerations:

Although the instrumentation package for a performance measurement flight may be quite sophisticated, including automated acquisition and telemetry capabilities, the basic guidelines for this equipment are relatively easy to define. They include:

The sensors should have proper range.

The sensors should be sufficiently rugged for the purpose.

The sensors should be unobtrusive, thereby causing minimal changes to the parameter being measured.

The readout, or acquisition/readout, equipment should not introduce significant errors and should provide legible displays with appropriate engineering units.

Several documents exist which provide details regarding the selection and use of instrumentation systems. Reference 5 provides typical installation requirements for the engine instrumentation. References 6 through 11 provide general information pertinent to basic airframe instrumentation (airspeed, altitude and temperature) required for performance testing. Reference 21 contains definitions of standard temperature measurement nomenclature which apply to both the airframe and the propulsion systems.

5.4 Flight Test Methods:

Specific discussion of flight test methods are contained in Reference 21 and Reference 22. A brief review of these tests is presented below:

5.4.1 Cruise Speed/Power Flight Test, Steady State Cruise: This type of test requires the aircraft to be stabilized in level, cruise flight while airspeed and power data is taken. Data is taken at various power settings between maximum and minimum at each of several altitudes. This data is then reduced to the drag polar format for comparison to the analytical model. The balance of thrust and drag elements resulting from this maneuver is illustrated in Figure 52. If the aircraft is flown at or near the full-scale reference condition, the relationship between the overall net

thrust, F'_N, and the airframe drag, D_{AFS}, is clearly established as

$$F'_N = D_{AFS} \quad (89)$$

Furthermore, deviations from the reference condition could be used to validate incremental changes in installed propulsive force from

$$\Sigma \Delta F = \Delta D \quad (90)$$

where the corresponding drag increment, ΔD, will be known from the throttle-independent airframe drag polars which constitute D_{AFS}. It is noted that only the aggregate of ΔF terms, denoted by the symbol Σ, may be determined without more-detailed instrumentation than is usually available in flight tests. Consequently, wind tunnel tests would be needed to assess the relative magnitudes of the ΔF terms.

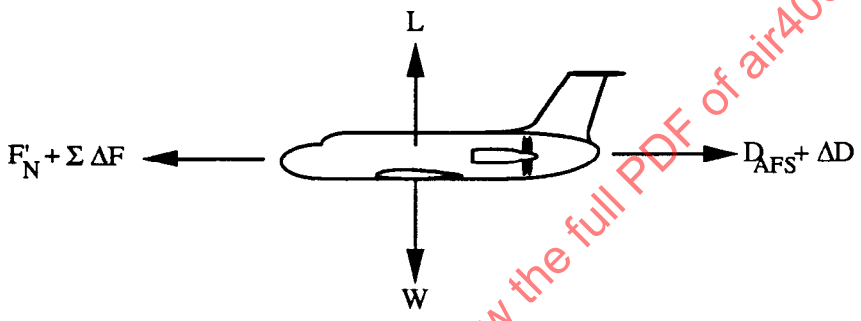

h = constant
L = W
V = constant

$$\Sigma \Delta F = \Delta F'_{net} - \Delta F_{inl} - \Delta D_{exh} - \Delta F_{trim} - \text{etc.}$$

$$F'_{net} + \Sigma \Delta F = D_{AFS} + \Delta D$$

Figure 52 - Constant Speed, Level Flight Validation of Overall Net Thrust, F'_N, at the Full Scale Reference Condition

5.4.2 Climb Tests: This test provides airspeed, power and rate-of-climb data for the aircraft at a number of constant airspeeds over numerous small altitude bands. The data may be converted to the drag polar format and it can readily be analyzed for maximum climb capabilities of the aircraft. The advantage of this test over the cruise speed power test is that high power, low airspeed data can be obtained. It has the disadvantage of repetitive, meticulous flight condition set-ups. This test requires rapid data acquisition at multiple points during each climb segment. Typically, various aircraft configurations (flap and gear position and engine out) are investigated using this method. Each segment described is at a quasi steady state condition, not a transient condition. The balance of forces in the flight path direction for this maneuver is illustrated in Figure 53. Here, the propulsive

increments over the level-flight thrust may be validated from

$$\Sigma \Delta F = W \sin \gamma \quad (91)$$

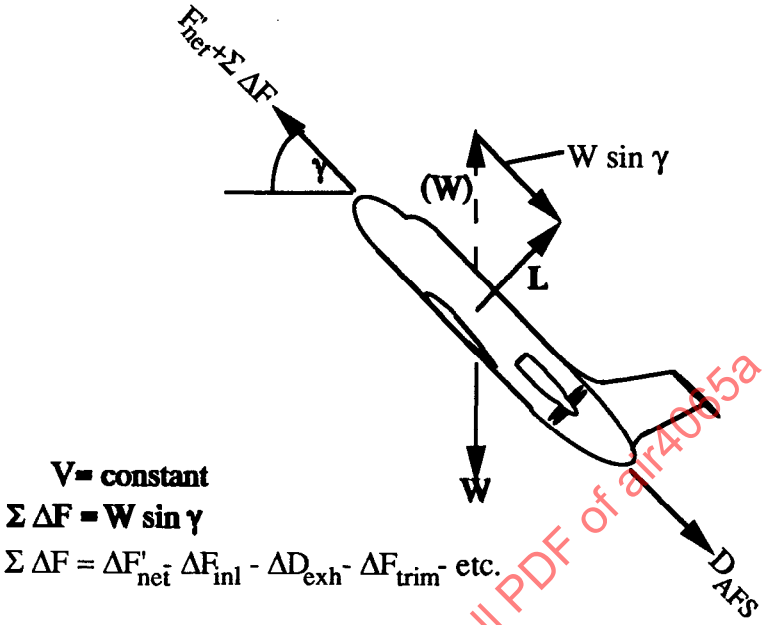

Figure 53 - Constant Speed Climb Validation of Thrust/Drag Increments from Full Scale Reference Condition

5.4.3 Descent (Including Feathered Descents): This test is similar to the climb test in the type of data acquired and the manner in which the data may be used. The advantage of this test is that it provides aircraft lift/drag data with minimal propulsion system interactions. In the extreme case of descents with the propulsion system inactive and the propellers feathered, observations of the aircraft basic drag characteristics can be made. The disadvantage of this test is the meticulous, repetitive test setup requirements and, in the feathered propeller case, the potential inability to restart the propulsion system following a planned descent segment. As in Section 5.4.2, each of these segments are at a quasi steady state condition.

5.4.4 Level Acceleration Tests: This test involves a steady acceleration from a low speed to high speed at a constant altitude. This test is used in lieu of the climb test for aircraft which have operating characteristics not conducive to the climb test profile (high climb performance, low endurance). The very nature of this test precludes an absolute steady state condition, (See SAE AIR 1703) for more general information on this type of testing). The balance of forces for this maneuver is illustrated in Figure 54. For the acceleration maneuver, the propulsive increments

over level-flight thrust at constant speed may be validated from

$$\Sigma \Delta F = \frac{W}{g}\frac{dV}{dt} \qquad (92)$$

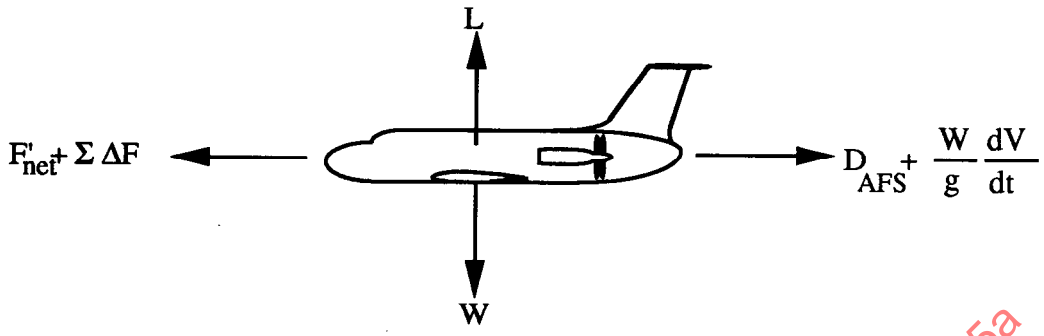

h = constant

$$\Sigma \Delta F = \Delta F'_{net} - \Delta F_{inl} - \Delta D_{exh} - \Delta F_{trim} - \text{etc.}$$

$$\Sigma \Delta F = \frac{W}{g}\frac{dV}{dt}$$

Figure 54 - Level Flight Acceleration Validation of Thrust/Drag Increments from Full Scale Reference Condition

5.4.5 Other Tests: Other tests may also be required to study propulsion system interactions. Any of the items discussed in paragraph 3.2.3 may require detail testing. Instrumentation validation or calibration tests, such as temperature probe ram recovery factor tests or propeller shaft torque meter calibration tests, may also be required.

5.5 Data Reduction Techniques:

Various techniques exist to convert flight test data into a form which can be directly compared to the analytical model. Care should be taken to assure that whatever technique is used relies on accepted aerodynamic and physical principals. References 21 and 22 offer convenient and accepted procedures. Included in these documents are the aerodynamic relationships required to progress through the steps shown in Figure 51.

6. NOTES:

6.1 Revision:

This is the initial publication of this document.

6.2 Warnings/Cautions:

This document contents are not intended to be used as a specification or any form of legal document. Other cautions & warnings are throughout the document as required.

6.3 Other:

None

6.4 Keywords:

IFTD
Inflight Thrust
Propeller
Propfan
Propulsion
Thrust
UDF

PREPARED BY SAE SUBCOMMITTEE E-33D, PROPFAN/PROPELLER IN-FLIGHT THRUST DETERMINATION

This Page Intentionally Blank

APPENDIX A

Actuator Disk Theory and The Isolated Propeller

NOMENCLATURE

A_{xx} - Cross sectional area at station xx

ΔD_{Hss} - Slipstream induced force on hub

ΔD_{SS} - Slipstream scrubbing force on propeller shaft (not the same as ΔD_{SS} in the report body

F'_N - Overall net thrust

p - Average static pressure

T_{fa} - Free air thrust

T_s - Apparent thrust

v - Delta velocity due to propeller in the plane of the propeller

V - Average velocity

V_0 - Free stream velocity

w - Delta velocity due to propeller at an infinite distance downstream

W_0 - Mass flow through the propeller

ρ - Ambient density of air

A.1 Actuator Disk Theory:

The actuator disc concept may by used to relate the overall net thrust to the flow conditions at the propeller. (These conditions are needed to estimate the force on a body immersed in the slip stream such as a nacelle.) To do this, a uniform, steady, incompressible adiabatic flow of inviscid fluid is assumed to pass through a vanishingly-thin disc resulting in the one-dimensional flow shown in Figure A1. Because the disc is very thin, the velocity on either side of the disc must be constant to preserve continuity, hence the free air thrust reduces to:

$$\text{Free Air Thrust, } T_{fa} = A(p_{13} - p_{12}) \qquad \text{(A1)}$$

Furthermore, the absence of dissipation allows equating the overall net thrust to the free air thrust.

$$\text{Thus:} \quad F'_N = T_{fa} \tag{A2}$$

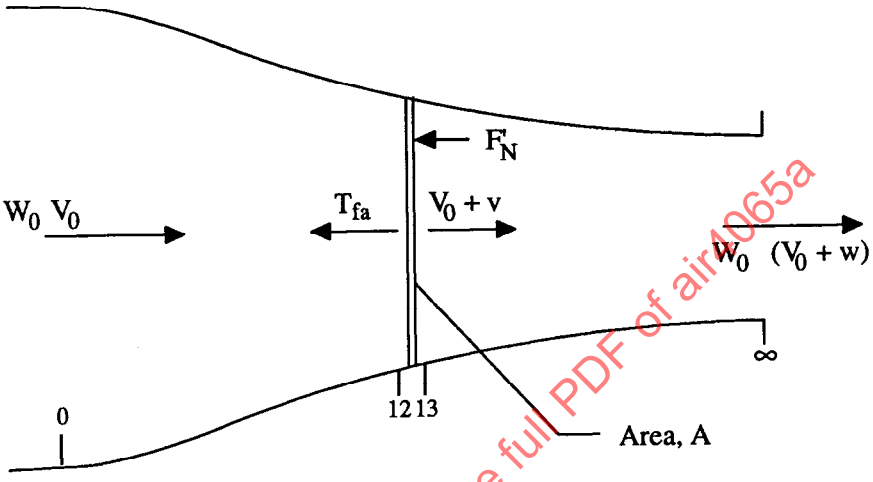

Figure A1 - Isolated Actuator Disc

Now, Bernoulli's equation may be applied in such flows to any two points on the same side of the disc.

Upstream:

$$p_{12} + \frac{\rho}{2}(V_0 + v)^2 = p_0 + \frac{\rho}{2} V_0^2 \tag{A3}$$

Downstream:

$$p_{13} + \frac{\rho}{2}(V_0 + v)^2 = p_0 + \frac{\rho}{2}(V_0 + w)^2 \tag{A4}$$

Subtracting:

$$p_{13} - p_{12} = \frac{\rho}{2}\left((V_0 + w)^2 - (V_0 + v)^2 - V_0^2 + (V_0 + v)^2\right) \tag{A5}$$

$$= \frac{\rho}{2}\left(2wV_0 + w^2\right) \tag{A6}$$

$$= \rho w\left(V_0 + \frac{1}{2} w\right) \tag{A7}$$

therefore:

$$T_{fa} = \rho w A \left(V_0 + \frac{1}{2} w \right) \quad \text{(A8)}$$

Next, the momentum equation applied to the streamtube equates the force T_{fa} to the total change in momentum flux between "o" and "∞".

$$T_{fa} = W_0 \Delta V = W_0 w \quad \text{(A9)}$$

and the mass flow is $W_0 = \rho A (V_0 + v)$ (A10)

These combine to give $T_{fa} = \rho w A (V_0 + v)$ (A11)

The two different expressions for T_{fa} given by (l) and (2), to both be true, require that

$$\frac{1}{2} w = v \quad \text{(A12)}$$

and substituting this into (2) gives:

$$T_{fa} = 2\rho v A (V_0 + v) = F'_N \quad \text{(A13)}$$

which defines the overall net or free air thrust of the isolated actuator disc in terms of velocity measurements at (or immediately behind) the disc. Equation (3) may be used to determine apparent thrust of a propeller as well, provided that the velocity measurements are time averaged and an appropriate adjustment is made for the swirl angle caused by blade rotation. These practical limitations on measurement accuracy combined with a not-so-well defined slipstream boundary immediately behind the propeller make the wake survey method less accurate than a direct force method.

A.2 The Isolated Propeller:

The thrust and power characteristics of an isolated propeller are normally provided by its manufacturer. These may be derived from wind tunnel test measurements and/or test cell measurements and are presented in dimensionless

form as tables or charts. Alternatively, they may be derived analytically from blade element theory or, more recently, from advanced flow field analysis methods. The measured thrust usually used to characterize propeller performance is the force (called free air thrust) shown as T_{fa} in Figure A2 depicting an isolated propeller test. The objective of the Propeller Test Rig (PTR) is to determine as accurately as possible the free air thrust, T_{fa} excluding any hub forces. In practice a small slipstream induced force increment ΔD_{Hss} may be implicit in the T_{fa} force.

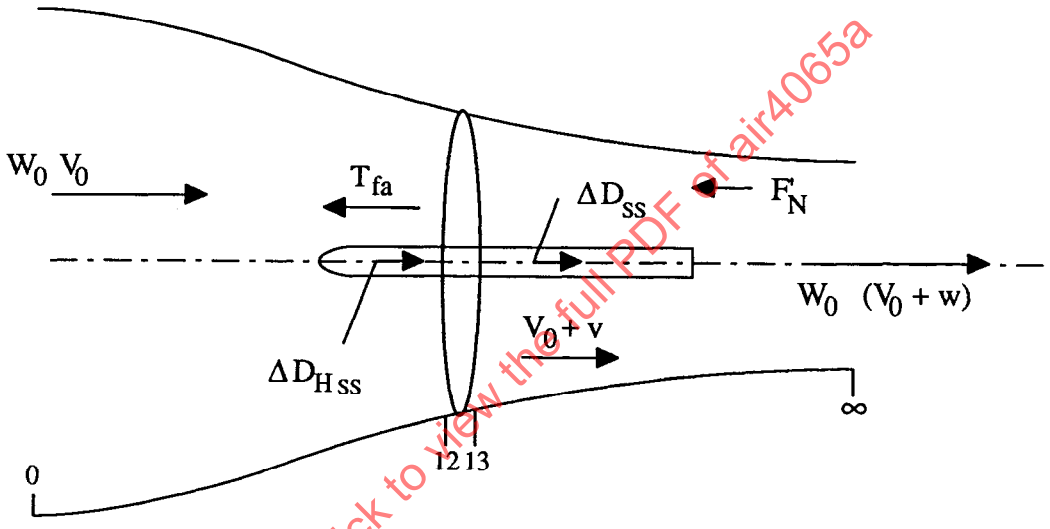

Figure A2 - "Isolated" Propeller Tested on a Propeller Test Rig (PTR)

The resulting net force therefore represents the blades-only part of the streamwise force component, and its definition may be expressed either in terms of stream quantities at the boundaries of an appropriate control volume or as the equivalent incremental force obtained from tests as follows:

Isolated Free Air Thrust,

$$T_{fa} = W_0(V_{13} - V_{12}) + p_{13}A_{13} - p_{12}A_{12} \text{ or} \quad \text{(A14)}$$

$$= T_{\text{blades on}} - T_{\text{blades off}} + \Delta D_{H_{ss}} \quad \text{(A15)}$$

where:
- W_0 = total mass flow through the prop
- V = average velocity
- p = average static pressure
- A = cross sectional area at station x

v = delta velocity due to propeller in plane of the propeller

w = delta velocity due to propeller at an infinite distance downstream

The force T_{fa} is more appropriately called isolated apparent thrust because it does not include hub and spinner forces, $T_{fa} = T_s$

Overall Net Thrust is defined in accordance with AIR 1703 as the reaction force which equates to the change in momentum flux between far upstream (sta. "0") and far downstream (sta. "∞"). It must, therefore, include all forces exerted by the internal flow on all surfaces wetted by the internal flow between stations "0" and "∞".

$$\text{Overall Net Thrust, } F'_N = W_0 (V_0 + w) - W_0 V_0 \quad \text{(A16)}$$

$$= W_0 w \quad \text{(A17)}$$

where F'_N = Overall Net Thrust

w = induced slipstream velocity at ∞

or alternatively as

$$F'_N = T_{fa} - D_s \quad \text{(A18)}$$

where D_s is the total downstream force exerted on the apparatus (PTR) by the propulsive stream. (Analogous to D_{nac} in Section 3.1.1.1)

APPENDIX B

Sample Calculation of Propfan Thrust (PW-Allison 578DX on the MD-80)

NOMENCLATURE

A	- Cross sectional area (identified by location)
C_d	- Core nozzle flow coefficient
C_D	- Drag coefficient
C_f	- Skin friction coefficient
C_p	- Power coefficient
C_s	- Stream thrust coefficient
C_t	- Thrust coefficient
C_v	- Core nozzle thrust coefficient
D	- Equivalent duct diameter
F_s	- Stream thrust
Δl	- Incremental duct length
MN	- Mach number
p_{amb}	- Ambient pressure
p_L	- Local static pressure
p_s	- Static pressure
$\Delta P_T/P_T$	- Total pressure loss (identified by system/component)
q	- Dynamic pressure ($P_T - p_s$)
R_N	- Reynolds number
T_s	- Apparent thrust
T_T	- Total Temperature
W_a	- Weight flow ~ lbs/sec
W_f	- Fuel flow ~ lbs/sec
W_g	- $W_a + W_f$ ~ lbs/sec

γ - Ratio of specific heats

δ - Ratio of ambient static pressure at altitude to S.L.Std static pressure

θ - Ratio of ambient static temperature at altitude to S.L.Std static temperature

β - Blade Angle at .75 Propeller Radius

B.1 Introduction

This appendix presents the flight measurements, supportive model testing, the step-by-step procedures and details of the calculations used to predict the in-flight thrust of the PW-Allison 578DX prop fan demonstrator engine that was flight tested on the MD-80 aircraft during the first half of C.Y. 1989. Of the optional methods and considerations covered in Sections 3 to 5 the methodology presented within this appendix is the one that best suits this particular propulsion system and its flight test installation. It is presented here as a typical numeric example to facilitate use of AIR 4065.

B.2 Propulsion System Description

The 578DX was a turboprop propulsion system demonstrator engine capable of producing 20,000 pounds thrust at sea level static conditions.

A cross-section of the 578-DX propulsion system is shown in Figure B1. The power section supplied by Allison includes a new low-pressure compressor (LPC) and intermediate support, modified Allison Model 571 gas generator and power turbine, and a new accessory gear box. The gear system supplied by Allison was a differential planetary configuration with a speed ratio of 8.3 to 1. This gear system permitted independent speed control of the two propfan rotors. The gear oil was cooled with an air/oil cooler assembly provided by Stewart Warner. The cooling air flow rate through the heat exchanger system was controlled with a modulating flap nozzle.

The propfan module, supplied by Hamilton Standard, included two rows of 11.6-foot diameter swept blades, six in the front row (counter-clockwise rotation viewed from the rear) and six in the rear row (clockwise rotation). This system had electrically actuated, variable blade pitch with mechanical pitch lock, full reverse and feathering capability, overspeed protection, and mechanical minimum blade angle features.

The engine exhaust system consisted of 9 lobes with circumferential width selected to avoid having the exhaust gases impinging on the propfan blades exceed an average temperature of 500 degrees F, and to minimize performance losses (only the root of the propfan blade is affected by the exhaust gases).

Figure B2 Shows the Lobe Nozzle Assembly viewed from the rear

Figures B3 and B4 show photographs of the propulsion system installed on the MD-80 flight test aircraft. Details of this propulsion system and the flight testing are available in the open literature in numerous publications, for example References B1 thru 4.

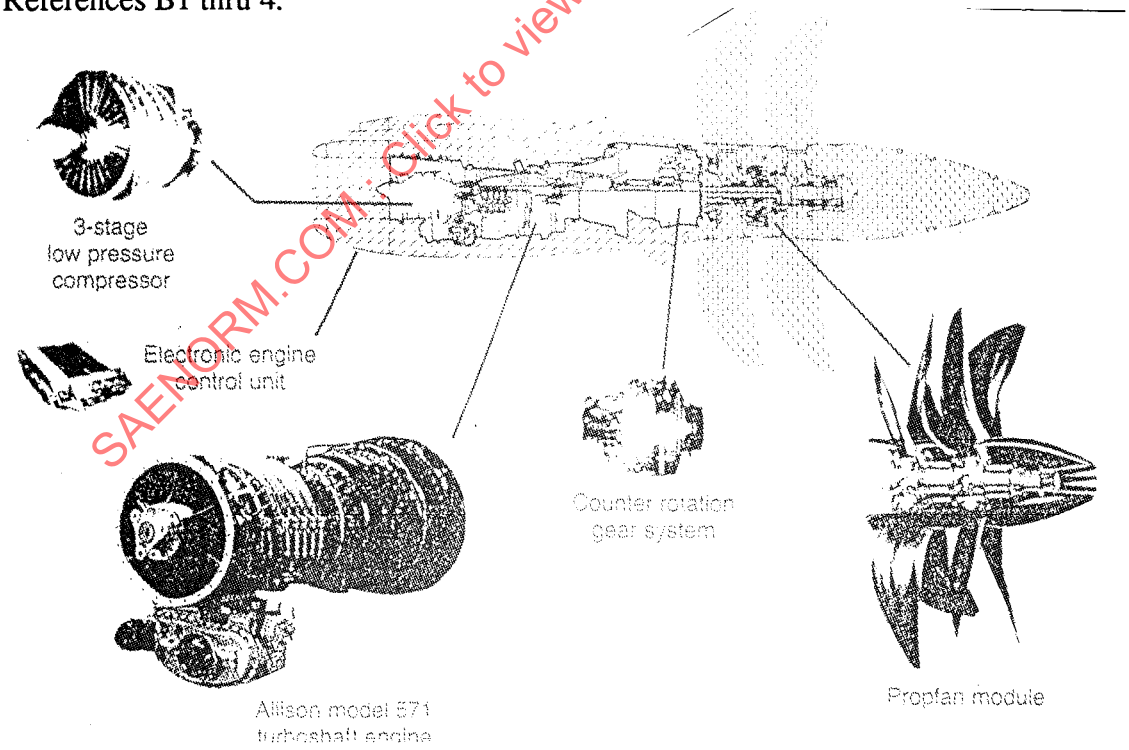

Figure B1 - 578-DX Propulsion System

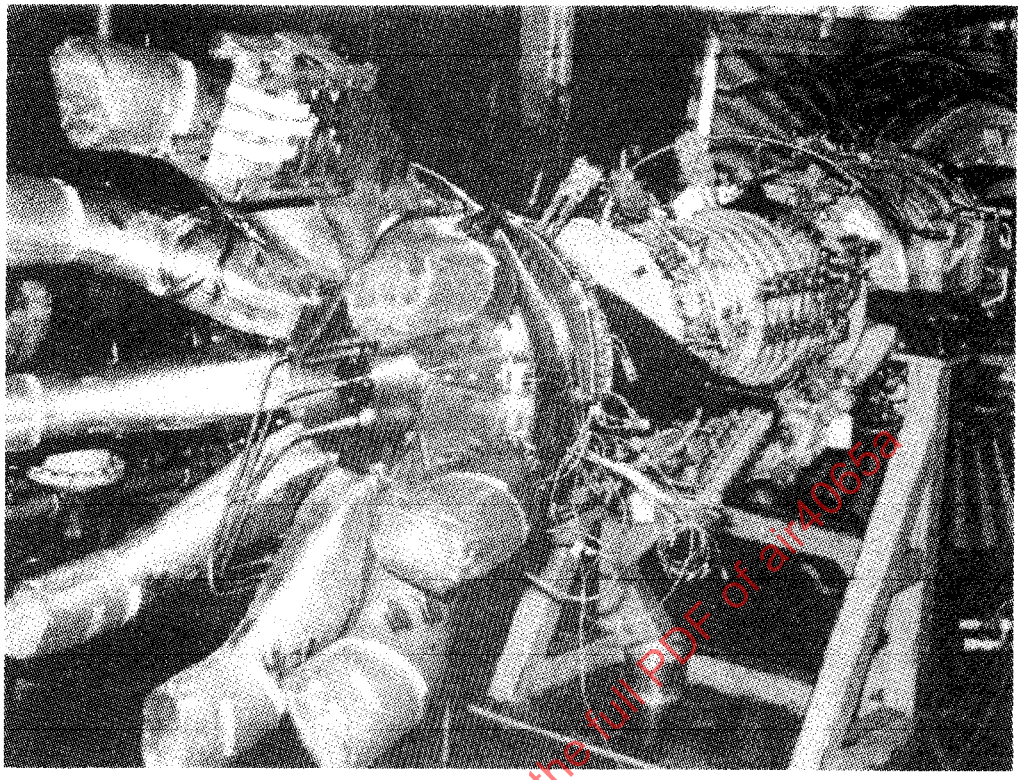

Figure B2 - 578-DX Lobe Nozzle Assembly

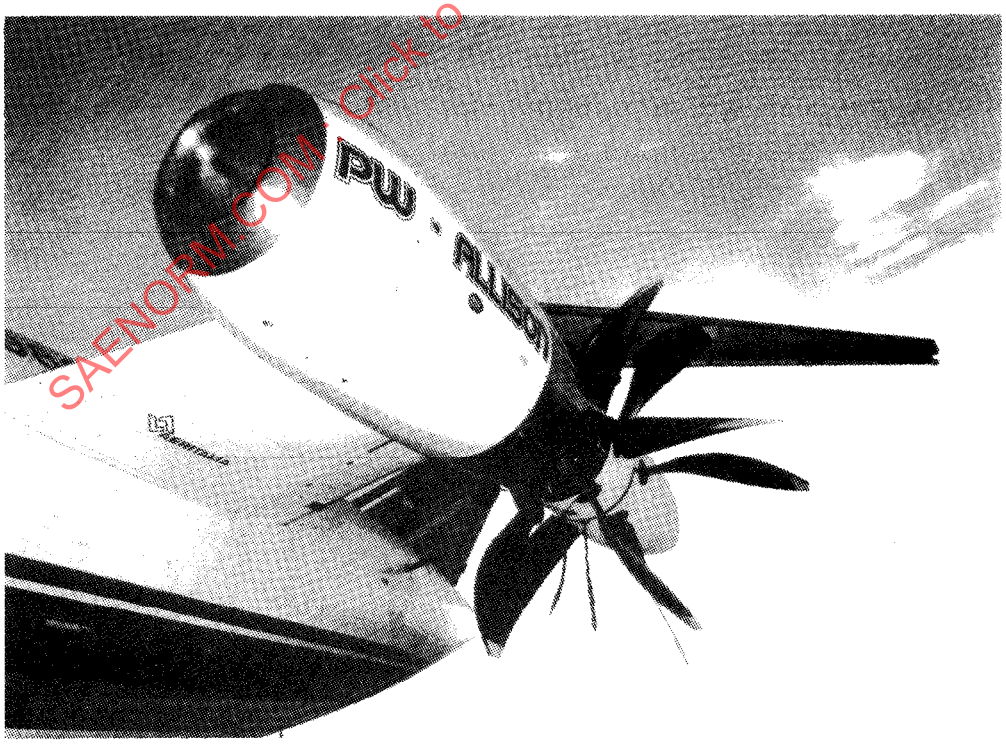

Figure B3 - 578-DX Installed on MD-80 Flight Test Aircraft

Figure B4 - 578-DX vs. JT8D-209 Installation

B.3 Thrust/Drag Accounting Definition:

The control volume used to calculate the S78DX net thrust is shown in Figure B5. Vectors pointing upstream (right to left) are the thrust terms; vectors pointing

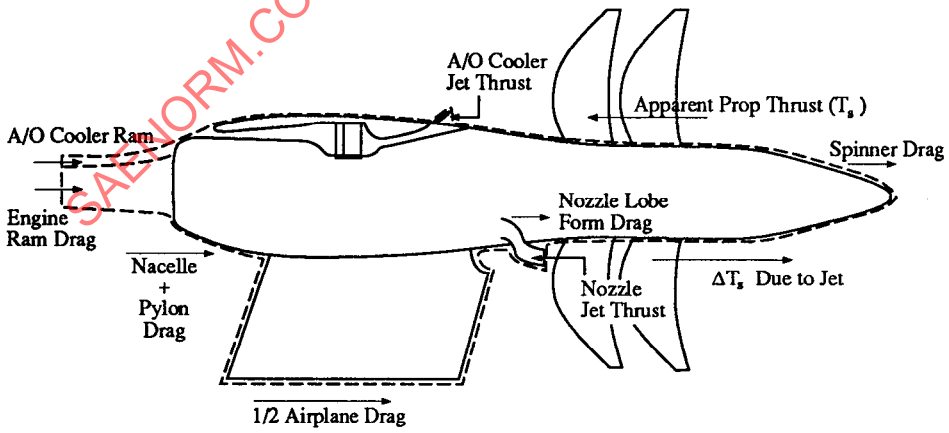

Figure B5 - Airplane and Engine Forces Used to Solve Momentum Equation

$$\left(\oint \vec{dF}=0\right)$$

downstream are drag terms (exception: degradation of apparent propeller thrust due to jet effects = ΔTs). Titles for the major thrust/drag components are indicated on the figure.

The momentum equation gives:

$$0 = \sum \left(\text{Thrust}^{1} - \text{Drag Components}\right) \qquad \text{(B1)}$$

Defining net thrust to be equal to the retarding airplane drag, the thrust/drag components can be rearranged and collected into the form:

$$\begin{aligned}\text{Net Thrust} = {} & \left(\begin{matrix}\text{Apparent}\\ \text{Propeller Thrust}\end{matrix} - \Delta T_s \text{ due to jet}\right) + \\ & \left(\begin{matrix}\text{Nozzle Jet}\\ \text{Thrust}\end{matrix} - \begin{matrix}\text{Engine Ram}\\ \text{Drag}\end{matrix}\right) - \\ & \left(\begin{matrix}\text{Nacelle}\\ \text{Drag}\end{matrix} + \begin{matrix}\text{Pylon}\\ \text{Drag}\end{matrix} + \begin{matrix}\text{Nozzle Lobe}\\ \text{Form Drag}\end{matrix} + \begin{matrix}\text{Spinner}\\ \text{Drag}\end{matrix}\right) + \\ & \left(\begin{matrix}\text{A/O Cooler}\\ \text{Jet Thrust}\end{matrix} - \text{A/O Cooler Ram}\right)\end{aligned} \qquad \text{(B2)}$$

These collections of thrust/drag components are solved in section B.7.

B.4 Measurements Recorded in Flight Test

There were 260 channels for data acquisition devoted to the propulsion system. The test priorities were (l) safety of operations, (2) system operability, (3) structural design data, (4) acoustics and finally (5) performance. The number of pieces of instrumentation were allocated accordingly. Fortunately, relatively few measurements are needed for calculating the propulsion system net thrust. These parameters are tabulated in Table B1. An in-flight thrust projection was made using the combination of these measured parameters, cycle analysis and model/rig/component test data.

The test point selected for this exercise was a low speed, low altitude climb condition. Values that approximate the data averaged from 5 repeat tests are

[1] This is a "Net Map".

tabulated next to the parameters in Table B1. The Mach numbers recorded during the five flights varied from 0.24 to 0.32. A nominal flight Mach number of 0.3 will be used in the sample calculations.

Table B1 - Measured Parameters Needed for Propulsion Thrust Determination

Example Case: Low Speed Climb Testing PWA-Allison 578DX in MD-80 - Average of 5 Flights

Aircraft	Approximate Values	Engine	Approximate Values
P2	14 psia	N Prop Fwd	1200 RPM
Altitude	2780 Ft	N Prop Aft	1200 RPM
Pamb	13.15 psia	Q (Torque) to Gear	3580 Ft-lbs
Tamb	7 °C	W Fuel Flow	3500 Lb/hr
MN	.24--- .32	2.4 Bleed Port	7%
		P 2.5 } From MN Probe	21.5 psia
		p_s 2.5 } From MN Probe	18.6 psia
		T 2.5 Synethsis (Control)	35 C
		p_sNozzle	13.4 psia
		N Power Turbine	10,300 RPM
		p_sA/O Cooler Inlet Press	13.73 psia
		T A/O Cooler Exit Temp.	139 °F

B.5 Model/Rig/Component Tests

B.5.1 Propeller Model: The J Method (Section 3.4.1) was used by Hamilton-Standard to calculate the propeller thrust. Initially these maps were generated using analytical predictions. The performance was later verified by model tests.using the test set-up shown in Figure B6. The counter rotating props were driven by air turbines from the rear. The propeller blades and hubs were metric with both thrust and torque being measured.

The propeller diameters were 24.1". This gives a Reynolds Number of approximately 700,000 when run in an atmospheric tunnel, which is large enough to avoid large scaling corrections (Section 4.0, Figure 30). The airfoil shapes simulated the full scale geometry when deflected by centrifugal load at high RPM. Consequently, the experimental measurements needed no adjustments for scale effects.

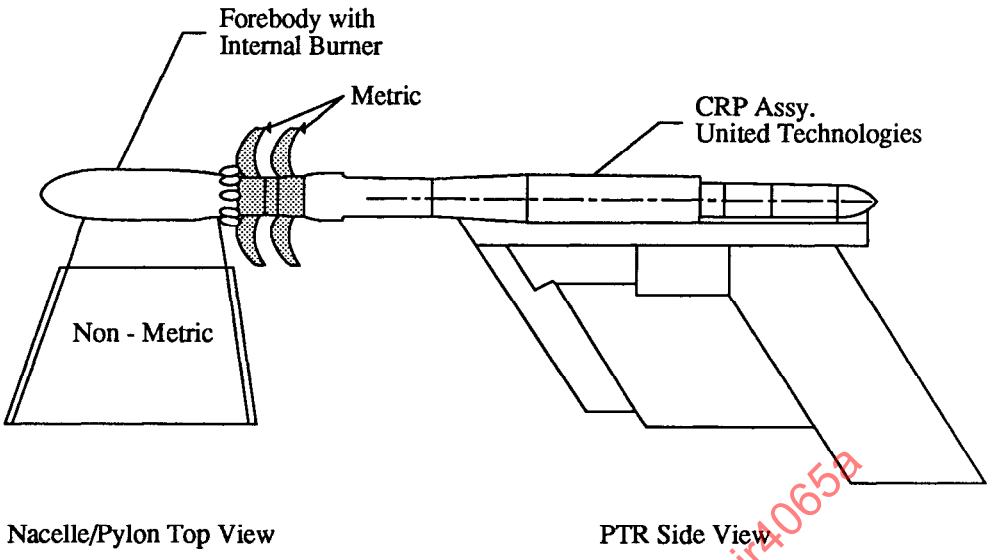

Figure B6 - Counter Rotation Propeller Test Rig - 2 Ft Diameter Blades

A non-metric simulation of the pylon, nacelle, and flowing nozzles was positioned in front of the props (Figure B7). The nacelle was contoured to retard the flow going into the first propfan row so that free stream velocity enters the root of the first blade. Also, the hubs of both propeller stages are cylindrical. Therefore, there is no need for pressure-area corrections to the recorded thrust. The blade thrust can be defined as free air thrust, apparent thrust, or net thrust (thrust definitions, Figure B1). The propeller thrust was obtained from the rotating balance data and is the difference between running with blades on v.s. blades off. This eliminates tare forces and the small amount of hub friction. The hub friction is bookkept as part of the nacelle drag. The measured parameters were: RPM, balance force thrust, balance torque, static and total pressures and temperatures of the external and nozzle flows. These allow calculation of power coefficient (C_p), thrust coefficient (C_t) and advance ratio J (see Basic Report Nomenclature). Maps of these were generated similar to the one shown in Figure B20.

The nozzle effect was demonstrated by establishing a basic set of maps without nozzles, and then map the blade efficiency shift that occurs when the nozzle lobes are installed and flowing at the exhaust conditions of the engine.

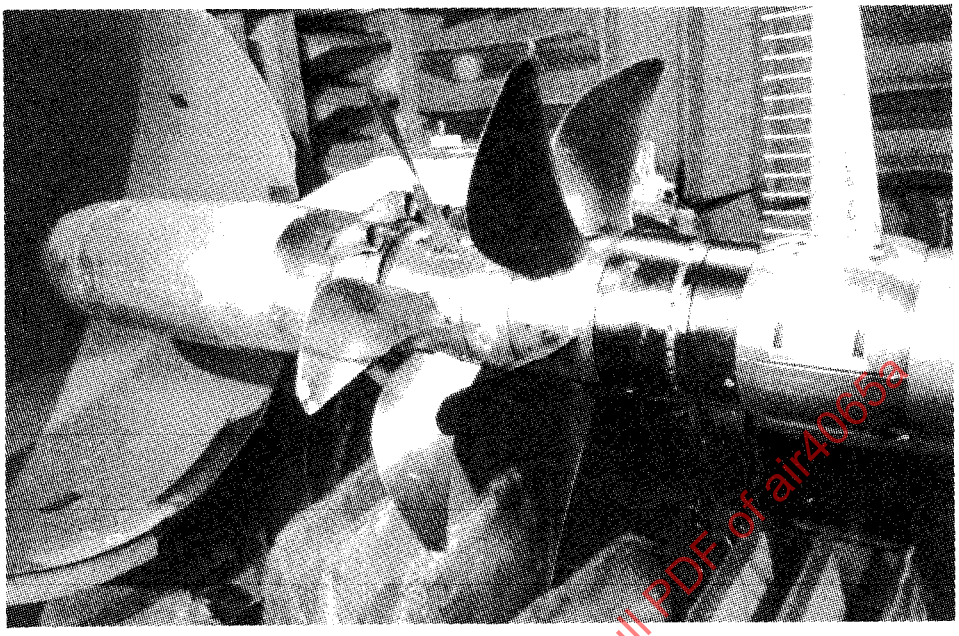

Figure B7 - Close Up Photo Showing Lobed Nozzles/Nacelle Positioned In Front of Test Propeller

B.5.2 Engine Exhaust Nozzle Model: Approximately 1/6th scale models of the engine exhaust system were tested to determine thrust coefficients (C_v) and flow coefficients (C_d). These are standard coefficients defined in AIR 1703. A photograph of one of the nozzle models is shown in Figure B8. A cross section of the test set up is shown in Figure B9. The model air supply has a calibrated venturi to determine airflow. The model is mounted on an upstream thrust balance to measure actual thrust. Charging station instrumentation (approximately 20 thermal couples and 40 pressure probes) at the nozzle entrance measure stagnation and static conditions for ideal thrust and ideal airflow calculations.

The charging station is located in a constant area section at a location that would coincide with the turbine exit guide vane discharge which is the exhaust system entrance.

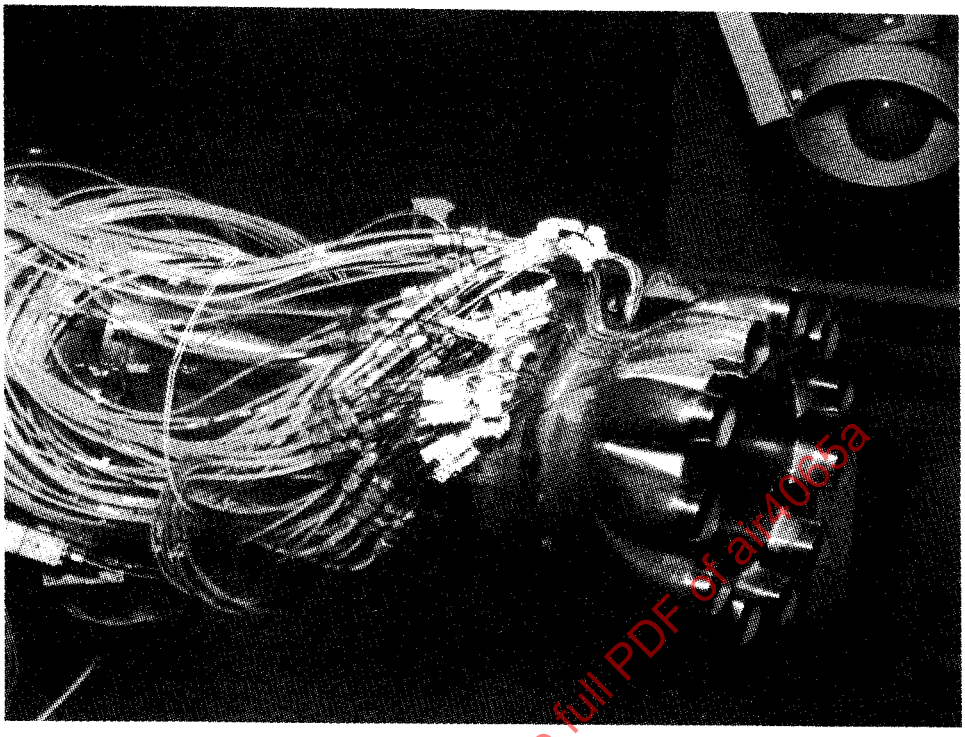

Figure B8 - 1/6th Scale Nozzle Model Tested Statically with Hot Gas

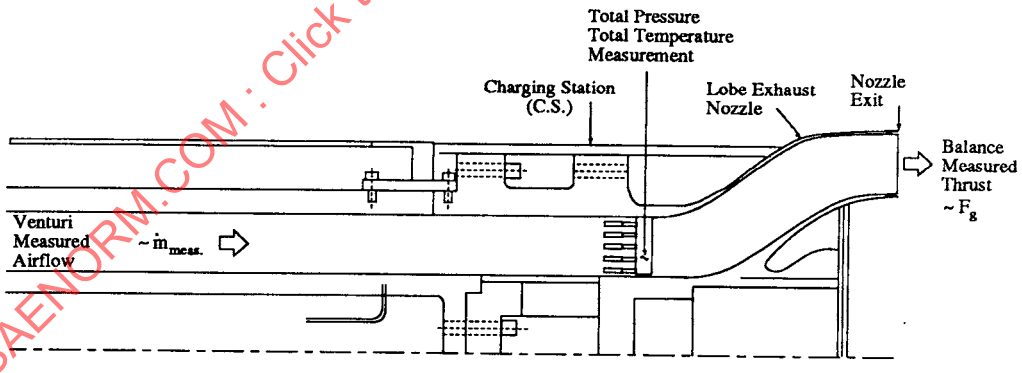

Figure B9 - Typical Nozzle Model Test Arrangement

The nozzle C_v and C_d curves are based on stagnation conditions at the nozzle exit (station 8). The charging station measurements must be adjusted for the pressure losses of the charging station instrumentation, and for the friction for the ducting from the nozzle entrance to the exit. Any other unaccountable losses that might

affect the actual thrust are buried in the C_{v8}, C_{d8} curves. The equations for adjusting from the charging station to station 8 are:

Skin friction total pressure loss is:

$$\left.\frac{\Delta P_T}{P_T}\right|_{S.F.} = \sum_{\text{Charging Station}}^{\text{Nozzle Exit}} -4C_f \frac{\gamma Mn^2}{2} \frac{\Delta l}{D} \qquad \text{(B3)}$$

Where
C_f = Skin friction coefficient
Mn = Local Mach number
Δl = Incremental duct length
D = Equivalent duct diameter
γ = Ratio of specific heats

Instrumentation total pressure loss is:

$$\left.\frac{\Delta P_T}{P_T}\right|_{Inst} = -\frac{\gamma Mn^2}{2} \frac{A_{Inst}}{A_{Flow}} C_D \qquad \text{(B4)}$$

Where
C_D = Drag coefficient based on frontal area
A_{Inst} = Instrumentation frontal area
A_{Flow} = Local cross-sectional area
Mn = Local Mach number

Total Losses:
$$\left.\frac{\Delta P_T}{P_T}\right|_{Model} = \left.\frac{\Delta P_T}{P_T}\right|_{\text{Skin Friction}} + \left.\frac{\Delta P_T}{P_T}\right|_{Inst} \qquad \text{(B5)}$$

having made these adjustments the coefficients are presented in the format for both model and full scale use as shown in Figure B10.

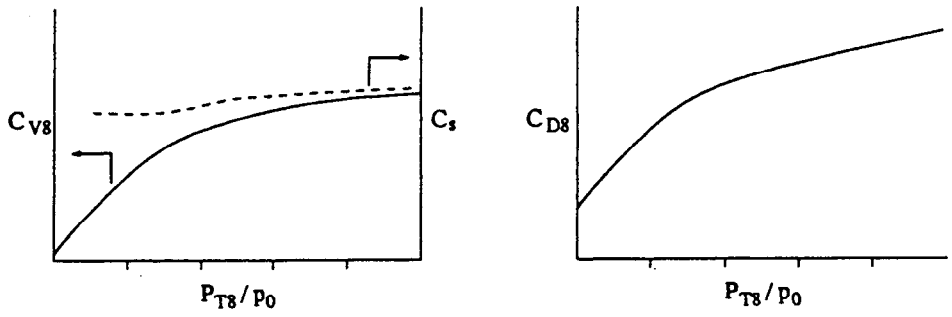

Figure B10 - Lobe Nozzle Thrust and Flow Coefficients

These curves can be used in a straightforward way at all times when the nozzles are choked (super-critical nozzle pressure ratios) or are being used in a static, quiescent environment when unchoked (exit static pressure equals local static pressure which in turn, equals ambient static pressure). p_{s8}, unchoked nozzle exit conditions will be affected by changes to the local environmental pressure, such as will occur when used in close proximity to the aspirated flow field in front of the propeller; installation interactions could also affect the local flow field changing the local static pressure to values either higher or lower than freestream static pressure. At the selected sample calculation test point, the local static pressure (average of 4 readings) was 13.4 psia, where as Pamb was 14.0. Even though the adjustment is small, at other flight conditions it can become more significant.

The adjustment for $p_L \neq p_0$ can be computed by solving the individual elements that go into C_v, some of which are a function of p_0, others of p_{s8}:

$$C_v = \frac{\text{Actual Thrust per pound of actual flow}}{\text{Ideal Thrust per pound of actual flow}} \quad \text{(B6)}$$

or

$$C_v = \frac{F_{Actual} / P_T A^*}{F_{Ideal} / P_T A^*} \quad \text{(B7)}$$

but

$$F_{Actual} = \left(\dot{m}V + pA\right)_{8_{Actual}} - p_{s_0}A_8 \quad \text{(B8)}$$

$$\text{so} \qquad C_V = \frac{\left(\frac{\dot{m}V + pA}{P_T A^*}\right)_{8\,\text{Actual}} - \frac{p_{s_0}}{P_{T_8}}\frac{A_8}{A^*}}{F_{\text{Ideal}} / P_T A^*} \tag{B9}$$

$\left(\frac{\dot{m}V + pA}{P_T A^*}\right)_{8\,\text{Actual}}$ is a function of $\left(\gamma, \frac{p_{s_0}}{P_{T_8}}\right)$. Calling this $F_s A / A^*$, and defining

$$C_{s_8} = \frac{\left(F_s A / A^*\right)_{\text{Actual}}}{\left(F_s A / A^*\right)_{\text{Ideal}}} \tag{B10}$$

can be arranged to solve for C_{s_8} or:

$$C_{s_8} = \frac{C_v \left(F_{\text{Ideal}} / P_T A^*\right) + \frac{p_{s_0}}{P_{T_8}}\frac{A_8}{A^*}}{\left(F_s \frac{A}{A^*}\right)_{8\,\text{Ideal}}} \tag{B11}$$

The model tests were conducted statically, so $p_{s_8} = p_{s_0}$. C_{s_8} was calculated and is also shown in Figure B10. So, to use the model data, when $p_{s_8} = p_{s_0}$, either the C_v curve can be used, or the C_s curve in combination with (1). When $p_{s_8} \neq p_{s_0}$, the appropriate pressure ratios must be used in (1) together with the C_s curve.

B.5.3 Air/Oil Cooler Calibrations: Stewart-Warner provided the heat exchanger system that cooled the propfan module gearbox oil. A schematic of this system is shown atop the engine in Figure B11. It consisted of: an air inlet, a diffuser, a dump diffuser to the radiator face, 2 radiators in tandem, each having 300 in^2 frontal area, a series of ejector nozzles behind the radiator driven by high compressor bleed air for static and low speed operation, a constant area mixing zone, and a modulating exhaust nozzle to control the amount of cooling airflow. A boilerplate version of this system was built and tested to prove heat exchanger effectiveness (Figures B11a through d). During these demonstrations the cooler airflow and system total pressure losses were calibrated. Both are needed for thrust/drag determination.

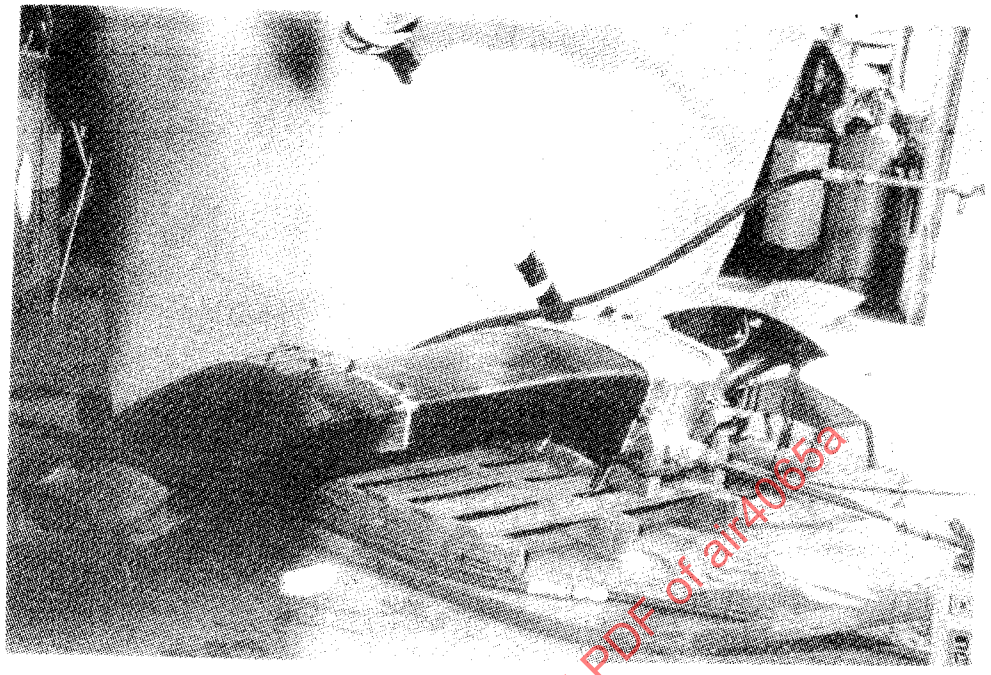

Overview of Rig

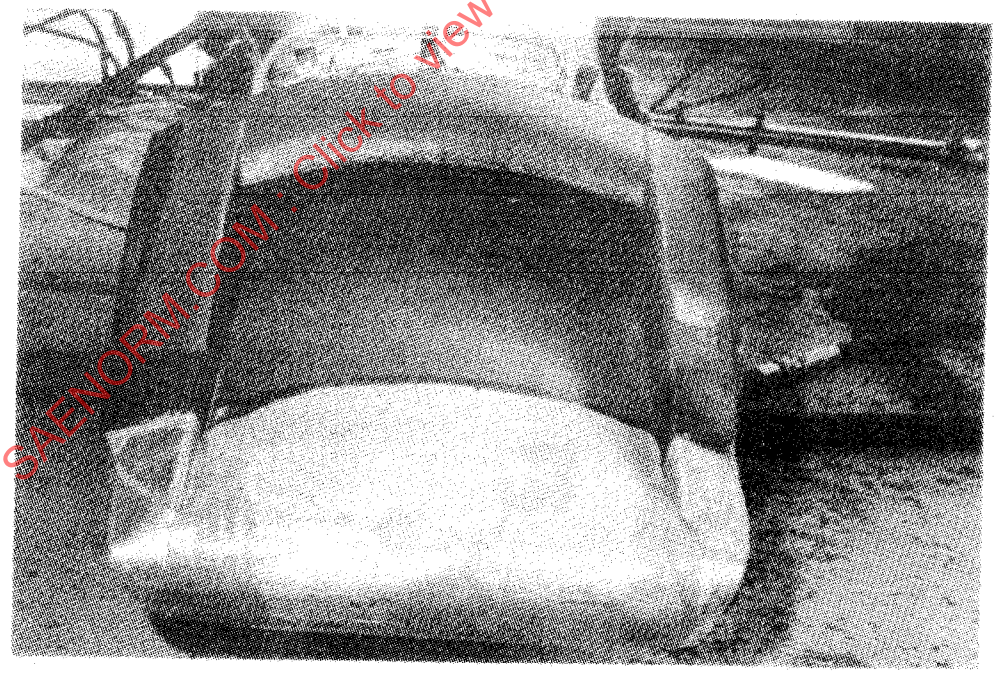

Front View (Inlet)

Figure B11 - Views of Rig (a and b)

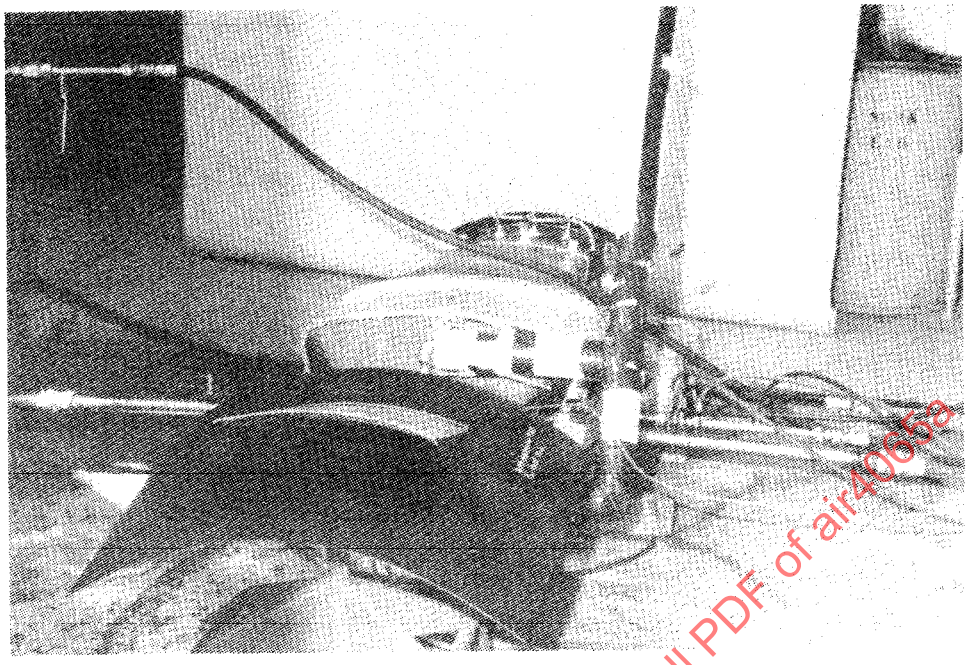

Rear View (Flap)

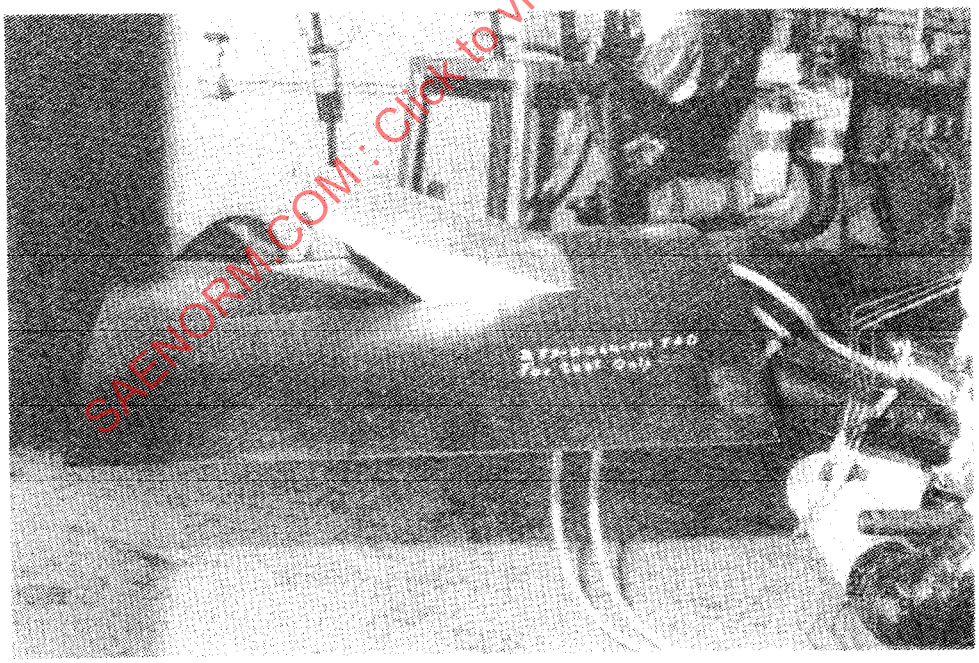

Side View (Flap)

Figure B11 - Views of Rig (c and d)

B.5.3.1 Inlet Flow Calibration: Air/Oil cooler flow rates were correlated with static pressure measurements taken 5.25 inches (see Figure B12) aft of the inlet highlite. Flow was measured using a calibrated 6 inch orifice plate. The resulting data were then non-dimensionalized and utilized per the correlation of Figure B13.

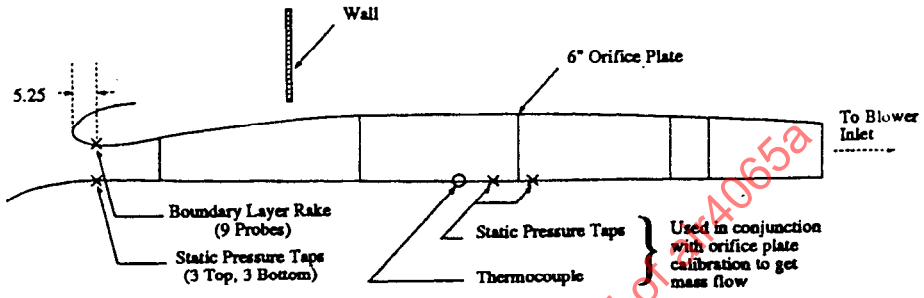

Figure B12 - Inlet Flow Calibration Instrumentation

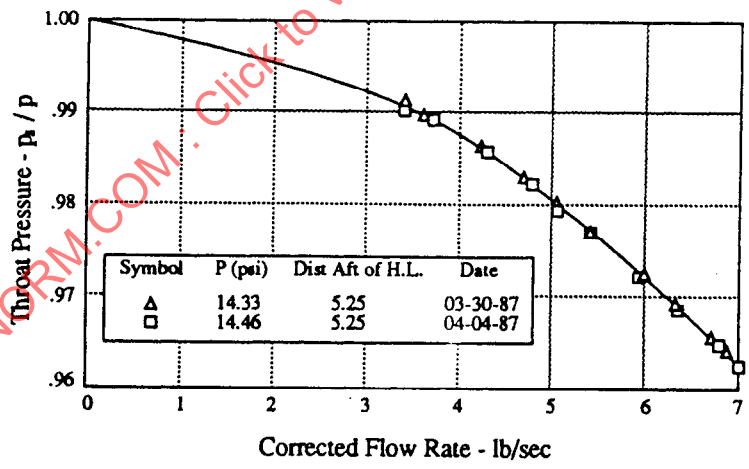

Figure B13 - Air/Oil Cooler Flow Calibration (Aft of Upper Lip Highlite)

B.5.3.2 Total Pressure Loss Through the Air/Oil Cooler System: The air flow path and the cumulative total pressure loss through the system are shown in Figure B14. The inlet and exhaust system losses are quite small and were estimated using skin friction calculations and dump diffuser correlations. The largest total pressure

loss occurs going through the radiator. This loss was calibrated by Stewart-Warner using the rig shown in Figure B15, producing the loss curve shown in Figure B16.

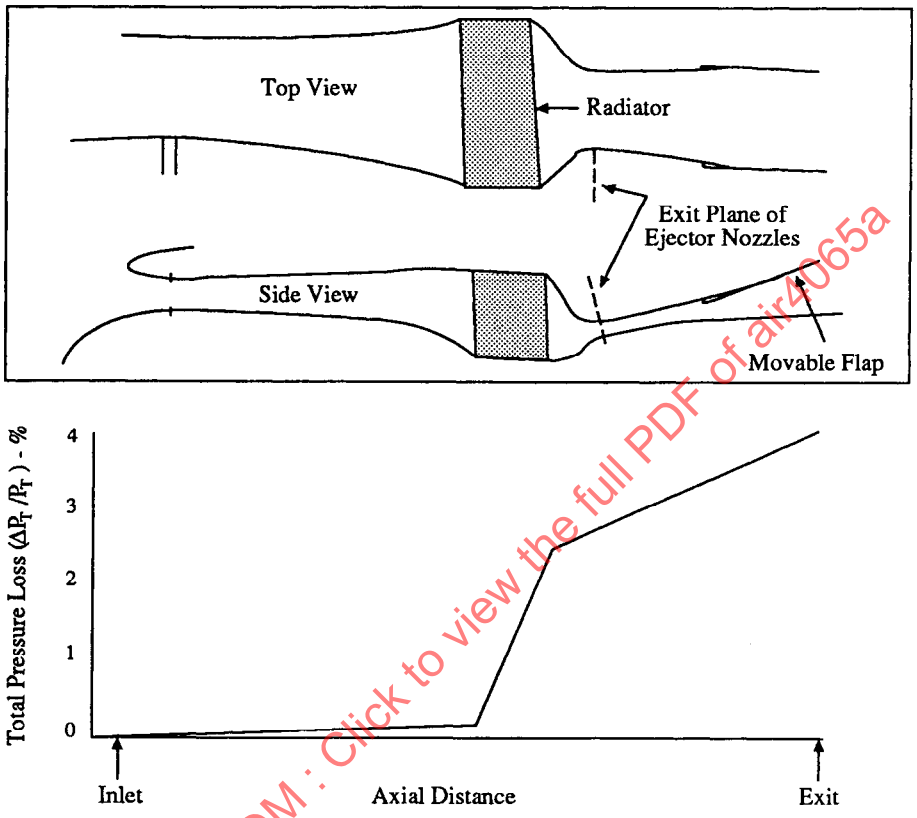

Figure B14 - Air/Oil Cooler System Losses

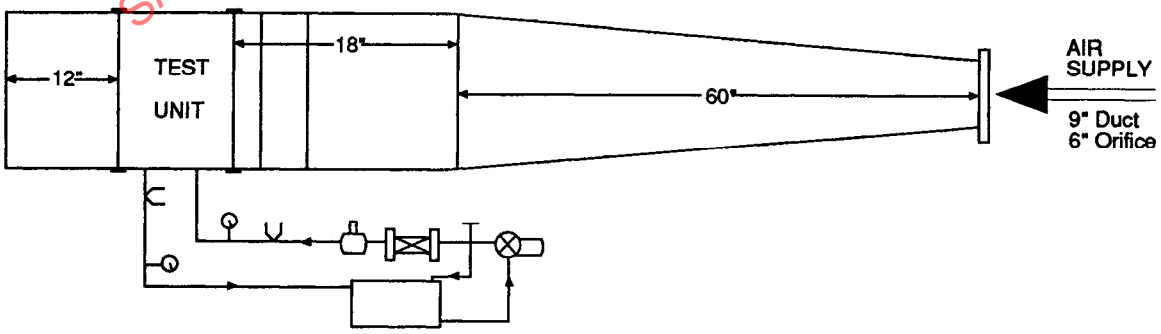

Figure B15 - Straight Duct Calibration (Installation and Instrumentation)

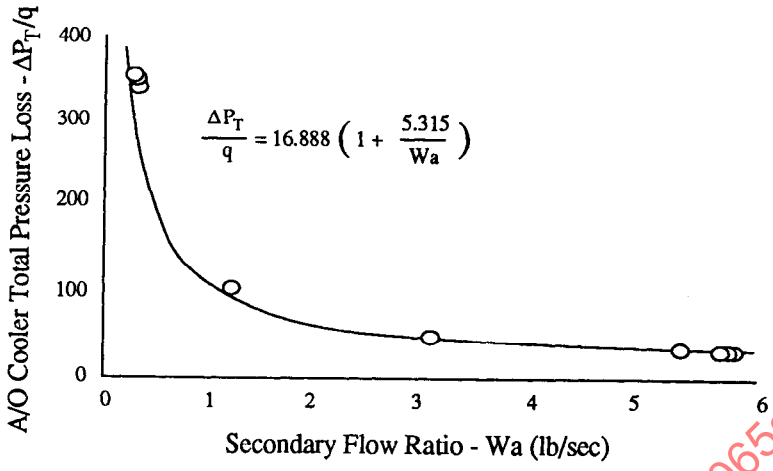

Figure B16 - Total Pressure Loss Through A/O Cooler

B.6 Engine Cycle Analysis

B.6.1 Introduction: During the planning phase of the MD-80/578DX flight test program, each technical discipline submitted their data acquisition desires. Typical of this type of test, the instrumentation being requested greatly exceeded measurement system capability. Since performance determination was not the highest of priorities in the program, data acquired specifically for that purpose was minimized. Consequently, the in-flight thrust calculation involved more cycle analysis than would have been required if we had the luxury of measuring conditions at major component interfaces. For example, to determine nozzle jet thrust requires having a nozzle thrust coefficient (C_v) and ideal thrust. Model tests gave C_v. With sufficient instrumentation at the nozzle entrance, stagnation conditions could be measured and ideal thrust determined directly. Without the power turbine exit/nozzle entrance interface measurements, these conditions had to be determined analytically by engine cycle matching analysis. The equations to execute these calculations are not complex, but involve numerous steps and in some cases iterations. These calculations were computerized, but for the sake of providing visibility, a detailed sample matching exercise is presented in the following text using the input from Table B1. The parameters are coded with designations Ml through M14 and Nl through N6 to facilitate tracking of the analysis (Table B2)

Table B2 - Measured Parameters as Used in Computerized Calculations

A. Engine

M1	N Prop Face	1200 Rpm
M2	N Prop Aft	1200 Rpm
M3	N Low	10300 Rpm
M4	Q (Torque) to Gear	3580 Ft-lb
M5	W Fuel Flow	3500 lb/hr
M6	$P_{2.5}$	(21.5/14.7) = 1.463
M7	$PS_{2.5}$	18.6 Psia
M8	P Burner	278 Psia
M9	P Nozzle Avg. of Four	13.4 Psia
M10	2.4 Bleed Stroke	7%
M11	T_2Control Sense	49.1 °F
M12	Prop Pitch Face	40.5 Deg
M13	Prop Pitch Aft	40.2 Deg
M14	$T_{2.5}$ Synthesis Control	35 °C (95 °F)
M15	$\delta_{2.5}$	(21.5/14.7) = 1.463
M16	$\theta_{2.5}$	(35 + 273)/288 = 1.034

B. Aircraft Parameters

N1	P_2	14.0 Psia
N2	Altitude (Press)	2780 Ft
N3	p_{amb}	13.15 Psia
N4	MN	0.3
N5	Calculated Air Speed	330 Ft/sec
N6	T_{amb}	44.6 °F

B.6.2 Calculate Turbine Discharge P_T and T_T: The basic approach is to calculate T_T exit based on overall energy balance, using airflow as measured by the calibrated Mn probe, plus fuel flow, less bleeds. Then to calculate the required $P_{T_{exit}}$.

(A.) Calculate Wg exit = Wa Mn probe - Wa downstream bleed + Wf/3600

(A.1) Wa Mn probe

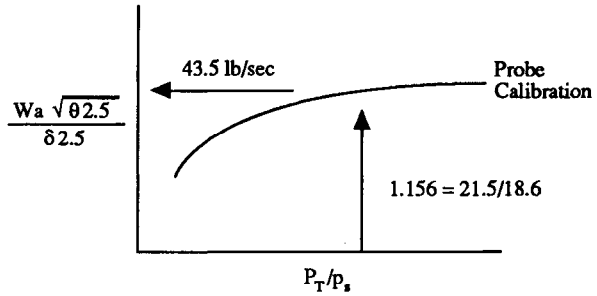

Figure B17 - Mn Probe Calibration

(A.2) $$\text{Wa Mn probe} = \text{Wa}\frac{\sqrt{\theta_{2.5}}}{\delta_{2.5}} \times \frac{\delta_{2.5}}{\sqrt{\theta_{2.5}}} \qquad \text{(B12)}$$

$$\text{Wa Mn probe} = \frac{43.5 \times 1.463}{1.034} = 61.5 \text{ lb/sec}$$

{Sources: B.6.2-A.1 and Table 2 (A.6 & A.14)}

(A.3) Is 10th bleed on: YES - subtract 0.7% Wa

NO - 0

YES: .007 x 61.5 = 0.4 lb/sec

Substituting back into general equation B.6.2.(A.)

(A.4) Wg exit = 61.5 - 0.4 + 3500/3600 = 62.1 lb/sec

{Sources: B.6.2-(A.2); B.6.2-(A.3); and Table B2,M3}

(B) Calculated T_{Texit} using energy equation, flows calculated above, T_{T2} measured, and measure power extracted to drive the gearbox. In equation form:

$$T_{Texit} = [T_2 C_p (Wa\ Mn\ Probe + Wa\ OB_{2.4B1}) + \quad \text{(B13)}$$

$$Wf \times H.V. - \frac{Q\ to\ gear \times N\ low}{5252} \times \frac{42.436}{60} - T_{2.4} C_p Wa_{2.4B1} -$$

$$T_{10th\ Bleed} C_p Wa_{10th\ Bleed}] / C_p Wg\ exit$$

(B.1) $\%Wa_{OB\ 2.4\ Bleed}$ = 2.4 Bleed Stroke x 1/2 (Slope of stroke vs. bleed at low stroke)

$Wa_{OB\ 2.4\ Bleed} = 7\% \times 1/2 = 3.5\%$

{Source: Table 2,M10}

$Wa_{OB\ 2.4\ Bleed} = 0.35 \times 61.5 = 2.2$ lb/sec

{Source: B.6.2-(A.2)}

(B.2) $T_{T\ 10th\ Bleed}$

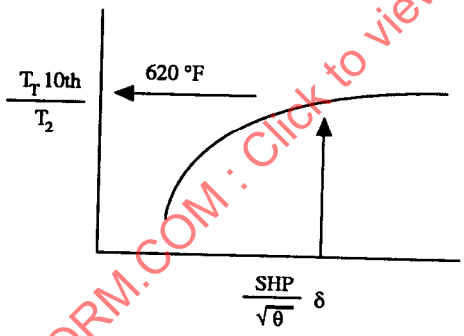

Figure B18 - Bleed Schedule

Substituting back into general equation B13:

(B.3) $$T_{T\ exit} = \left[(9.5 + 273)\ 1.8 \times 0.24\ (61.5 + 2.2) + \frac{3500}{3600} \times 18400 - \frac{3580 \times 10300}{5252} \frac{42.436}{60} - (620 + 460)\ 0.24 \times 0.4 \right] / (62.1 \times 0.24)$$

{Sources: Table 2,M11; B.6.2-(A.2); B.6.2-(B.1); Table B2,M5, M4, M3; B.6.2-(B.2); B.6.2-(A.3); and B.6.2-(A.4)}

$$T_{T\,exit} = [508.5 \times 0.24 \times 63.7 + 17889 - 7021 * 0.707 - 1080 * 0.24 \times 0.4] / (62.1 \times 0.24)$$

$$T_{T\,exit} = \frac{7811 + 17889 - 4963\text{-}104}{14.9} = \frac{20596}{14.9} = 1382°R$$

(C) Calculate $P_{T\,exit}$ by successive iteration using nozzle flow parameter curve measured in model test program.

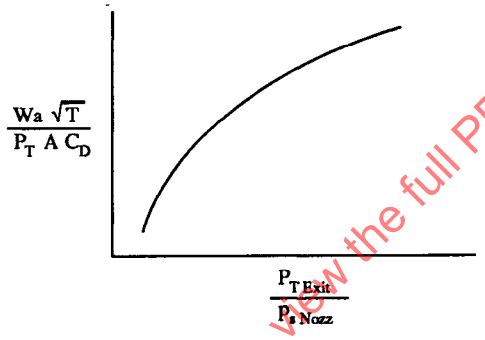

Figure B19 - Nozzle Flow Parameter Curve

(C.1) Assume $P_{T\,exit} = 1.5 \times p_{Nozz}$

$= 1.5 \times M9 = 1.5 \times 13.4 = 20.1$ Psia (B14)

(C.2) Look up $\frac{Wa\sqrt{T}}{P_T A C_D}$ from nozzle curve:

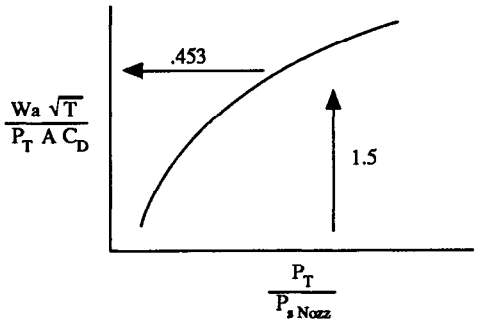

Figure B20 - Nozzle Curve

(C.3) Calculate $P_{T\ exit} = \frac{Wa\sqrt{T}}{AC_d} \Big/ \frac{Wa\sqrt{T}}{P_T AC_d}$ (B15)

{Source: C_d vs. $\frac{P_T}{P_S}$ curve}

$$P_{T\ exit} = \frac{62.1\sqrt{1382}}{300 \times 0.974 \times 0.453} = \frac{2308.6}{127.9} = 17.45 \text{ Psia}$$

{Sources: B.6.2-(A.4); B.6.2-(B.3) and B.6.2-(C.2)}

(C.4) Compare C.1 to C.3: 20.1 = 17.45
Recycle through iteration until C1 = C3 = 19.1 Psia

B.6.3 Calculate Power Extraction to Drive Propellers

(A.1) Power into gear $= \frac{Q \times N_L}{5252}$ (B16)

{Sources: Table B2, M4 and M3}

Power into gear $= \frac{3580 \times 10300}{5252} = 7021$ Shp

(A.2) Gear System Efficiency
From Full Scale Gear Rig Test

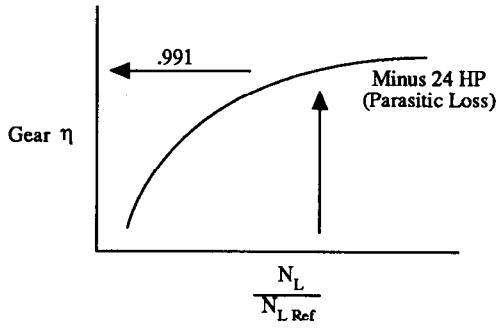

Figure B21 - Gear Efficiency

(A.3) Power into propeller = Power into Gear x Gear η - 24 (B17)

Power into propeller = 7021 x 0.991 - 24 = 6934 Hp

$= 3{,}813{,}700 \frac{\text{ft-lb}}{\text{sec}}$

{Sources: B.6.3-(A.1) and B.6.3-(A.2)}

B.7 Numerical Example to Quantify and Sum Thrust/Drag Components

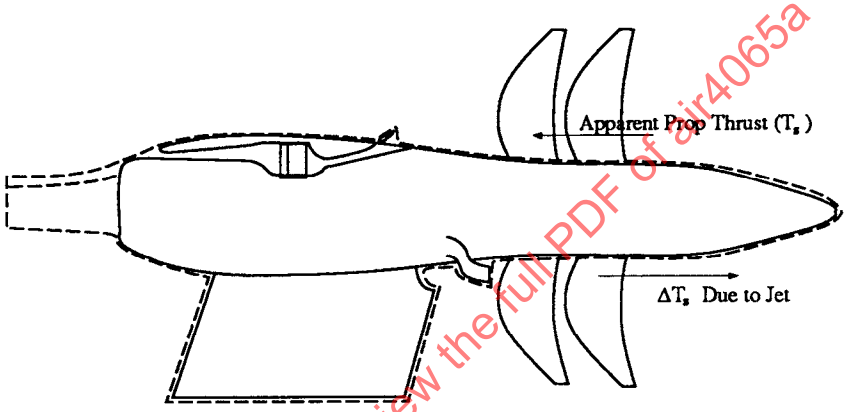

Figure B22 - Propeller Thrust Contribution

B.7.1 Propeller Thrust Contribution: The map method for quantifying propeller thrust relates C_p, C_T and J at a given flight speed and a given blade angle. The approach to quantifying the propeller thrust was to use the cycle analysis power extraction calculation from B.6.3 to compute C_p, and measurements to determine J, β and flight Mach number. C_T maps provided by Hamilton-Standard were then used to calculate blade thrust.

The most straight forward way of generating the maps is to conduct parametric tests of the model described in section B.5.1, installed behind a nacelle/pylon simulation with flowing exhaust nozzles. However, thrust projections were required before the tests could be conducted. Hamilton-Standard generated these thrust projections analytically. Airfoil strip analysis was performed at numerous cuts through the blade going from root to tip. Free air blade thrust and torque was computed by resolving the incremental air foil forces into axial and tangential components. Then, summing these cuts radially, efficiencies were determined

and mapped. Because the velocity triangles are off-design when the blade passes behind the engine exhaust nozzle, the calculations were repeated over the root sections affected by the jet plume and a debit to efficiency was determined. The root performance debit was proportioned by the % of the circumference occupied by the exhaust jet.

The following numerical example shows how the maps, cycle analysis and flight measurements (Table B2) were combined to calculate propeller thrust.

B.7.1.1 Calculate C_p Treating Counter Rotating 2 Row Propfan as One Equivalent:

System: $$C_p = \frac{\text{Power into Prop}}{\rho\, N^3\, D^5} \qquad \text{(B18)}$$

A.1 $$N_{Prop} = \frac{N_{Face} + N_{Aft}}{2} \qquad \text{(B19)}$$

$$= \frac{1200 + 1200}{2} = 1200$$

{Sources: Table B2, M1 and M2}

Substituting back into general equation for C_p:

A.2 $$C_p = \frac{\text{Power into Prop}}{\rho\, N^3\, D^5}$$

$$= \frac{(3{,}813{,}700)}{0.00216\left(\frac{1200}{60}\right)^3 (11.6)^5} = 1.0508$$

{Sources: B.6.3-(A.3) and Table B2, N1}

B.7.1.2 Computation of J: T = 7°C = 504°R:

$$\text{Sonic Velocity} = \sqrt{\gamma * G * R * T} = 1100.6 \text{ ft/sec}$$

Flight Mach No. = 0.3

Flight Speed = Mach No. * Sonic Velocity = 330.2 ft/sec

N = 1200 rpm / 60 = 20 rps

D = 11.5 ft

J = V / (N * D) = 1.43

B.7.1.3 Calculation of Free Apparent from Thrust Hamilton Standard Provided Propfan Map:

(A) Look up C_{Ts}

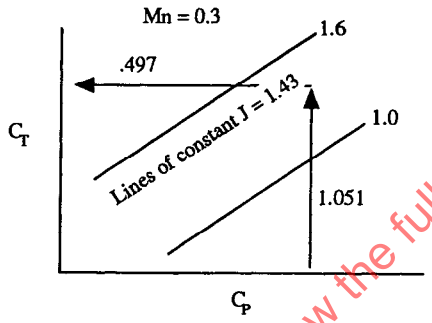

Figure B23 - Propfan Map

(B) Calculated propeller efficiency

$$\eta_{Prop} = \frac{C_{Ts}}{C_P} \times J = \frac{0.497 \times 1.43}{1.051} = 0.677 \quad \text{(B20)}$$

B.7.1.4 Calculate Jet Exhaust Impact on Propeller Efficiency and Thrust:

(A.1) Look up $V_J - V_0$ effect on propeller efficiencies on curve provided by Hamilton Standard.

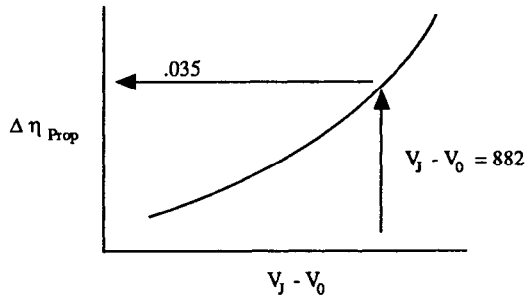

Figure B24 - Loss in Propeller Efficiency due to Jet Effect

(A.2) Compute Warm Propeller Effect

$\eta_{Prop} = 0.677 - 0.035 = 0.642$

{Sources: B.7.1.3-(B) and B.7.1.4.-(A.1)}

(A.3) Compute Warm Propeller C_T

$$C_{T\ Warm\ Prop} = \frac{\eta_{Warm\ Prop} \times C_p}{J} = \frac{0.642 \times 1.051}{1.43} = 0.472$$

(A.4) Compute Warm Propeller F_N

$$F_{N\ Warm\ Prop} = C_T\ D^4\ N^2\ \rho$$

$$= 0.472\ (11.6)^4 \left(\frac{1200}{60}\right)^2\ 0.00216$$

$$= 7390\ lb$$

{Sources: B.7.1.4-(A.3) and B.7.1.1-A.1}

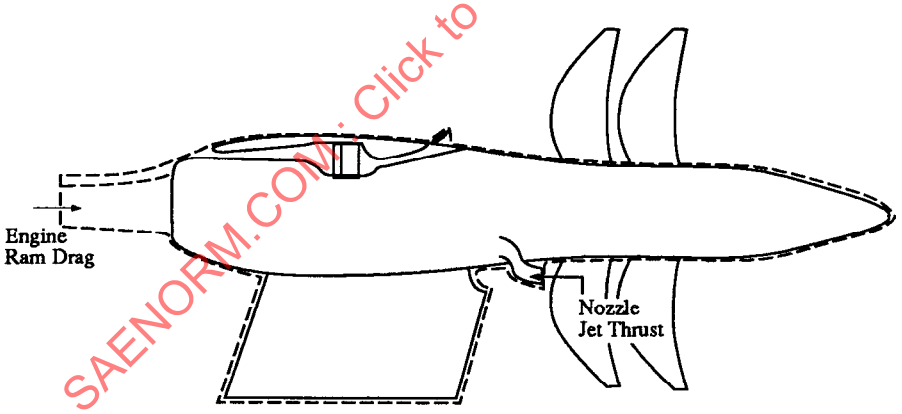

Figure B25 - Engine Inlet Ram Drag

B.7.2 Engine Inlet Ram Drag and Nozzle Jet Thrust

B.7.2.1 Engine Inlet Ram Drag: Engine inlet ram drag is the product of captured engine air times free stream velocity:

$$\text{Engine Ram Drag} = \dot{m}_{Engine}\, V_0$$

where: $V_0 = 330$ fps

{Source: Table B2, N5 }

and: $\dot{m}$ = Calibrated Mn Probe + Bleed
= (61.5 lb/sec) + (2.2 lb/sec)
= 64 lb/sec

{Sources: Table B2, N4 and N6}

so: $$\text{Engine Ram Drag} = \frac{\dot{m}\, V_0}{g} = \frac{330 \times 64}{32.2} = 656 \text{ lbf} \qquad \text{(B21)}$$

B.7.2.2 Nozzle Jet Thrust: Nozzle jet thrust = C_v (F_{Ideal}); but, since $P_{s8} \neq P_{s0}$, and the flow is unchoked, the static nozzle C_v curves can not be used directly. Instead the C_{s8} curve together with (1) from section B.5.2 were used.

It should be noted that the nozzle exit total pressure (P_{T8}) was determined from the engine cycle conditions at the turbine exit and adjusted for full scale nozzle total pressure loss ($\Delta P_T/P_T$) using methods described in section B.5.2. Nozzle exit total pressure then becomes:

$$P_{T8} = P_{T7}\left(1 - \frac{\Delta P_T}{P_T}\right)$$

where: P_{T7} = 19.1 {Source: B.6.2-C.4)

and $\frac{\Delta P_T}{P_T}$ = .012

P_{T8} = 19.1 (1 - .012) = 18.87 psia

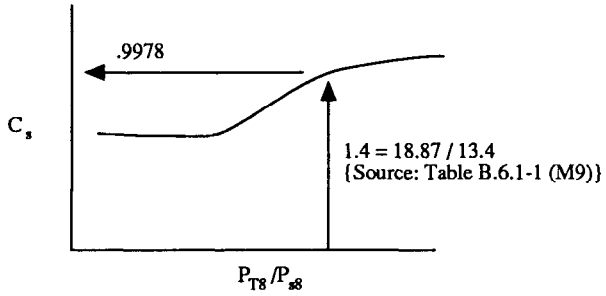

Figure B26 - C_s vs P_{T8}/P_{s8}

$$C_v = \frac{C_{s8}\left(F_s \frac{A}{A^*}\right)_{8\,Ideal} - \frac{P_{s0}}{P_{T8}}\left(\frac{A_8}{A^*}\right)}{\frac{F_{Ideal}}{P_T A^*}} \qquad \text{(B22)}$$

where: $\frac{P_{s0}}{P_{T8}} = \frac{14}{18.87} = .7419$ {Source: Table 2, N1}

$\frac{P_{s8}}{P_{T8}} = \frac{13.4}{18.87} = .7100$ {Source: Table 2, M9}

$\frac{A}{A^*}$ and $\left(F_s \frac{A}{A^*}\right)_{8\,Ideal} = f(\gamma, Mn_8)$ using $\gamma = 1.35$

{Source: compressible flow tables}:

$\left(F_s \frac{A}{A^*}\right)_{8\,Ideal} = 1.311$

$\frac{A}{A^*} = 1.076$

$\frac{F_{Ideal}}{P_T A^*} = f\left(\gamma \frac{P_{s0}}{P_{T8}}\right) = .5125$

so: $C_v = \frac{(.9978)\,(1.311) - (.7419)\,(1.076)}{.5125}$

$C_v = .9967$

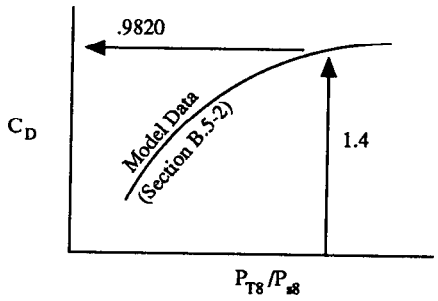

Figure B27 - C_D vs P_{T8}/P_{s8}

$$\text{and} \quad \text{Jet Thrust} = C_v \left(\frac{F_{Ideal}}{P_T A^*} \right) (P_{T8}) \left(\frac{A_8 C_D}{A_8 A^*} \right) \qquad \text{(B23)}$$

$$= (.9967)\ (.5125)\ (18.87)\ \frac{300}{1.076}\ (.9820)$$

$$\text{Jet Thrust} = 2640 \text{ lbf}$$

B.7.3 Nacelle/Pylon and Nozzle Lobe Drag:

B.7.3.1 Nacelle/Pylon Drag:

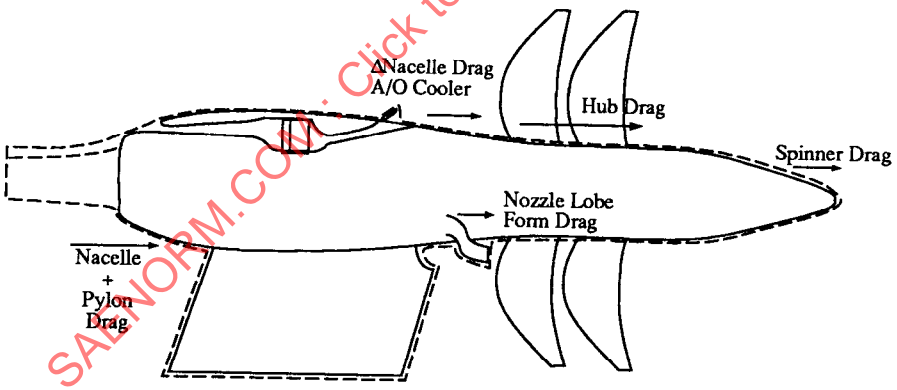

Figure B28 - Nacelle and Pylon Drag

The Nacelle and Pylon drag includes:

Inlet additive and spillage
Nacelle
Nacelle drag increment due to air/oil cooler system bulge

Pylon (to waterline at propeller tip)
Hubs
Aft cone or spinner
Nozzle lobes
Excrescences, steps, gaps, surface irregularities, etc.

At the low flight speeds of this test case, linearized potential flow panel methods can be used to calculate the flow field around the nacelle. Actuator disks were used to simulate the props, sinks simulate the inlet flow, and sources simulate the nozzle flow (Figure B29). This, combined with calibrated boundary layer analysis gave assurance that there were no localized supersonic flow regions, hence no threat of shock induced pressure drag, nor was there any threat of flow separation. Hence, the only losses were: (1) skin friction; (2) the pressure drag associated with the displaced streamlines in the aft end due to boundary layer growth; and (3) form drag of the nozzle lobes.

The friction and boundary layer induced pressure drag calculations use with the equation for flat plate friction:

$$\text{Drag} = K \times C_f \times \frac{q \times A_{wet}}{(1 + .16\ MN^2)^{0.6}} \qquad \text{(B24)}$$

where: K = a constant to adjust smooth flat plate friction coefficient for:

- Roughness
- Surface imperfections, steps, gaps, etc.
- Adjustment to estimate boundary layer induced pressure drag

K = 1.2

C_f = Schultz-Grunow flat plate skin friction coefficient

$$C_f = \frac{.427}{(\text{Log } R_N - .407)^{2.64}}$$

$$\frac{R_N}{l_{nac}} = \frac{\rho V}{\mu} = 1.51 \times 10^7 \times Mn_\infty \times P_{amb} \times \left(\frac{T_{amb} + 198.72}{T_{amb}^2}\right)$$

$$= 1.51 \times 10^7 \times 0.3 \times 13.28 \times \left(\frac{504.6 + 198.72}{504.6^2}\right)$$

$$= 17566 \text{ / inch}$$

Nacelle length = 282 in

$R_N =$ 49.5×10^6

then, $C_f = \dfrac{.427}{(\text{Log}(49.5 \times 10^6) - .407)^{2.64}} = .002255$

$q =$ Local Free Stream Dynamic Pressure

Awet = Local wetted area (Figure B30)

$(1 + .16\ Mn^2)$ = Skin friction compressibility factor (Ref. B5)

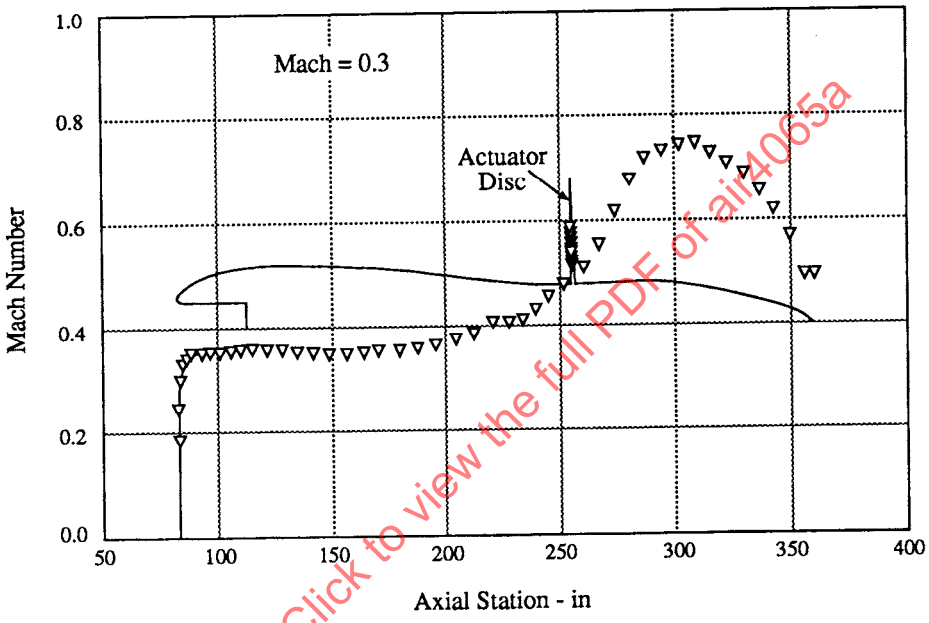

Figure B29 - Nacelle Mach Number Distributions

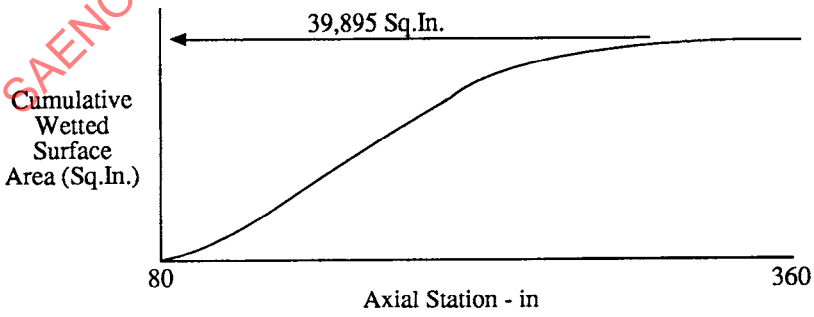

Figure B30 - Surface Area Distribution

Integrating the local drag increments using P_{T0} in front of the actuator disc, and adding the propeller pressure rise for conditions behind the actuator disc gives:

Nacelle and Pylon Drag = 124.2 lb

.B.7.3.2 Nozzle Lobe Drag: Nozzle lobe drag can be calculated using:

Δ Drag Nozzle Lobe = C_D x q_∞ x A_{ref} x Number of Lobes

where: $C_D \sim f(t, l, \alpha)$ see reference B6

t = lobe thickness = 5.4 in
l = lobe length protruding into freestream flow = 18 in
α = angle lobe makes with freestream flow = 50°
C_D = .037
q_∞ = .84
A_{ref} = t x l = 5.4 x 18 = 97.2 in^2
number of lobes = 9
Δ Drag Nozzle Lobe = .037 x .84 x 97.2 x 9 = 27.1 lbf
Nacelle and Pylon Drag = 124.2 + 27.1 = 151.3 lbf

B.7.4 (Thrust-Drag) Contribution of Air/Oil Cooler:

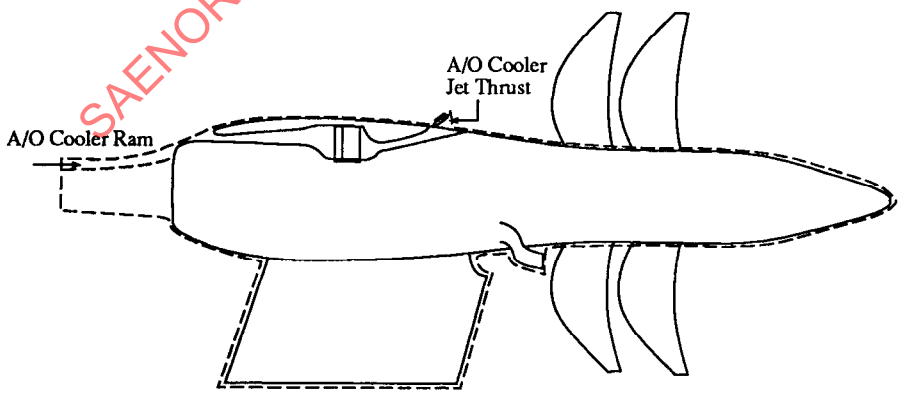

Figure B31 - Air/Oil Cooler Ram Drag

B.7.4.1 Air/Oil Cooler Ram Drag = $\dot{m}\, V_0$: Air/Oil cooler mass flow through duct:

$$\text{Pressure ratio in duct} = \frac{P_s}{P_t} = \frac{13.73}{14} = .977$$

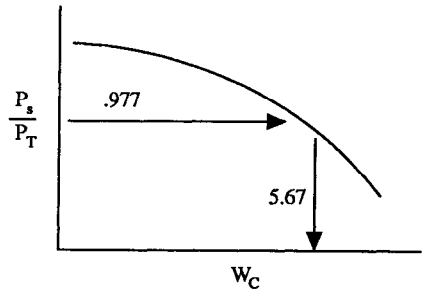

Figure B32 - Mass Flow Calibration (From Figure B13)

$$\dot{m} = W_c \frac{P_t\ /14.7}{\sqrt{T_t\ /\ 518}} = \frac{5.67\ /14/\ 14.7}{\sqrt{524\ /\ 518}} = 5.37$$

Ram Drag of air/oil cooler = W V_0

V_0 was previously computed as 330 ft/sec

Thus: $$\text{Ram Drag} = \frac{5.37\ (330)}{32.2} = 55 \text{ lbf}$$

B.7.4.2 A/O Cooler Jet Thrust: Despite the pressure losses in the air/oil cooler system, the heat exchange adds energy to the air side of the system producing thrust. This nozzle thrust can be computed similar to the C_v method described in Section B.7.2.2. The nozzle for the air side of the air/oil cooler system was rectangular and discharged the flow at a 15° angle relative to the thrust axis. The thrust computation used a standard C_v curve for a conical nozzle, with a debit for the asymmetry of a rectangular nozzle, and a debit for the flow angle (Figure B33). There was no static pressure data taken at the nozzle exit so it is assumed that $P_{s\,exit} = P_{s0}$, so the standard C_v equation can be used to calculate the cooler jet thrust.

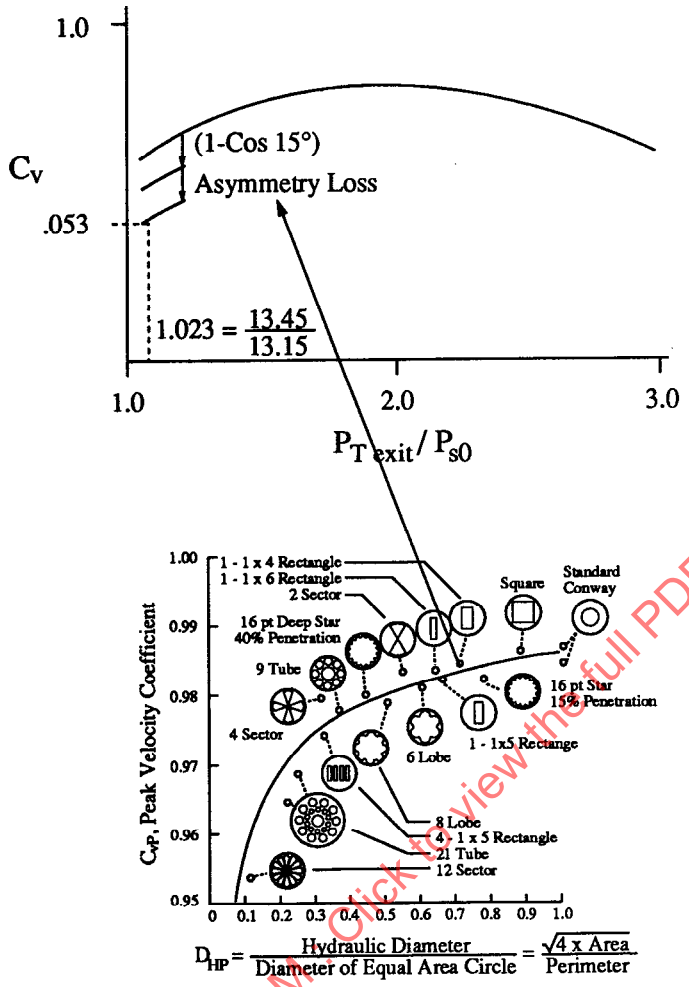

Reference B.7.4-2

Figure B33 - Standard C_v Curve with Debits for Cross Section Shape and 15° Flow Angle

Total Pressure Loss in System:

Figure B31 presents the loss distribution for w = 5.37 lb/sec and freestream Mach number of 0.3. The system loss is 3.9%.

$$P_{Te} = (1 - .039)\, P_T = (1 - .039)\, 14 = 13.454$$

$$\text{A/O Jet thrust} = C_v \left(\frac{F_{Ideal}}{P_T\, A^*} \right) (P_T)\, (A^*)$$

where: $P_T = 13.454$

$P_s = P_{s0} = 13.15$

{Sources: Table 2, (B1) and (B3)}

$$\left(\frac{F_{Ideal}}{P_T A^*}\right) = f(\gamma, P_{s0}/P_T) = .145$$

{Source: Compressible flow tables}

$T_t = 599\ °R$

{Source: Measurement, Table B1}

$$A^* = \frac{\dot{m}\sqrt{T_T}}{.532\ P_T} = \frac{5.37\sqrt{599}}{.532\ (13.45)} = 18.36 \text{ sq. in.}$$

A/O Cooler Jet Thrust = (.953) (.145) (13.454) (18.36) = 34.1 lbf

B.7.5 Summation of Forces to Quantify Net Thrust

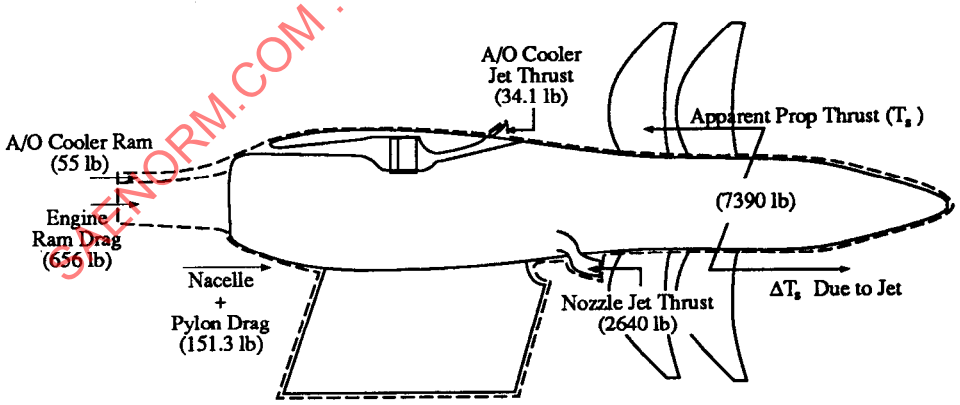

Figure B34 - Summation of Forces to Quantify Net Thrust

Net Thrust = (Thrust - Drag) **(B25)**

= (7390 + 2640 + 34.1) - (656 + 55 + 151.3)

= (10,064.1) - (862.3)

Net Thrust = 9201.8 lb

{Sources: B.7.1.4-(A.4); B.7.2.2; B.7.4.2; B.7.2.1;B.7.4.1 and B.7.3}

B.8 Comparison of In-Flight Thrust Calculation to In-Flight Thrust Inferred from MD-80 Aircraft Characteristics:

The rate of climb of the MD-80 test aircraft when powered with JT8D-200 engines had been measured on numerous occasions and is well defined at the Douglas Aircraft Company. The thrust-EPR relationship for the JT8D-200 is also well defined by Pratt & Whitney. Consequently a thrust setting v.s. climb gradient is well established for the test aircraft and offers a way of giving an independent indication of the propulsion system net thrust.

In order to determine thrust from rate of climb measurements, adjustments to the airplane characteristics must be made when a new propulsion system is installed. Thrust vector orientation changes, interference drag changes, pylon length changes, and changes to the airplane's lift, drag and trim moments all affect the rate of climb characteristic. Data for these adjustments was acquired using full span airplane models that included flow-through simulations of the JT8D-200 nacelle, and l' diameter turbo-powered simulators of a propfan. Low speed wind tunnel tests were conducted at the United Technology Research Center (UTRC) main wind tunnel, and high speed tests were conducted at NASA Ames Research Center to acquire the data needed for adjusting the aircraft characteristics. For example, the procedure for establishing changes to airplane interference drag is to:

(l) Test a clean airplane model (no nacelles)

(2) Test the nacelles isolated

(3) Test the airplane model with nacelles installed

Adding (1) and (2) and subtracting from (3) yields interference drag. Doing this first with the JT8D flow-through nacelles then comparing to the propfan TPS measured forces yields interference drag shifts. It should be pointed out that the propulsion simulator did not have the blades on a rotating thrust balance. Therefore, any changes in blade thrust that occur when going from an isolated flow field to installed in the airplane flow field are part of what's being called interference drag. The propeller blades simulated the Hamilton Standard's SR-2 blade and did not duplicate the aerodynamics of the full scale SR-9 blades. Hence shifts in blade thrust due to the aerodynamic installation in the airplane are not properly simulated. Also, the nacelle shape more closely represented a 0.4 hub to tip diameter ratio propeller design, whereas the 578DX's diameter ratio was 0.286. These dissimilarities increase the uncertainty of using rate of climb data for thrust validation. Despite these shortcomings, this comparison was of interest and is shown in Figure B35. The projected propulsion system thrust agrees within nominally 2% of the thrust implied by the airplane flight test/wind tunnel data. At the time of publication of this document it was not known if either in-flight thrust value is correct, or which is closer to the true propulsion systems in-flight thrust. It was encouraging that they agreed this well.

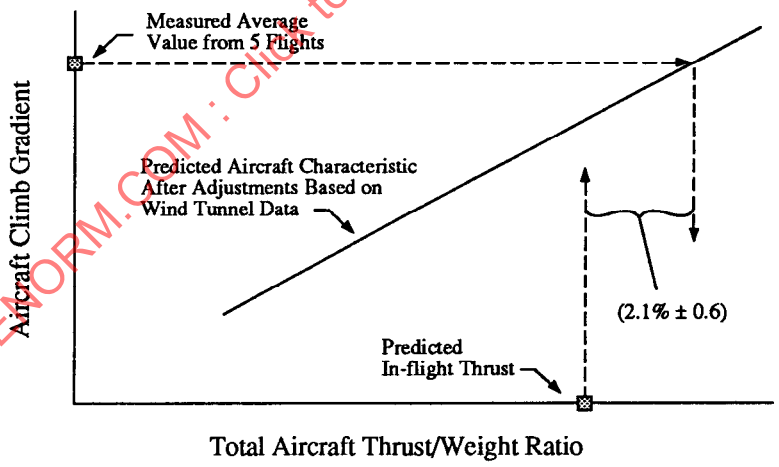

Figure B35 - In-flight Thrust Calculation Comparison

B.9 References

B1 Chapman, D. C., Sevich, G. J., and Smith, D. E.,"Preparing a Propfan Propulsion System For Flight Test", AIAA paper No. 87-1731

B2 Chapman, D. C., Godston, J., and Smith, D. E., "Testing of the 578-DX Propfan Propulsion System" 24th Joint AIAA/SAE/ASME Propulsion Conference, July, 1988.

B3 Chapman, D. C., Fleury, R. E., and Smith, D. E., "Flight Test on 578-DX Geared Propfan Propulsion System", 25th Joint AIAA/SAE/ASME Propulsion Conference, July, 1989.

B4 Bettner, J. L., Godston, J., Shattuck, C. D., "Propfan Propulsion System Design Considerations" 34th ASME International Gas Turbine and Aeroengine Congress and Exposition, June 1989.

B5 B. S. Stratford and G. S. Beavers, "The Calculation of the Compressible Turbulent Boundary Layer in an Arbitrary Pressure Gradient-A Correlation of Certain Previous Methods", R. & M. No. 3207, Aeronautical Research Council; London, England, 1961.

B6 Fluid Dynamic Drag by S. F. Horner, Page 8-11, Figure 25

APPENDIX C

In-Flight Thrust and Correlation Methodology Using Blade Angle and Torque

(Theta Method)

C.1 Introduction

The basic approach of evaluating in-flight thrust consists of two parts. The first part is the direct method when the installed power plant characteristics are known and the thrust of the power plant is estimated, knowing the flight Mach number, ambient conditions and the measured values of the power plant performance parameters. The second part is the indirect method which consists of evaluating the aircraft drag from the drag polar. The criteria for the acceptance of either method is the agreement between the estimated thrust and the drag. Both of these, i.e., the power plant performance map and the aircraft drag polar depend on extensive scale model testing both statically and in wind tunnels to arrive at full scale performance prediction. Given a set of performance characteristics, the inaccuracies arise from scaling the data from the scale model and the complex correlation schemes used in evaluating the unknowns in this instance the thrust, from the knowns. Any effort in improving these accuracies is a step in the right direction. However, it is important to point out that all of the correlation techniques available for constructing the power plant performance map are based on sound aerodynamic principles. In addition, the correlation technique should lend itself to verification of power plant characteristics from full scale test data. Consequently the objectives of the overall power plant performance correlation techniques from scale model testing can be summarized as simplicity, prediction accuracy, reduced installation effects and verification by full scale static engine tests.

C.2 Installation Effects

In the case of installed counter rotating propellers due to the differences in the inflow angle and the Mach number, the torque and thrust coefficients at any given propeller tip speed can be significantly different than the isolated propeller. Depending on the control system characteristics of the given engine, the installed propeller blade angles (θ_1 = forward, θ_2 = aft) and the individual propeller speeds may vary from the isolated case, for a given free stream Mach number and thrust requirement. Consequently, there is a need for developing two different performance maps, one for the forward propeller, and the other for the aft propeller. For the purpose of illustration, data acquired on GE-NASA unducted fan engine demonstrator scale model fan blades are used. The cases considered

are low speed data with pylon and a simulated fuselage as shown in Figure C1 up to 16 degrees angle of attack, and the high speed data with pylon up to 2 degrees angle of attack (α). As evident from Figures C2 and C3, both the total torque and thrust coefficient, at constant advance ratio, is significantly different between zero angle of attack and angle of attack cases. These differences are amplified in Figures C4 through C 7 where the individual rotor torque and thrust coefficient for the high speed cases are plotted as a function of advance ratio. The torque and thrust coefficients at a given advance ratio change considerably for constant pitch angle and free stream Mach number. However, the changes between the two rotors are in the opposite direction from each other, such that the net change in total thrust and torque coefficients are smaller than for individual rotors alone. The above data was used to illustrate the effect of inflow condition changes on performance. In the case of the installed propeller, significant inflow differences are to be expected due to the presence of the wing, pylon, and fuselage, which can lead to corresponding changes in torque and thrust coefficients as seen in Figures C2 through C7.

For a given free stream Mach number and advance ratio, both the torque and thrust coefficients are unique for each blade pitch angle combination. Since the blade pitch angle combination which produces the same propeller thrust is different between installed and uninstalled inflow conditions, all accounting methods should include the knowledge of blade pitch angle changes. The relative error due to neglecting the blade pitch angles should be evaluated before arriving at an appropriate method for determining the installed propeller thrust.

C.3 Propeller Performance Based On Blade Pitch Angle

The details of the blade angle method have been discussed in Section 3.4.2 earlier. The propeller thrust and torque coefficients can be related by the blade pitch angle and flight Mach number as:

$$C_T = f(C_Q, \theta, Mn)$$